Metabotropic Glutamate Receptor 7: Implications for the Etiology and Treatment of Neurodevelopmental Disorders

By

Nicole Marie Fisher

Dissertation

Submitted to the Faculty of the

Graduate School of Vanderbilt University

in partial fulfillment of the requirements

for the degree of

DOCTOR OF PHILOSOPHY

in

Pharmacology

December 12, 2020

Nashville, Tennessee

Approved:

Colleen M. Niswender, Ph.D.

P. Jeffrey Conn, Ph.D.

Danny G. Winder, Ph.D.

Vsevolod V. Gurevich, Ph.D.

Eric Delpire, Ph.D.

To all patients and families affected by rare genetic disorders

ACKNOWLEDGMENTS

I have been tremendously lucky to have the support of so many people throughout the course of graduate school. I would first like to thank Colleen Niswender for taking me on as a student and for being an all-around terrific mentor. Colleen has many qualities that I admire and strive to emulate: a positive attitude, resilience to failure, openness to try anything once, and genuine respect for those who work with her. I also appreciate the freedom and independence that she gave me as a graduate student, which challenged me to grow in many ways. Thank you to Rocco Gogliotti, who mentored me from day one and has continually shown a sincere interest in my training. I am particularly grateful for Rocco's tireless efforts to teach me to align figures properly, a skill that has finally stuck after 5+ years. I would also like to thank my co-mentor Jeff Conn, along with my other committee members, for their helpful scientific input and for always being advocates for my success. And thank you to those in the Pharmacology department who have provided support and encouragement including Karen Gieg, Christine Konradi, Sean Davies and Joey Barnett.

I would also like to thank our collaborator Aqeela Al-Hashim of King Fahad Medical City in Riyadh, Saudi Arabia for providing the clinical information in Chapter 5 and for all of her helpful input. It was truly rewarding and motivating to connect with patients carrying the mutation I was studying at the bench. Similarly, thank you to Sar Peters and Cary Fu, two clinicians who I had the opportunity to shadow through the Vanderbilt Program in Molecular Medicine, for introducing me to patients with Rett syndrome and MECP2 Duplication syndrome. This work could not have been done without use of the Vanderbilt Mouse Neurobehavioral Core (with much help from John Allison) and the Vanderbilt Genome Editing Resource. I would also like to acknowledge funding provided by the National Institute of Mental Health, the Department of Defense and Rettsyndrome.org.

I have had the privilege to work with many talented people at Vanderbilt, including great labmates who created a fun, positive, and stimulating work environment. Thank you to Sean, James, Sheryl, Chris and Mabel for being supportive peers, thank you to all the postdocs who gave me helpful advice, and a special thank you to the RAs and undergrads for keeping me up-to-date on the hip lingo. Many of these people also made direct contributions to this work, specifically Rocco, Rob, Sheryl, Branden, Mabel, Aditi, Hana, Susmi, and Annalise. I would also like to thank Matt and Holly for all the hard work that they do to support the lab.

Thank you to all of my Nashville friends who have explored the city with me and shared many delicious meals, particularly Meredith, Laura, Chloe, Michael T., Alissa, FJ, Kelly and Michael D. I will miss our “Hot Chicken Christmas” parties. I have also enjoyed the friendship of many Pharmacology students, including my best friend and fiancé, Eric Figueroa. Eric, thank you for taking me to so many concerts, for running a half marathon with me, for being my quarantine companion, and for always believing in me. With our mutual love and support, I feel like we can do anything. I can’t wait for our next chapter and to see where else life takes us.

Finally, I need to thank my very large and supportive family. Thank you to my three big brothers, Nathan, Jason and Jonathan, for being the best role models. Thank you to my three sister-in-laws, Krissy, Kayla and Kristin, for their support, and a special thank you to Krissy for introducing me to biomedical research as a career path and for being a great example of a female scientist balancing work and family. Thank you to my niece, Sophie, and to my nephews, Luke and Tanner, for giving me an escape from adult worries. I can’t wait to watch you grow up and follow your own passions. And most importantly, thank you to my parents, Mark and Debbi, who have loved me unconditionally and supported me in every possible way. Thank you for teaching me the value of education and hard work, and for encouraging my curiosity. I could not have had a better upbringing, which is the foundation upon which I have built all other aspects of my life.

TABLE OF CONTENTS

LIST OF TABLES

LIST OF FIGURES

CHAPTER I. Introduction

Preface

This chapter includes text from a review published in *Frontiers in Molecular Neuroscience*[1] along with additional information. Content from the review was written in collaboration with Mabel Seto.

Overview

The work described herein investigates the contribution of the metabotropic glutamate receptor 7 ($mGlu_7$) to neurodevelopmental disorders. In this introduction, I will summarize what is currently known about neurodevelopmental disorders and $mGlu_7$ separately. In the following chapters, I will present data that evaluates $mGlu_7$ as a therapeutic target and investigates $mGlu_7$ loss of function as a cause of neurodevelopmental disease.

Neurodevelopmental disorders (NDDs)

Neurodevelopmental disorders (NDDs) are a group of conditions that present in early life and are characterized by the failure to meet typical developmental milestones. These disorders affect a significant fraction of the population. According to a recent survey, nearly 18% of children between 3 to 17 years old in the United States were reported to have a developmental disability from 2015 to 2017[2]. The current Diagnostic and Statistical Manual of Mental Disorders (DSM-V) categorizes neurodevelopmental disorders into six groups: intellectual disabilities (ID), learning disorders, communication disorders, autism spectrum disorders (ASD), attention-deficit hyperactivity disorder (ADHD), and motor disorders[3]. There is often overlap between these groups; for example, 32% of patients with ASD also fulfill the diagnosis for ID[4]. In addition, NDDs are associated with many co-morbidities, including but not limited to: epilepsy, mood disorders, breathing abnormalities, sleep problems and gastrointestinal issues[5,6]. Individuals with NDDs can struggle to develop interpersonal relationships and face immense challenges in school and in the

workforce. Treatment options remain limited; thus, there is a great need to understand the pathophysiology of these disorders and to identify novel points of intervention to improve the quality of life of these patients and their caretakers. Advances in sequencing technologies and recent whole exome sequencing studies have yielded significant insights into underlying causes of these disorders. These findings will be discussed in detail for each NDD class in the sections below.

Autism spectrum disorder

ASD is characterized by deficits in social communication accompanied by restrictive and/or repetitive sensory-motor behaviors[7]. Symptoms include lack of social-emotional reciprocity, deficits in non-verbal communication and problems maintaining relationships. Abnormal sensory-motor behaviors include repetitive movements, insistence on sameness, fixated interests and hyper-reactivity to sensory input. It is recognized that ASD is highly heterogeneous and that symptom presentation and severity can vary greatly from individual to individual. ASD has a prevalence of about 1.5% in developed countries[8] and 2.5% in the United States[2]. Current treatments focus on behavioral therapy and promoting individual strengths to help those with ASD succeed. There are no medications that target the core symptoms of ASD; rather, medications are used to manage comorbidities such as irritability, anxiety, and ADHD.

A recent meta-analysis estimated that 74-93% of the risk for ASD is heritable[9]; however, several environmental factors have also been suggested. These include parental age, maternal infection and medication use during pregnancy[7]. Nonetheless, there has been a large effort to understand ASD genetics in hopes to gain insights into the underlying neurobiology and to improve diagnosis and treatment. In about 5-10% of cases, ASD is found in patients with co-occurring monogenetic syndromes. The most common include Fragile X syndrome, Tuberous Sclerosis, and Rett syndrome, which are caused by mutations in the genes *FMR1*, *TSC1/2*, and *MECP2*, respectively[10]. With increased prevalence of whole exome sequencing, other high-risk

genes have been identified. In the largest ASD exome sequencing study to date (N = 35,584 total samples, N = 11,986 with ASD), Satterstorm et al. identified 102 high-risk genes[11]. Most of these genes are expressed early in development and play roles in either gene regulation or neuronal communication. Interestingly, 49 of these genes showed higher frequencies in individuals with severe developmental delay, while 51 showed higher frequency in those with ASD alone. As the list of ASD susceptibility continues to grow, it is increasingly recognized that ASD likely arises from the interaction of many genes in addition to environmental factors.

Attention-deficit hyperactivity disorder

Attention-deficit hyperactivity disorder (ADHD) is characterized by inattention, hyperactivity and impulsivity[3], which can have a negative impact on academic achievement and interpersonal relationships. ADHD is usually diagnosed during childhood with symptoms often persisting into adolescence and adulthood. Its estimated world-wide prevalence is 7.2% in children and 3.4% in adults[12,13]. ADHD treatment consists of a combination of behavioral therapy and medication. Psychostimulants, such as methylphenidate and amphetamine are considered to be the first-line treatment for ADHD[14]. Both of these drugs block the reuptake of dopamine and norepinephrine thus increasing the action of these neurotransmitters. Amphetamine additionally reverses the dopamine transporter and causes an efflux of dopamine. However, these stimulants have side effects that include appetite suppression, dry mouth, insomnia and nausea in addition to concerns that they may negatively impact the growth trajectory of children. Several nonstimulant options are available to those who respond poorly to stimulants, including atomoxetine, guanfacine and clonidine, which act on the norepinephrine system.

Twin studies have estimated that the heritability of ADHD falls around 60-80%[15,16]. These estimates can be greatly influenced by the method of data collection (e.g. self-report versus parent or teacher report, assessment of distinct behaviors versus clinical ADHD diagnosis, etc.). Regardless, it is generally accepted that there is high heritability of ADHD. Early candidate gene

approaches identified variants in pathways associated with dopaminergic or noradrenergic transmission with significant genetic association[17]. These variants implicated six genes: the serotonin transporter gene (*5HTT*), the dopamine transporter gene (*DAT1*), the D_4 dopamine receptor gene (*DRD4*), the D_5 dopamine receptor gene (*DRD5*) the serotonin 1B receptor gene (*HTR1B*) and the gene for the vesicle-regulating protein SNAP25 (*SNAP25*).[18] Genome-wide association and whole exome sequencing studies have identified many more genes associated with ADHD which are reviewed in reference 16. Of interest to this dissertation, enrichment for copy number variations (CNVs) in glutamatergic genes have been identified in two independent studies[19,20]. Involvement of glutamatergic transmission is further supported by deficits in rat models of ADHD[21] and alterations in glutamate/glutamine levels demonstrated in human imaging studies[22].

Intellectual disability

Intellectual disability (ID) is a prominent feature of many neurodevelopmental disorders and is often identified early in childhood along with other developmental delays. According to the DSM-V, ID is clinically defined as having deficits in both intellectual and adaptive functioning before the age of 18 years. Intellectual functioning encompasses skills such as reasoning, problem solving and planning, while adaptive function refers to the ability to meet societal standards for personal independence and social responsibility. Intellectual functioning is usually evaluated with a standardized test that quantifies an intellectual quotient (IQ). The criteria for ID is fulfilled if an individual's IQ is below 70, or two standard deviations below the mean of the general population[3]. In a recent survey, ID was estimated to affect about 1% of the US population[2]. Global developmental delay is a diagnosis given to children under 5 years of age who show deficits in intellectual functioning, but are unable to undergo systematic assessments[3].

Many cases of ID can be explained by genetic abnormalities. The first to be described was Down syndrome, which results from trisomy of chromosome 21 and is still the most common

cause of ID[23]. Fragile X syndrome was also an early recognized form of ID and is caused by mutations in the X-linked gene *FMR1*[24]*.* The X chromosome has been extensively studied and over 100 genes on this chromosome have been associated with ID. Each one accounts for a small number of cases, but collectively they can explain 5-10% of ID in males[25]. Exome sequencing studies have now identified over 700 genes linked to ID and ID-associated syndromes[26]. In 2015, the Deciphering Developmental Disabilities study sequenced the exomes of over 1,000 children with severe undiagnosed neurodevelopmental disease and yielded a molecular diagnosis rate of 28%. The most common cause was reported to be *de novo* mutations[27]. A later study estimated that nearly half of severe developmental disorders can be attributed to *de novo* mutations, and that the occurrence of these mutations positively correlates with parental age[28]. While ID caused by autosomal recessive mutations is rare in populations of European decent, it is much more common in cultures with consanguineous marriage. For example, in one study only 3% of cases could be explained by recessive mutations in a European population whereas 31% of cases could be explained by recessive mutations in a Pakistani population[29]. Studies focused on consanguineous families have been incredibly successful in identifying novel ID genes[30–32]. Similar to ASD, many ID-linked genes play roles in synaptic structure and function. Thus, much effort has been devoted to understanding synaptic deficits in animal models of ID and developing therapies that act to restore proper synaptic function[33].

Epilepsy

Epilepsy is defined by the occurrence of at least two unprovoked seizures spaced greater than 24 hours apart. A seizure is a “a transient occurrence of signs and/or symptoms due to abnormal excessive or synchronous neuronal activity in the brain” as defined by the International League Against Epilepsy[34]. Seizures can be further classified based on onset (focal, generalized, or unknown) and motor characteristics (motor vs. non-motor). Seizures that involve movement can be further described by terms such as tonic (stiffening of muscles), clonic (jerking of muscles),

tonic-clonic, myoclonic, aclonic, etc. Epilepsy is highly co-morbid with neurodevelopmental disorders: epilepsy is diagnosed in about 21% of patients with ASD and ID and in 6% of patients with ASD without ID[35]. In the case of epileptic encephalopathies, recurrent seizures early in life can lead to severe cognitive and behavioral impairment[36].

There are many known causes of epilepsy including stroke, trauma, brain lesions, neoplasms, infection and autoimmune syndromes; however, a large proportion of epilepsy cases are idiopathic and believed to be influenced by genetic factors[37]. In rare cases, a single gene mutation can explain familial epilepsies. For example, mutations in *CHRNA4,* encoding the nicotinic acetylcholine receptor α4 subunit, are found in a form of autosomal-dominant nocturnal frontal lobe epilepsy[38], and mutations in the gene encoding epitempin, *LGI1,* are a cause of autosomal-dominant partial epilepsy with auditory features[39]. In recent years, whole exome sequencing studies have revealed that *de novo* mutations also make a significant contribution. Most cases of Dravet syndrome, a severe epileptic encephalopathy, are caused by *de novo* mutations in *SCN1A,* a gene that encodes a subunit of voltage-gated sodium channels. As another example, *de novo* gain of function mutations in *KCNT1*, which encodes a sodium-activated potassium channel, have been identified in infants with severe seizures[40]. A recent analysis found that 84 genes have been reported as a cause of epilepsy or syndromes with epilepsy as a core symptom[41]. When grouped based on protein function, ion channel genes were heavily enriched (28/84), which is consistent with the direct role of ion channels in neuronal excitability.

A variety of antiepileptic drugs are currently available to help manage seizures and decrease their occurrence. Some of these drugs act by dampening the excitability of glutamatergic neurons via inhibition of voltage-gated sodium channels and ionotropic glutamate receptors. Others promote inhibitory synaptic transmission by potentiating GABA receptors, inhibiting GABA reuptake or increasing GABA biosynthesis[42]. While effective for a subset patients, about 30% of individuals do not respond[43]. Drug-resistant epilepsy is sometimes treated with a

ketogenic diet in which fat becomes the main energy source for the brain. The mechanism behind the efficacy of this diet is unknown but postulated to involve inhibition of vesicular glutamate loading, inhibition of ATP-sensitive potassium channels, and effects on mitochondrial respiration[44]. Precision medicine efforts are currently underway to develop improved therapies that are tailored to specific subtypes of epilepsy[45].

Metabotropic glutamate receptor 7 ($mGlu_7$)

The metabotropic glutamate receptors

Excitatory neurotransmission in the brain is mediated in large part by the neurotransmitter glutamate, which exerts its effects by activating ionotropic and metabotropic glutamate receptors. The ionotropic glutamate receptors include AMPA, NMDA and kainate receptors. Upon glutamate binding, these receptors open to allow the influx of cations (Na^+, Ca^{2+}), which leads to dendritic depolarization and increased probability of action potential firing. The metabotropic glutamate (mGlu) receptors, on the other hand, are G protein-coupled receptors (GPCRs) that activate intracellular signal cascades to modulate synaptic transmission and plasticity on a slower time scale. mGlu receptor activation leads to a myriad of post-translational effects on synaptic proteins (receptors, ion channels, scaffolding proteins, etc.), and can also impact gene transcription and local protein synthesis. For a review encompassing all glutamate receptors and potential crosstalk, see reference 46, as this dissertation will focus on the metabotropic glutamate receptors.

The mGlu receptors are a family of Class C GPCRs that can be further divided into three groups based on their sequence homology, G-protein coupling, and cellular localization (Figure 1A). Group I includes $mGlu_1$ and $mGlu_5$, which canonically couple to G_q to activate the phospholipase C signaling cascade and are typically found in the postsynaptic membrane. Conversely, Group II and Group III receptors couple to $G_{i/o}$ proteins and are typically found in the

presynaptic membrane. Group II includes $mGlu_2$ and $mGlu_3$ while Group III includes $mGlu_4$, $mGlu_6$, $mGlu_7$, and $mGlu_8$[47].

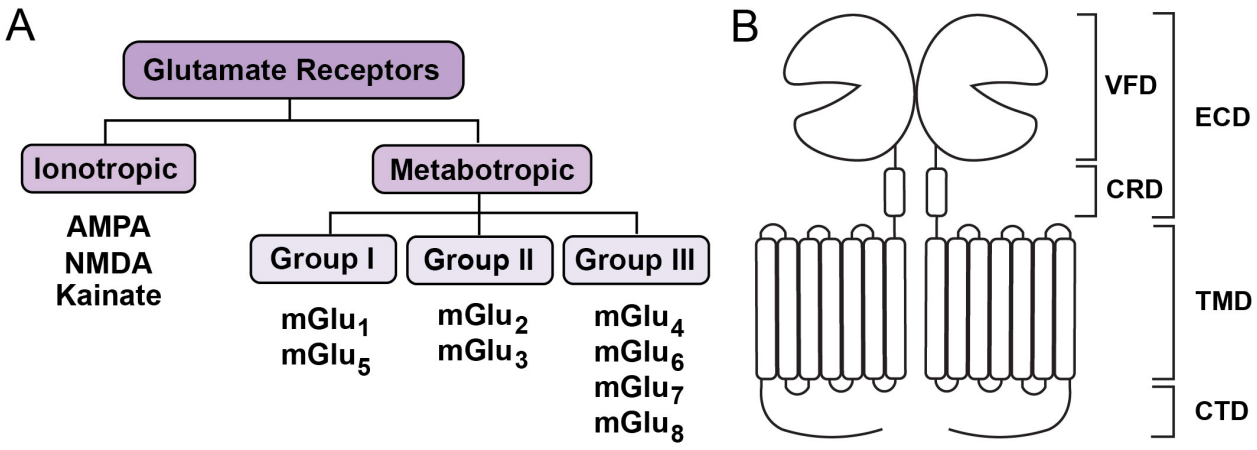

Figure 1. Organization and structure of metabotropic glutamate receptors.

A) Organization of glutamate receptors. B) Structure of metabotropic glutamate receptors. VFD = Venus flytrap domain, CRD = cysteine-rich domain, ECD = extracellular domain, TMD = transmembrane domain, CTD = C-terminal domain.

Characteristic of Class C GPCRs, all mGlu receptors have a large *N*-terminal extracellular domain (ECD) which comprises a ligand-binding domain and a cysteine-rich domain (CRD). The receptors then have a heptahelical transmembrane domain and an intracellular C-terminal tail (Figure 1B). The large ligand-binding domain consists of two lobes that sit on top of one another, similar to a Venus flytrap. For this reason, the ligand binding is often referred to as the "Venus flytrap domain" (VFD). The metabotropic glutamate receptors function as constitutive dimers[48,49], and dimerization primarily occurs at the level of the VFDs[50–54]. Glutamate binds to a cleft in between the two lobes of the VFD[47,50,51] allowing for three potential states: open-open, open-closed, and closed-closed. It is thought that glutamate binding to one VFD alone is sufficient for activation (open-closed), but that full activation is achieved when both VFDs are ligand bound (closed-closed)[55]. Upon glutamate binding, the VFDs undergo a large conformational rearrangement that brings the two CRDs into close proximity[50]. The CRDs contain cysteine residues that form inter-subunit disulfide bonds that are critical for propagating signals from the

VFDs to the rest of the receptor[56]. Interactions between the CRDs and the second extracellular loops enable rearrangement of the transmembrane domains such that the helices rotate to create an interface between the sixth helix of each subunit[54]. The structural details of how this rearrangement leads to G protein activation are presently unknown.

$mGlu_7$ expression, signaling and regulation

This dissertation focuses exclusively on the $mGlu_7$ receptor, which is encoded by the gene *GRM7* in humans. There are fifteen splice variants of *GRM7*, six of which are predicted to be protein coding[57]. The two major isoforms, $mGlu_{7a}$ and $mGlu_{7b}$, differ at their C-termini and several studies have shown that these distinct C-terminal tails mediate different protein-protein interactions[58]. Of note, $mGlu_{7a}$ contains a PDZ-binding domain at its extreme C-terminus that allows for interaction with protein interacting with C kinase (PICK1)[59,60]. $mGlu_{7a}$ has widespread expression in the CNS whereas $mGlu_{7b}$ expression is more restricted to distinct regions including the hippocampus, ventral pallidum, and globus pallidus[61,62,63]. Three other isoforms with distinct C-termini have been detected in the brain but have yet to be characterized in detail[64]. $mGlu_7$ is expressed in several peripheral tissues as well, including the testes, uterus, placenta and adrenal gland[64].

In the CNS, $mGlu_7$ receptors are primarily localized to presynaptic active zones in neurons where they can act as auto- or hetero-receptors to inhibit the release of their endogenous ligand, glutamate, the main excitatory neurotransmitter, or γ-aminobutyric acid (GABA), the main inhibitory neurotransmitter, respectively[65–67]. Compared to the other Group III mGlu receptors, $mGlu_7$ exhibits an extremely low affinity for glutamate (high μM to mM as opposed to high nM to low μM for the other Group III mGlu receptors). Because of this low affinity, it has been suggested that $mGlu_7$ functions as an “emergency brake” in the case of elevated glutamate levels[47]. This idea is supported by the observation that $mGlu_7$ knockout mice exhibit spontaneous seizures under certain contexts[68]. Another theory is that $mGlu_7$ forms heterodimers with other mGlu

subtypes and that these heterodimers have unique characteristics from homodimers. It has been demonstrated that $mGlu_7$ *can* dimerize with group II and other group III mGlu receptors[69,70] and in one interesting study, $mGlu_{2/7}$ heterodimers were shown to have increased affinity and efficacy compared to $mGlu_{7/7}$ or $mGlu_{2/2}$ homodimers[71]. However, the existence of heterodimers containing $mGlu_7$ has not yet been demonstrated in the brain. A recent analysis of single cell RNA-sequencing data from mouse cortex revealed that $mGlu_7$ is co-expressed within the same cell with other mGlu subtypes *in vivo*[70]; therefore, $mGlu_7$ heterodimerization remains an open and exciting avenue of research.

$mGlu_7$ and the other Group III mGlu receptors couple to $G_{i/o}$, which inhibits adenylyl cyclase activity and reduces intracellular cyclic adenosine monophosphate (cAMP) concentrations[47]. Furthermore, $mGlu_7$ activation can result in K^+ influx via $G_{\beta\gamma}$-mediated opening of G protein-activated inwardly rectifying potassium (GIRK) ion channels[72,73] and inhibition of Ca^{2+} currents through N- and P/Q- type calcium channels[74]. Recruitment of β-arrestins to $mGlu_7$ has also been shown to impact ERK1/2 and JNK signaling in recombinant cells[75]. In addition to agonist-induced activation, $mGlu_7$ has been shown to exhibit constitutive activity in some cell types and circuits[76–78].

Inhibition of neurotransmitter release by $mGlu_7$ at synapses is believed to be mediated primarily through inhibition of N-type and P/Q-type calcium channels[74,79–81]. Millán et al. demonstrated that activation of cerebrocortical $mGlu_7$ with the agonist L-AP4 inhibited N-type calcium channels. This effect could be blocked by pertussis toxin, but not by inhibitors of protein kinase A (PKA) and protein kinase C (PKC)[79]. Perroy et al. demonstrated that $mGlu_7$ activation inhibited P/Q-type calcium channels in cultured cerebellar granule cells via a pathway involving $G_{i/o}$ proteins, phospholipase C (PLC), and PKC[82]. It has also been demonstrated that the scaffolding protein, PICK1, facilitates the interaction between $mGlu_7$ and PKC, and is required for receptor-mediated P/Q-type calcium channel inhibition in cultured cerebellar granule cells[81]. In contrast, Martín et al. demonstrated that $mGlu_7$ inhibited hippocampal P/Q-type calcium channels

in a PKC-independent manner[74]. $mGlu_7$-mediated inhibition of glutamate release has also been shown to be dependent on interactions with calmodulin (CaM), where activated CaM allows for the displacement of $G_{\beta\gamma}$ from $mGlu_7$ and the subsequent downregulation of calcium influx into the cell via calcium channel inhibition[72]. Moreover, $mGlu_7$'s interactions with MacMARCKS (macrophage myristoylated alanine-rich C-kinase substrate) competitively antagonizes CaM-mediated calcium channel inhibition[83]. Interestingly, it has been shown that prolonged exposure to the agonist L-AP4 can lead to $mGlu_7$-mediated *potentiation* of neurotransmitter release via activation of PLC, hydrolysis of phosphatidylinositol (4,5)-bisphosphate, and activation of Munc-13, a protein that primes synaptic vesicles for release[84,85].

$mGlu_7$ signaling is regulated through several mechanisms including phosphorylation, internalization, and other protein-protein interactions. $mGlu_7$ is known to be phosphorylated at serine 862 by PKC, and this phosphorylation is regulated by $mGlu_7$'s interaction with PICK1[60]. Phosphorylation at this site promotes binding of PICK1 and stable surface expression of $mGlu_7$, while simultaneously decreasing the binding affinity of CaM[86]. Phosphorylation at serine 862 is removed by protein phosphatase 1 (PP1) leading to increased receptor internalization and decreased $mGlu_7$ surface expression[87]. $mGlu_7$ has been shown to undergo both constitutive and activity-induced endocytosis[88,89]. Upon agonist stimulation, the ubiquitin ligase Nedd4 is recruited to $mGlu_7$ by β-arrestins, allowing for ubiquitination of $mGlu_7$. The ubiquitinated receptor then undergoes endocytosis followed by proteasomal or lysosomal degradation[90]. Recently, activity of group III mGlu receptors have been shown to be regulated by the postsynaptic adhesion protein extracellular-leucine-rich repeat fibronectin type III domain containing 1/2 (ELFN1 and ELFN2)[91,92]. ELFN1 recruits high presynaptic expression of $mGlu_7$ at distinct synapses[17] and promotes the constitutive activity of $mGlu_7$ leading to low presynaptic release probability[78].

$mGlu_7$ in synaptic transmission and plasticity

$mGlu_7$'s position within the active zone and its ability to modulate neurotransmitter release has led to numerous studies focused on its role in synaptic plasticity. Two major forms of synaptic plasticity include long-term potentiation (LTP) and long-term depression (LTD), which are persistent changes in synaptic strength that are thought to be correlates of learning and memory[93,94]. The role of $mGlu_7$ in synaptic plasticity has been best characterized within the hippocampus at several distinct synapses. $mGlu_7$ was first reported to mediate a form of LTD occurring in stratum radiatum interneurons within area CA3[95]. At excitatory synapses onto interneurons expressing calcium-permeable AMPA receptors, LTP could be induced by high frequency stimulation and blocked by the Group II and Group III mGlu antagonist LY341495. Further pharmacological experiments confirmed the specific involvement of $mGlu_7$: only a high concentration of L-AP4 depressed synaptic transmission at these synapses and a Group II mGlu agonist showed no effect. A similar form of plasticity was later described at mossy fiber inputs onto stratum lucidum interneurons (SLINs) in area CA3[96]. At SLINs expressing calcium-permeable AMPA receptors, high frequency stimulation of mossy fibers induced an LTD that required $mGlu_7$ activation and PKC-dependent depression of neurotransmitter release through P/Q-type voltage gated calcium channels[96,97]. Interestingly, in slices pre-treated with L-AP4, internalization of $mGlu_7$ receptors revealed the ability of these synapses to undergo LTP instead of LTD in response to the same electrical stimulus. Surface expression of $mGlu_7$, therefore, regulates the direction of plasticity at these synapses, making $mGlu_7$ a "metaplastic switch" that can modulate feedforward inhibition in area CA3.

An additional class of interneurons in which $mGlu_7$-mediated plasticity has been implicated is the oriens-lacunosum-moleculare (OLM) interneuron population within the stratum oriens of areas CA3 and CA1. At excitatory inputs onto OLM interneurons, $mGlu_7$ expression is preferentially enriched[65] and proposed to be recruited by the postsynaptic adhesion protein ELFN1[17]. Sylwestrak and Ghosh demonstrated that ELFN1 knockdown in OLM interneurons

decreases short-term facilitation and increases presynaptic release probability. Conversely, overexpression of ELFN1 in parvalbumin interneurons leads to short-term facilitation when these synapses typically undergo short-term depression[98]. In slices from *Elfn1*$^{-/-}$ mice, presynaptic release probability, short term facilitation, and LTP are reduced in patch-clamp recordings from OLM interneurons[17]. Although this evidence is indirect, it suggests that $mGlu_7$ may be involved in these forms of synaptic plasticity since $mGlu_7$ is likely to be a major regulator of presynaptic release probability at these synapses due to its recruitment by ELFN1. At cortical synapses onto somatostatin-expressing interneurons, the ELFN1-$mGlu_7$ interaction promotes constitutive activity of $mGlu_7$[78]. This contributes to low release probability and allows for the characteristic short-term facilitation at these synapses.

In addition to its role as an autoreceptor on excitatory terminals, $mGlu_7$ is also located on the terminals of interneurons within the hippocampus and modulates the release of GABA[66,99]. This function of $mGlu_7$ is required for LTP in wild-type animals at Schaffer Collateral-CA1 (SC-CA1) synapses through a mechanism of disinhibition[100]. Importantly, deficits in LTP at this particular synapse have been reported in several models of NDDs[101–103]. At SC-CA1 synapses, $mGlu_7$ is the only presynaptic mGlu receptor present in adult animals and activation of $mGlu_7$ has been repeatedly shown to reduce field potentials at SC-CA1[73,104,105]. Klar et al. demonstrated that $mGlu_7$ activation by the agonist LSP4-2022 also reduces evoked inhibitory postsynaptic currents recorded from CA1 pyramidal cells. LTP induced by high-frequency stimulation was blocked by the negative allosteric modulator (NAM) ADX71743, but only when GABAergic transmission was intact[100]. Recently, we showed that a chemically distinct $mGlu_7$ NAM, VU6010608, also blocked LTP induced by high-frequency stimulation at SC-CA1 synapses[106]. Interestingly, hippocampal slices from *Grm7*$^{-/-}$ mice have been reported to exhibit similar levels of LTP when compared to wild-type controls, but decreased short-term potentiation following high-frequency stimulation[107]. In these studies, slices from *Grm7*$^{-/-}$ mice showed reduced facilitation during the high-frequency train, an effect that was also seen with ADX71743 by Klar et al. The presence of LTP in *Grm7*$^{-/-}$

slices may be due to compensatory mechanisms during development, such as retained expression of $mGlu_8$, which is present at SC-CA1 synapses earlier in development[105]. Re-expression of $mGlu_8$ is not unprecedented as the selective $mGlu_8$ agonist (S)-3,4-DCPG was recently shown to reduce synaptic transmission at SC-CA1 in slices from pilocarpine-treated rats, but not in those of age-matched controls[108]. While further studies will be needed to explain the current discrepancy between genetic and pharmacological approaches, these data indicate that $mGlu_7$ regulates high-frequency transmission at SC-CA1 synapses. Recently, Martin et al. demonstrated that prolonged activation of $mGlu_7$ leads to potentiation of excitatory postsynaptic currents recorded from pyramidal cells in CA1[109]. This potentiation of neurotransmitter release is dependent on PLC and the vesicle release proteins Munc13-2 and Rim1α. These studies indicate that, under conditions of high-frequency stimulation, $mGlu_7$ activation favors potentiation of excitatory transmission, which could be an additional mechanism by which $mGlu_7$ modulates long-term plasticity in the hippocampus.

Beyond the hippocampus, a role for $mGlu_7$ in LTP has also been established within the amygdala. Synaptic plasticity in the hippocampus is believed to underlie associative learning and working memory, whereas plasticity in the amygdala is associated with aversion and emotional learning[110,111]. The allosteric agonist AMN082 has been shown to block LTP at thalamo-amygdala synapses in slices from rats and mice[112,113]. This effect correlates with the ability of direct injection of AMN082 into the amygdala to block the acquisition of fear-potentiated startle behavior in rats[112] and fear learning in mice[112,113]. Interestingly, *Grm7*$^{-/-}$ mice exhibited a general deficit in fear learning and decreased LTP at thalamo-amygdala synapses[113]. Reduction of LTP by both an agonist and gene ablation may be explained by AMN082's ability to cause rapid internalization of $mGlu_7$ receptors[89]. This would suggest that AMN082 can act as a functional antagonist by decreasing surface expression and, therefore, receptor signaling. This hypothesis is further supported by the ability of the $mGlu_7$ antagonist XAP044 to block LTP within the amygdala, inhibit acquisition of conditioned fear, and reduce anxiety-like behavior[114]. Together, these studies

demonstrate that $mGlu_7$ promotes plasticity within the amygdala, which is in line with its involvement in behaviors of fear and anxiety.

Role of $mGlu_7$ in NDD-associated phenotypes

Core symptoms and comorbidities of NDDs can include, but are not limited to: cognitive impairment, seizures, mood disorders, social deficits, and motor impairments[5,6]. Many studies have demonstrated that modulation of $mGlu_7$ function via genetic and/or pharmacologic techniques is able to mimic some of these phenotypes in animal models, and these studies will be reviewed here.

Cognition

$mGlu_7$ knockout animals (*Grm7*$^{-/-}$) show deficits in tasks that test cognitive functioning. In a conditioned taste aversion task, which measures amygdala-dependent aversive learning, mice were given saccharin along with an intraperitoneal injection of the control, saline, or lithium chloride (LiCl), which evokes malaise. In this task, *Grm7*$^{-/-}$ mice did not associate the adverse effects of LiCl to saccharin in comparison to wild-type littermates, exhibiting a deficit in fear learning[115]. In addition, Masugi et al. and Goddyn et al. demonstrated that *Grm7*$^{-/-}$ mice exhibit less freezing than wild-type animals in cued and contextual fear conditioning paradigms[115–117]. Together, these results indicate a role for $mGlu_7$ in aversion learning, and also suggest that the loss of $mGlu_7$ causes impairments in these learning paradigms.

$mGlu_7$ has also been demonstrated to play a role in cognitive tasks that do not rely on fearful or aversive stimuli. Callaerts-Vegh et al. showed that *Grm7*$^{-/-}$ mice exhibit impaired short-term working memory in 4- and 8-arm radial maze tasks, committing more errors (visits to previously baited arms or un-baited arms) than their wild-type counterparts. Conversely, *Grm7*$^{-/-}$ mice performed similarly to wild-type animals in radial maze tasks when they were modified to assess long-term memory[118]. Furthermore, both Goddyn et al. and Callaerts-Vegh et al. have reported that the loss of $mGlu_7$ causes increased latency to locate a platform in the Morris water

maze task of spatial memory[117,118]. Interestingly, *Grm7*$^{-/-}$ mice performed similarly to wild-type animals after increased training and in un-cued trials[118]. Together, these data demonstrate that $mGlu_7$ may play specific roles in tasks involving working and spatial memory.

Pharmacological studies have further confirmed a role for $mGlu_7$ in learning and memory. Hikichi et al. showed that administration of MMPIP, an $mGlu_7$ negative allosteric modulator (NAM), to wild-type mice reduced performance in object recognition and location tasks, suggesting that $mGlu_7$ is also involved in recognition memory[119]. MMPIP also attenuated conditioned taste aversion learning in rats[120]. Interestingly, MMPIP improved cognitive performance in Y-maze and object recognition assays in a mouse model of neuropathic pain with no effect on sham-treated animals[121]. MMPIP exhibits cellular background-dependent differences *in vitro*, and also had no effect in an electrophysiological study of SC-CA1 synapses in the hippocampus[122], which may complicate interpretation of *in vivo* data. Inhibition of $mGlu_7$ with the antagonist XAP044 also resulted in reduced freezing in mice during a contextual fear conditioning task, further supporting a role for $mGlu_7$ in amygdala function[114]. Activation of $mGlu_7$ with an allosteric agonist, AMN082, has been shown to modulate both the acquisition and extinction of conditioned fear, though the results seem to contradict findings from studies performed with XAP044 and *Grm7*$^{-/-}$ animals[112–114,116,123,124]. Administration of AMN082 impaired the acquisition and enhanced the extinction of fear learning[112,113,123,124], but knockout animals exhibited similar phenotypes in conditioned fear paradigms[113,116]. AMN082 has been shown to have task-dependent effects, where $mGlu_7$ activation facilitated between-session extinction, but not within-session extinction in a fear conditioning model[113,125]. AMN082 was also shown to have effects in social fear; it impaired extinction and recall when administered prior to the social fear extinction task, but not when given before social fear conditioning[126]. However, Ahnaou et al. demonstrated that AMN082 produced similar sleep-wake and hypothermia phenotypes in *Grm7*$^{-/-}$ and wild-type mice, suggesting that there may be off-target effects elicited by the compound[127]. Additionally, administration of

VU6005649, an $mGlu_{7/8}$ positive allosteric modulator (PAM), to wild-type mice, has been shown to increase freezing in contextual fear conditioning[128].

Seizures

Seizures are often present in patients with NDDs, and $mGlu_7$ and its interacting proteins have been implicated in seizure activity. Sansig et al. observed that *Grm7*$^{-/-}$ mice suffered from spontaneous sensory stimulus-seizures and were also more susceptible to subconvulsant doses of pentylenetetrazole (PTZ) and bicuculline than their heterozygous or wild-type littermates[68]. In addition, reduction of $mGlu_7$ activity with the NAM ADX71743 was sufficient to induce absence seizures[77]. Disruption of proteins that interact with $mGlu_7$ can also induce seizures in mice. For example, PICK1 is a PDZ-domain containing protein that interacts with the C-terminus of $mGlu_7$. As mentioned, interaction with PICK1 is important for stable $mGlu_7$ cell surface expression, proper trafficking of $mGlu_7$ to presynaptic active zones, and also for inhibition of P/Q-type calcium channels[81,86]. It has been reported that disruption of the interaction between PICK1 and $mGlu_7$ results in an absence-like seizure phenotype in mice[129,130].

Another $mGlu_7$-interacting protein implicated in seizures is ELFN1, a transmembrane protein that has been demonstrated to recruit $mGlu_7$ to distinct cell populations in the hippocampus and cortex[17]. Most recently, ELFN1 was also shown to be a trans-synaptic allosteric modulator of Group III mGlu receptors; receptor modulation occurs through an ELFN1-mediated alteration of G protein-coupling efficiency to the Group III mGlu receptors[91]. Of note, ELFN1 mutations clustered in the region required for $mGlu_7$ recruitment have been found in patients with epilepsy and ADHD[17,131], and ELFN1 knockout (*Elfn1*$^{-/-}$) animals exhibit a similar seizure phenotype as *Grm7*$^{-/-}$ animals[17]. Interestingly, *Elfn1*$^{-/-}$ mice also exhibit ADHD-like phenotypes such as hyperactivity and impulsivity. Dolan et al. showed that *Elfn1*$^{-/-}$ animals display hyperlocomotion and increased activity in an open field. However, administration of amphetamine to *Elfn1*$^{-/-}$ mice was able to attenuate hyperlocomotion, similar to the effects of stimulant therapies

for ADHD patients[131]. Tomioka et al. also demonstrated that *Elfn1*$^{-/-}$ mice displayed more spontaneous activity than wild-type animals and also exhibited decreased immobility in a forced swim test, which are behaviors suggestive of hyperactivity. *Elfn1*$^{-/-}$ mice spent more time in the open arms during an elevated plus maze (EPM) task compared to wild-type littermates. These data are typically indicative of anxiolytic effects; however, *Elfn1*$^{-/-}$ mice showed no preference between the light and dark boxes of the light-dark box transition task. Based on this finding, the authors hypothesized that the results of the EPM were indicative of impulsivity. Together, these data suggest a role for the ELFN1-mGlu$_7$ complex in seizures and in other disorders.

Mood Disorders

mGlu$_7$ modulation has also been demonstrated to impact behavioral models of mood disorders such as anxiety or depression, which are common comorbidities seen in NDDs[132]. The amygdala and hippocampus, areas of high mGlu$_7$ expression, are brain regions also known for their importance in anti-anxiety and anti-depressive action[133]. In comparison to cognitive tasks, where reductions in mGlu$_7$ cause deficits, the loss of mGlu$_7$ has been reported to result in anti-depressive and anxiolytic effects. For example, Cryan et al. showed that *Grm7*$^{-/-}$ animals spend more time in the open arms than their wild-type counterparts in an EPM paradigm, demonstrating that the loss of the receptor causes anxiolytic activity[134]. In a light-dark box task, *Grm7*$^{-/-}$ animals exhibited a reduced latency to enter a covered, dark compartment as well as an increased number of transitions into an open, brightly lit compartment than wild-type mice[134]. Callaerts-Vegh et al. demonstrated that *Grm7*$^{-/-}$ mice bury fewer marbles than wild-type animals in a marble burying task, which also measures anxiety-like behavior in rodents[118]. ADX71743, the mGlu$_7$-selective NAM, had similar effects in EPM, and reduced marble burying in wild-type mice[135]. Administration of the NAM MMPIP also reduced marble burying, consistent with the *Grm7*$^{-/-}$ phenotype[121]. In tail suspension or forced swim tasks, where immobility is indicative of depression-like behavior, *Grm7*$^{-/-}$ mice were less immobile than wild-type animals[134]. In wild-type mice, the antagonist

XAP044 increased time in open arms in EPM and decreased immobility in tail suspension, recapitulating data from studies using knockout animals[114]. In a mouse model of neuropathic pain, the NAM MMPIP also reduced immobility time during tail suspension[121]. The $mGlu_7$ agonist AMN082 reduced immobility in tail suspension and forced swim tasks, and MMPIP was able to block the effect of AMN082[136,137]. In summary, $mGlu_7$ has been implicated in a range of behaviors in rodent models, many of which mimic those reported in rodent models of NDDs.

$mGlu_7$ as a therapeutic target for Rett syndrome

Preclinical research in the NDD field has focused largely on mouse models of genetic syndromes due to their high construct validity. Rett syndrome (RTT) is a monogenetic disorder in which $mGlu_7$ has recently gained particular interest as a potential therapeutic target[138]. RTT is a debilitating NDD affecting 1 in 20,000 births and is characterized by a period of normal development followed by sudden developmental regression and loss of acquired skills at 6 to 18 months of age. Following regression, RTT patients are burdened by life-long symptoms that include repetitive hand clasping, limited speech, intellectual disability, motor impairment, apneas and epilepsy[139]. The majority of RTT cases can be attributed to loss-of-function mutations in the X-linked gene *MECP2*, which encodes the transcriptional regulator methyl-CpG binding protein 2 (MeCP2)[140]. Since this discovery, nearly two decades of research have yielded significant insight into the functions of MeCP2 within the brain. Of note, *MECP2* mutations have also been identified in patients with ASD and ID independent of a RTT diagnosis[141,142], suggesting that pathways involving MeCP2 may underlie NDDs more broadly. MeCP2 is canonically thought to repress gene transcription through binding to methylated CpG dinucleotides and recruiting repressor complexes; however, MeCP2 has also been shown to activate gene transcription and play roles in long-range regulation of chromatin structure, mRNA splicing and micro-RNA processing[143]. Although MeCP2 is involved in prenatal and postnatal development[144–146], phenotypes of *Mecp2* knockout mice can be reversed if *Mecp2* expression is reintroduced in adult animals[147].

Conversely, ablation of *Mecp2* expression in adult mice following normal development is sufficient to recapitulate the phenotype of constitutive *Mecp2* knockout mice[148]. MeCP2 is thus critical for proper neuronal function throughout life and there exists a therapeutic window to improve disease severity, even at adult stages. These proof-of-concept studies have fueled programs to develop *MECP2* replacement strategies, along with parallel efforts to identify targets downstream of MeCP2 dysfunction that may be amenable to pharmacological manipulation.

$mGlu_7$ is one of three metabotropic glutamate receptors found to be decreased at the mRNA level in a RTT mouse model[146]. These mGlu receptors represent a potential point of access to normalize synaptic function in RTT. Consistent with this initial report, we have shown that $mGlu_7$ protein expression is significantly decreased in motor cortex autopsy samples from RTT patients compared to those of controls matched for age, sex and postmortem interval[138]. In global *Mecp2* knockout mice, $mGlu_7$ protein expression was decreased in a brain-region specific manner with a notable reduction in hippocampal synaptosomal fractions. This correlated with reduced depression of synaptic transmission at SC-CA1 synapses by LSP4-2022 in slices from RTT model mice, which could be restored by a positive allosteric modulator (PAM). Additionally, pre-application of two structurally distinct Group III mGlu receptor PAMs, VU0422288 and VU0155094, to slices was able to restore deficient LTP at SC-CA1 synapses in RTT model mice. Ablation of *Mecp2* selectively from GABAergic neurons is sufficient for LTP impairment[149]; therefore, rescue of LTP by $mGlu_7$ potentiation is consistent with the proposed model by which $mGlu_7$-mediated inhibition of GABA release is required for LTP at SC-CA1 synapses[100].

At the behavioral level, $mGlu_7$ potentiation by intraperitoneal administration of the brain penetrant PAM, VU0422288, was able to improve performance in assays of cognition in RTT model mice[138]. While many studies in *Grm7*$^{-/-}$ mice have implicated a role for $mGlu_7$ in learning and memory[116,118,150], this is the first report of $mGlu_7$ activity being modulated in a positive direction to reverse a deficit in cognition. VU0422288 was also able to increase performance in a social novelty task and reduce the number of apneas detected by whole body plethysmography[138].

These data suggest that $mGlu_7$ potentiation may be a valid approach to address multiple RTT-associated symptom domains. It is important to note that these experiments used mice with a global deletion of *Mecp2*. As RTT is most commonly caused by *MECP2* point mutations in humans, it will be important to elucidate the effect of various point mutations on $mGlu_7$ expression/function to identify patient subpopulations that would be predicted to benefit from an $mGlu_7$ PAM.

Genetic associations between *GRM7* and NDDs

Genetic associations between NDDs and *GRM7*, the gene that encodes $mGlu_7$ in humans, provide a link between experiments in rodent models and the clinical population. ASD affects as much as 1% of the world's population[151], and family studies have suggested that the heritability of ASD is about 83%[152], which indicates a strong genetic component. Heterozygous deletions in *GRM7* have been identified in three ASD patients by Gai et al[153], and in one patient by Liu et al[154]. The latter patient exhibited language and cognitive impairments as well as hyperactivity, stereotyped behaviors, and deficits in social interaction. An additional ASD patient with a *de novo* point mutation in *GRM7*, resulting in a change from arginine to glutamate at amino acid 622, has also been reported[155]. This mutation affects the third transmembrane portion of the receptor. Two single nucleotide polymorphisms (SNPs) were reported to have significant association with ASD in a group of 22 patients[156]. These SNPs are rs6782011 and rs779867, which encode a C to T change in intron 6 and a T to C or T to G change in intron 5 in *GRM7*, respectively. In an Iranian cohort of 518 ASD patients, however, only rs779867 was identified as a SNP that associates *GRM7* with ASD[157]. rs779867 is a T to C or T to G polymorphism in intron 5 hypothesized to have effects on a mortality factor-related gene (MRG) protein binding motif. MRG motif-binding proteins are thought to bind chromatin and function in the regulation of gene transcription[158].

Attention deficit hyperactivity disorder (ADHD) is characterized by inattention, hyperactivity and impulsivity (DSM-V). Its estimated prevalence around the world is 7.2% in

children and 3.4% in adults[12,13]. A genome wide copy-number variation study revealed that rs7623055, which encodes a G to C or G to T change, was significantly associated with ADHD, and also identified 6 different heterozygous deletions in *GRM7* in patients with ADHD[19]. Additionally, rs37952452 was found to have an association with ADHD in a study of 202 patients in Korea, though it was not significantly associated when using a case-control approach[159]. In contrast, neither rs37952452 nor rs7623055 were found to be significantly associated with ADHD in a later study[160]. Interestingly, ADHD patients with the G/A genotype of rs37952452 showed an improved response to methylphenidate in comparison to those with the G/G genotype[161].

Rare mutations in *GRM7* have also been implicated in undiagnosed NDDs. Whole-exome sequencing in 31 consanguineous Arab families with developmental delay and/or intellectual disability revealed two families with mutations in *GRM7*. Two brothers in the same family were homozygous for a 461T/C variant, which results in the missense mutation I154T in the ligand binding domain of $mGlu_7$. The same study also identified two siblings (brother and sister) that are compound heterozygous for the mutations 1972C/T and 2024C/A, which lead to missense mutations, R658W and T675K, respectively, in the third transmembrane domain. These four patients share symptoms that include developmental delay, ID, brain malformations and seizures[31]. In a different set of consanguineous families, exome sequencing identified two female cousins with the homozygous mutation 1757G/A, which results in a premature truncation of $mGlu_7$ prior to its first transmembrane domain (W568*). These patients exhibit seizures, profound ID, microcephaly and leukodystrophy[32]. A search of the DECIPHER database[162] identified 69 patients with a deletion or duplication that included *GRM7,* although most of these also affected other genes. Three of these patients had a deletion or duplication restricted to the *GRM7* gene and their phenotypes are included in Table 1.

Table 1. Summary of *GRM7* variants identified in patients with NDDs as of May 2018.
Columns 3-4 refer to transcript NM_000844.3.

Mutation Type	Chromo-some 3 Position	Nucleotide/ Protein Change	Location in Transcript	Zygosity	Phenotype	Source
Duplication	6209671-6981117		5' UTR and Exon 1	Heterozygous	Behavioral abnormality, ID	DECIPHER 289768
Point mutation	6861849	c.461T>C p.I154T	Exon 1	Homozygous	Developmental delay, seizures, hypotonia, atrophy, thin corpus callosum	31
Deletion	6979874-7003319		Intron 1-2	Heterozygous	ADHD	19
Deletion	6980446-7001696		Intron 1-2	Heterozygous	ADHD	19
Deletion	7053179-7144453		Intron 1-2 and Exon 2	Heterozygous	ASD, ADHD	153,19
Deletion	70664629-7172715		Exon 2	Heterozygous	ASD	153
Deletion	7065422-7172715		Exon 2	Heterozygous	ASD	153
Deletion	7183953-7197236		Intron 2-3	Heterozygous	ADHD	19
Deletion	7257514-7442882		Exon 3-5	Heterozygous	Global developmental delay	DECIPHER 356330
Deletion	7221090-7524552		Exon 3-7	Heterozygous	ASD	154
Point mutation	7578663	c.1757 G>A p.W586*	Exon 8	Homozygous	Developmental delay, ID, microcephaly, seizures, leukodystrophy	32
Point mutation	7578771	c.1865 G>A p.R622Q	Exon 8	Heterozygous	ASD	155
Point mutation	7578878, 7578930	c.1972C>T p.R658W, c.2024C>A p.T675K	Exon 8	Compound Heterozygous	Developmental delay, ID, hypotonia, hypomyelination, brain atrophy, seziures	31
Duplication	7509664-7878406		Exon 8-10	Heterozygous	Intellectual disability, microcephaly	DECIPHER 288108

CHAPTER II. Evaluation of $mGlu_7$ as a therapeutic target in a mouse model of *MECP2* Duplication syndrome

Preface

The work in this chapter is reprinted with permission from reference 163. Copyright (2018) American Chemical Society. Sheryl Anne Vermudez performed the RT-PCR experiments in Figure 2A, Branden Stansley contributed partly to the electrophysiology data set in Figure 3, and Rocco Gogliotti performed the behavioral experiments in Figure 6. All other experiments were performed and analyzed by me.

Introduction

Loss-of-function mutations in the Methyl-CpG-Binding Protein 2 (*MECP2*) gene are present in 95% of patients with the neurodevelopmental disorder Rett syndrome (RTT)[140,164]. Conversely, duplication of the *MECP2* locus results in a syndrome characterized by infantile hypotonia, recurrent respiratory infections, limited speech, seizures, intellectual disability and autism-like behaviors[165,166]. While decades of research have yielded significant insights into the pathophysiology of RTT, our understanding of *MECP2* Duplication syndrome (MDS) remains limited. Recently, Sztainberg et al. reported that antisense oligonucleotide and/or genetic reduction of *MECP2* expression improves phenotypes in *MeCP2-Tg1* mice, a model of MDS[167], suggesting that symptoms of MDS may be reversible in patients. These data provide rationale to identify processes downstream of *MECP2* dysregulation that can be therapeutically targeted to restore proper neuronal function.

In support of this strategy, we previously identified the metabotropic glutamate receptor 7 ($mGlu_7$) as a potential therapeutic target in a clinical population as well as in a mouse model of RTT[138]. $mGlu_7$ is a G protein-coupled receptor expressed widely throughout the brain at glutamatergic and GABAergic presynaptic terminals[66,168]. $mGlu_7$ activation inhibits neurotransmitter release and plays important roles in synaptic plasticity in the hippocampus and

amygdala[74,79,100,112,114]. Additionally, a heterozygous *GRM7* mutation has been reported in a patient with idiopathic autism and homozygous mutations have been linked to severe neurological disease[31,32,154]. We have demonstrated that *GRM7* expression is activated by MeCP2 binding *in vitro* and that $mGlu_7$ protein expression is decreased in brain samples from RTT patient autopsies and model mice[138]. Furthermore, positive allosteric modulation of $mGlu_7$ activity restores long-term potentiation at Schaffer Collateral CA1 (SC-CA1) synapses in the hippocampus and improves cognition, social interaction and respiratory phenotypes in *Mecp2*$^{+/-}$ female mice[138].

From our findings in RTT model mice, we hypothesized that MeCP2 overexpression would drive increased $mGlu_7$ expression in *MeCP2-Tg1* mice. This hypothesis was consistent with previous literature reporting that *MeCP2-Tg1* mice display opposing hippocampal phenotypes when compared to RTT model mice. Specifically, slices from *MeCP2-Tg1* mice have been shown to display increased paired-pulse ratio and augmented long-term potentiation at SC-CA1 synapses[167,169]. Behaviorally, *MeCP2-Tg1* mice exhibit elevated contextual fear freezing at 20 weeks of age[169]. Another model of MDS, the *Tau-Mecp2* model, also exhibits elevated fear memory, suggesting that overexpression of Mecp2 in the CNS underlies this phenotype[170]. Given that positive modulation of $mGlu_7$ activity restores decreased LTP and contextual fear freezing in *Mecp2*$^{+/-}$ mice, we further hypothesized that genetic reduction or negative modulation of $mGlu_7$ activity would normalize hippocampal-dependent phenotypes in *MeCP2-Tg1* animals.

Here, we report that $mGlu_7$ protein expression is selectively upregulated in the hippocampus of *MeCP2-Tg1* mice, but this increase does not translate to a functional increase in $mGlu_7$ activity at SC-CA1 synapses. In contrast to our hypothesis, genetic reduction or negative modulation of $mGlu_7$ activity shows no efficacy in ameliorating exaggerated contextual fear learning or anxiety-like behavior in this mouse model of MDS.

Results

Analysis of $mGlu_7$ and MeCP2 expression in *MeCP2-Tg1* mice

To test the hypothesis that MeCP2 overexpression leads to increased $mGlu_7$ expression, we isolated cortex, hippocampus, and striatum samples from 20-week-old *MeCP2-Tg1* mice and wildtype (WT) littermates on a pure FVB/N background for mRNA and protein analysis. *Grm7* mRNA expression detected by quantitative real-time polymerase chain reaction (qRT-PCR) was unchanged in all brain regions examined (Figure 2A). Western blotting confirmed global MeCP2 overexpression by 2-3 fold in samples from *MeCP2-Tg1* mice (Figure 2C); however, elevated $mGlu_7$ protein expression was only detected in hippocampal tissue (Figure 2D).

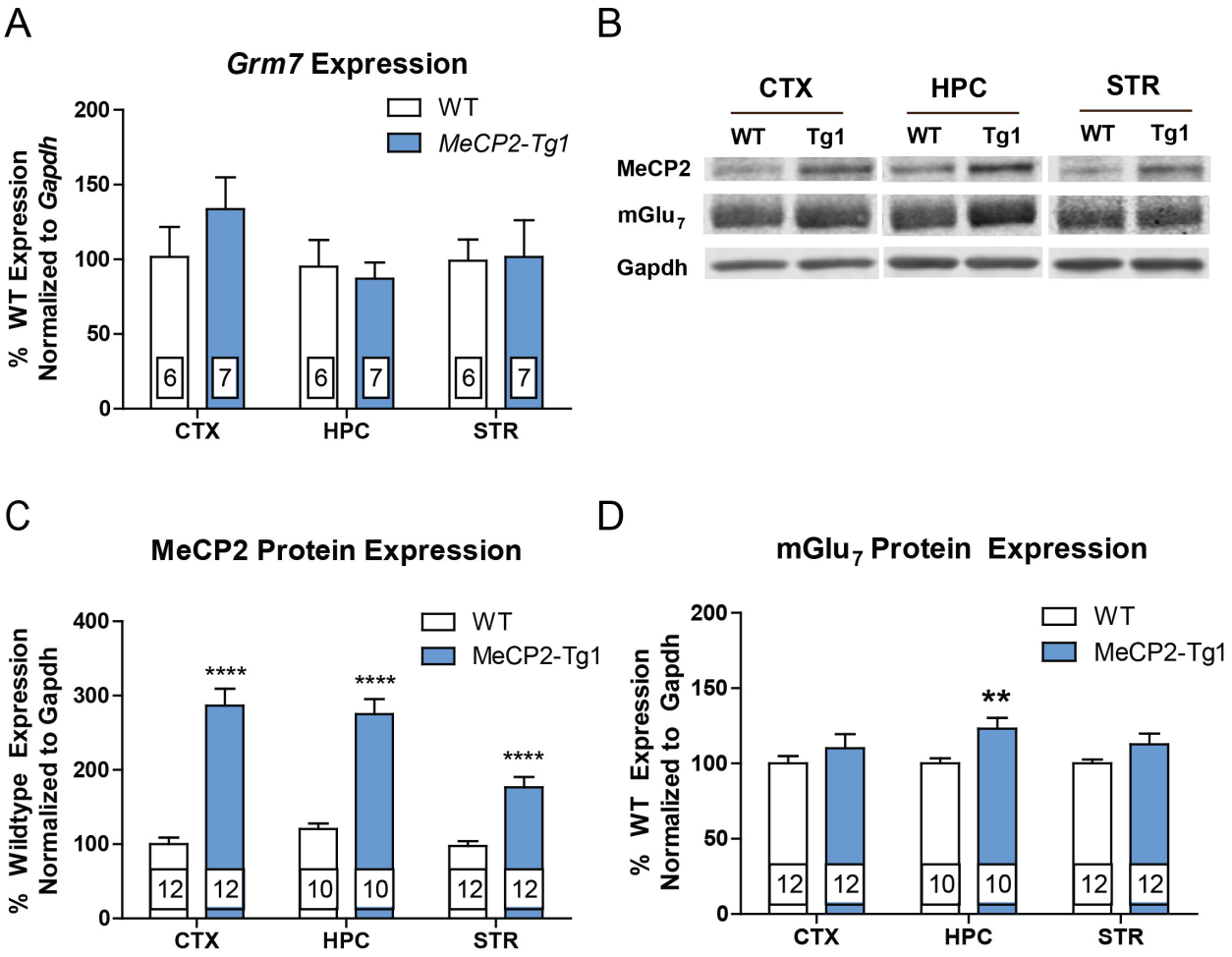

Figure 2. Total $mGlu_7$ protein expression is selectively increased in the hippocampus of MeCP2-Tg1 mice.

A) *Grm7* mRNA expression is not changed in samples from *MeCP2-Tg1* mice (N = 6-7 samples per genotype). B) Representative Western blots showing total $mGlu_7$ and MeCP2 protein expression. C) Quantification of MeCP2 expression from total protein isolates: Cortex (WT 100.1 ± 8.7% (N = 12) vs. *MeCP2-Tg1* 286.6 ± 22.5% (N = 12), ****p < 0.0001) Hippocampus (WT 110 ± 6.2% (N = 10) vs. *MeCP2-Tg1* 232.3 ± 17.6% (N = 10), ****p < 0.0001) Striatum (WT 97.5 ± 6.7% (N = 12) vs. 176.6 ± 13.8% (N = 12), ****p < 0.0001), Student's t-tests for each region. D) Quantification of $mGlu_7$ expression from total protein isolates: Cortex (WT 100 ± 4.8% (N = 12) vs. MeCP2-Tg1 110.2 ± 9.2% (N = 12)), Hippocampus (WT 100.0 ± 3.5% (N = 10) vs. 123.0 ± 7.2% (N = 10), *p < 0.05), Striatum (WT 100 ± 2.5% (N = 12) vs. MeCP2-Tg1 112.7 ± 7.1% (N = 12)), Student's t-tests for each region.

$mGlu_7$ function is unchanged at SC-CA1 synapses in *MeCP2-Tg1* mice

To characterize the functional effects of elevated $mGlu_7$ protein expression within the hippocampus, we performed *ex vivo* brain slice electrophysiology at SC-CA1 synapses. Similar to previous reports[167,169], slices from 20-week-old *MeCP2-Tg1* mice displayed unchanged input-output curves (Figure 3A); however, decreased input-output slope has been reported in younger mice[171]. Increased paired-pulse ratio was also observed (Figure 3B), which often corresponds with a decrease in presynaptic glutamate release. Since $mGlu_7$ is a presynaptic regulator of neurotransmitter release, this result was consistent with increased $mGlu_7$ protein expression observed in total protein extracted from hippocampal tissue (Figure 2D) and directly opposed our findings in *Mecp2*$^{-/y}$ and *Mecp2*$^{+/-}$ animals[138].

To test whether $mGlu_7$ receptor activity was increased, we recorded field excitatory postsynaptic potentials (fEPSPs) at SC-CA1 and bath applied the Group III mGlu receptor agonist, LSP4-2022. Application of 100 μM LSP4-2022 depressed synaptic transmission in WT and *MeCP2-Tg1* slices, with no difference in the maximal depression of fEPSP slope (Figure 3C-D). While LSP4-2022 also activates $mGlu_4$ and $mGlu_8$, $mGlu_7$ is believed to be the only presynaptic mGlu receptor at SC-CA1 synapses, making this an ideal synapse to probe $mGlu_7$ function[104,105]. Since an increase in total $mGlu_7$ protein expression did not translate to an increase in $mGlu_7$ activity in this functional readout, we next tested whether $mGlu_7$ expression was increased in synaptosome fractions. In contrast to the total protein Western blots, we did not observe a significant increase in $mGlu_7$ expression in synaptosome fractions (Figure 3E-F). Taken together, these data suggest that increased cellular $mGlu_7$ does not necessarily lead to increased receptor surface expression and activity at this synapse.

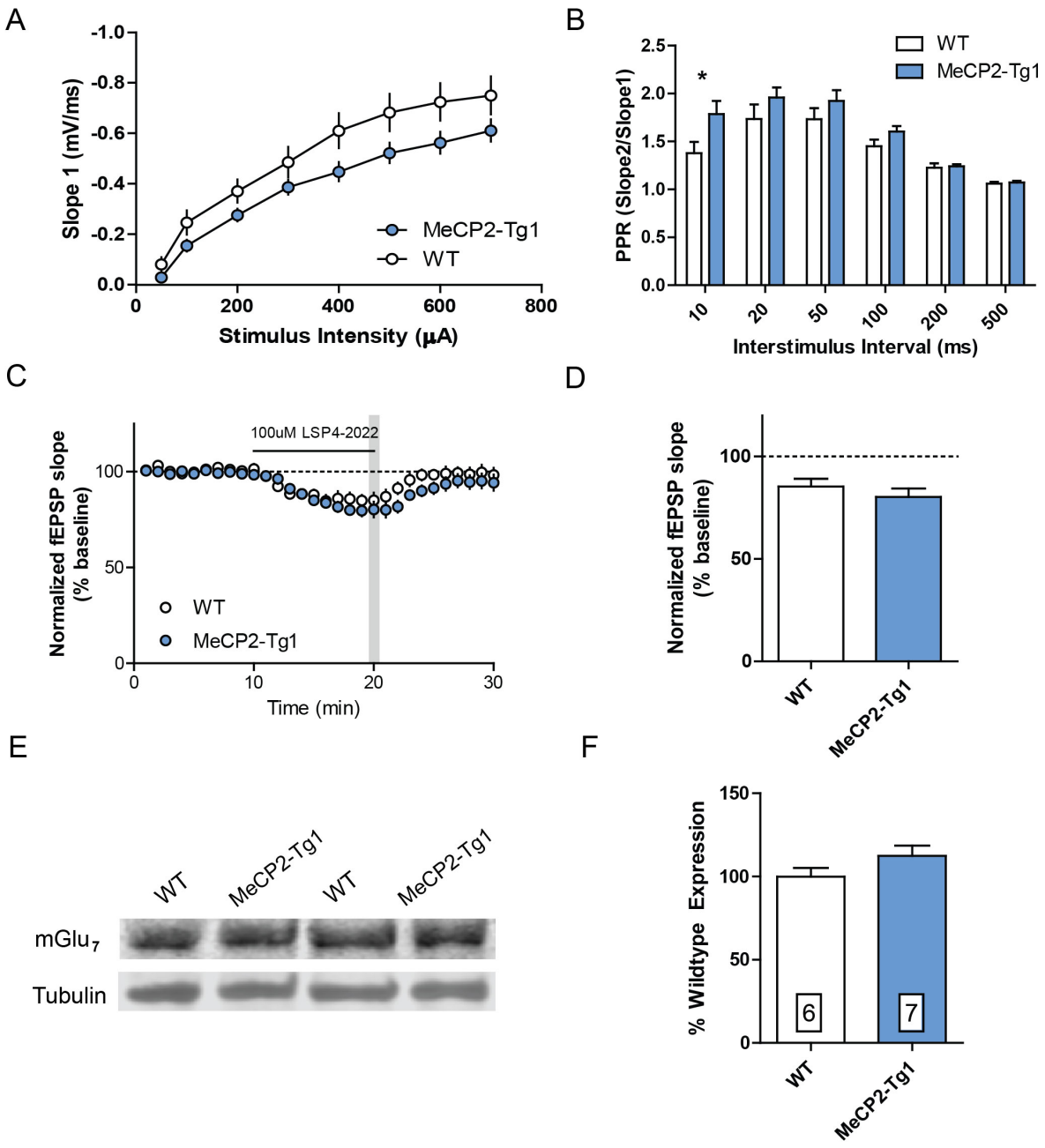

Figure 3. $mGlu_7$ function is not affected by MECP2 duplication at SC-CA1 synapses in mice.

A) Input-output curves were not significantly different between slices derived from 20-week-old WT and *MeCP2-Tg1* mice (N = 8 slices / 5-6 mice). Two-way ANOVA. B) Paired pulse ratios were significantly increased at a 10ms interstimulus interval in *MeCP2-Tg1* slices (N = 7 slices/ 7 mice, *p < 0.05). Two-way ANOVA with Bonferroni post hoc comparisons. (C-D) Depression by 100 µM LSP4-2022 at minute 20 (gray bar) was not significantly different between genotypes. WT 85.4 ± 3.8 (N = 8 slices, 5 mice) vs. *MeCP2-Tg1* 80.2 ± 4.1 (N = 8 slices, 6 mice), Student's t test. E) Representative $mGlu_7$ Western blots from synaptosomal protein isolates. F) Quantification of $mGlu_7$ protein expression was not significantly different between genotypes. WT 100 ± 5.2% (N = 6 mice) vs *MeCP2-Tg1* 112.4 ± 6.2% (N = 7 mice). Student's t-test.

LTP at SC-CA1 synapses is unchanged in *MeCP2-Tg1* mice

In contrast to *Mecp2*$^{+/-}$ mice, 20-week-old *MeCP2-Tg1* mice have been reported to display increased LTP at SC-CA1 when compared to littermate controls[167,169]. We have previously demonstrated that activation of $mGlu_7$ on GABAergic interneurons is required for the induction of LTP at this synapse; $mGlu_7$ activation decreases GABA release and leads to the disinhibition of excitatory neurons[100]. We therefore hypothesized that negative modulation of $mGlu_7$ activity might normalize LTP in *MeCP2-Tg1* slices despite the lack of increase in receptor function. We induced LTP with high frequency stimulation (two 1s trains at 100Hz, 20s interstimulus interval) and monitored fEPSPs for 60 minutes; however, contrary to previous reports[167,169], we observed no change in LTP between WT and *MeCP2-Tg1* slices (Figure 4A-B).

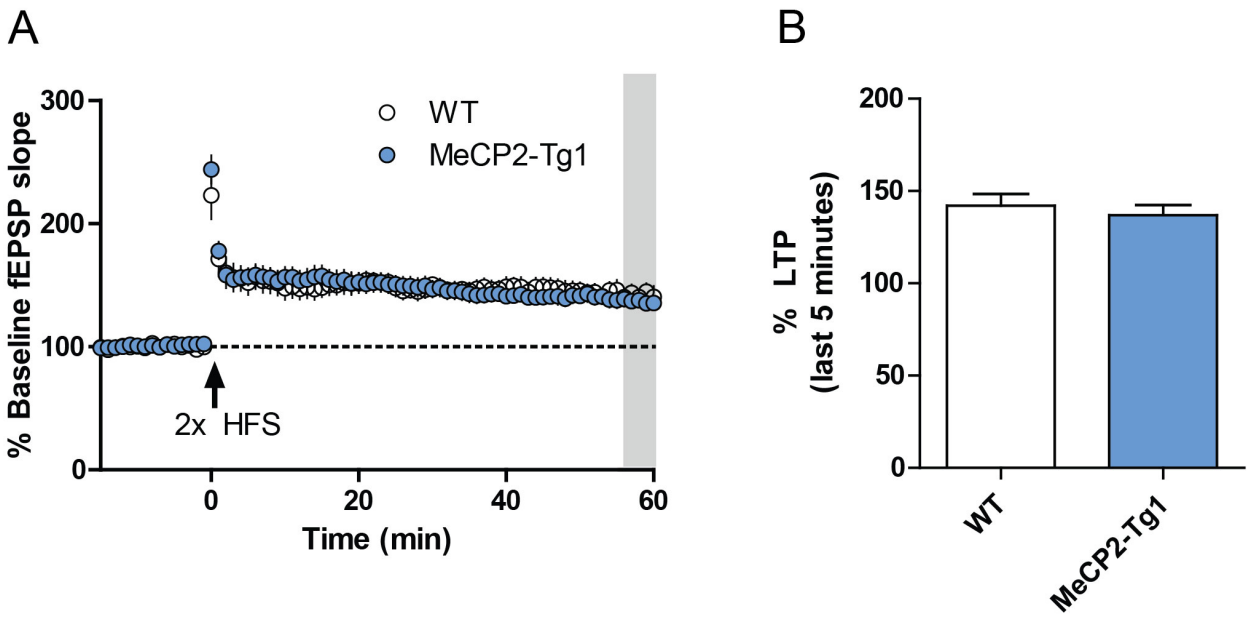

Figure 4. LTP induced by HFS is unchanged at the SC-CA1 synapses in slices from 20-week-old MeCP2-Tg1 mice.
A) After a 15-minute baseline recording, LTP was induced by 2 trains of HFS and fEPSPs were monitored for 60 minutes. B) Quantification of percent LTP during the last 5 minutes of recording (gray bar). WT 142.1 ± 6.4 (N = 8 slices/9 mice) vs. *MeCP2-Tg1* 137.0 ± 5.4 (N = 13 slices, 9 mice), Student's t-test.

Genetic reduction of $mGlu_7$ expression does not impact anxiety-like behavior or contextual fear learning in *MeCP2-Tg1* mice

MeCP2-Tg1 mice exhibit increased anxiety-like behavior and increased contextual fear learning[169,172], which are phenotypes opposite to those observed in *Grm7*$^{-/-}$ mice and *Mecp2*$^{+/-}$ mice[113,115]. We previously demonstrated that increasing $mGlu_7$ activity with the positive allosteric modulator (PAM) VU0422288 normalized anxiolytic behavior and fear learning in *Mecp2*$^{+/-}$ mice. We therefore hypothesized that either a genetic or pharmacological reduction of $mGlu_7$ function might normalize behavior in *MeCP2-Tg1* mice in a similar manner. We crossed female *MeCP2-Tg1* mice (FVB/N) with male *Grm7*$^{+/-}$ mice (C57BL/6J) to genetically reduce $mGlu_7$ expression in the context of MeCP2 overexpression and studied the F1 offspring. We first confirmed that $mGlu_7$ protein levels were significantly reduced in total protein and synaptosomal isolates from these animals (Figure 5A-B). We next performed the elevated plus maze to examine anxiety-like behavior and contextual fear conditioning as a measure of hippocampal-dependent memory. Genetic reduction of $mGlu_7$ expression did not mitigate increased anxiety-like behavior in *MeCP2-Tg1* mice as measured by time spent in the open arms of an elevated plus maze (Figure 5C). Furthermore, independent of *Grm7* genotype, mice with the *MECP2* transgene displayed heightened freezing when re-exposed to the conditioning context 24 hours post training along with delayed extinction learning when re-exposed to the conditioning context for 7 subsequent days (Figure 5D).

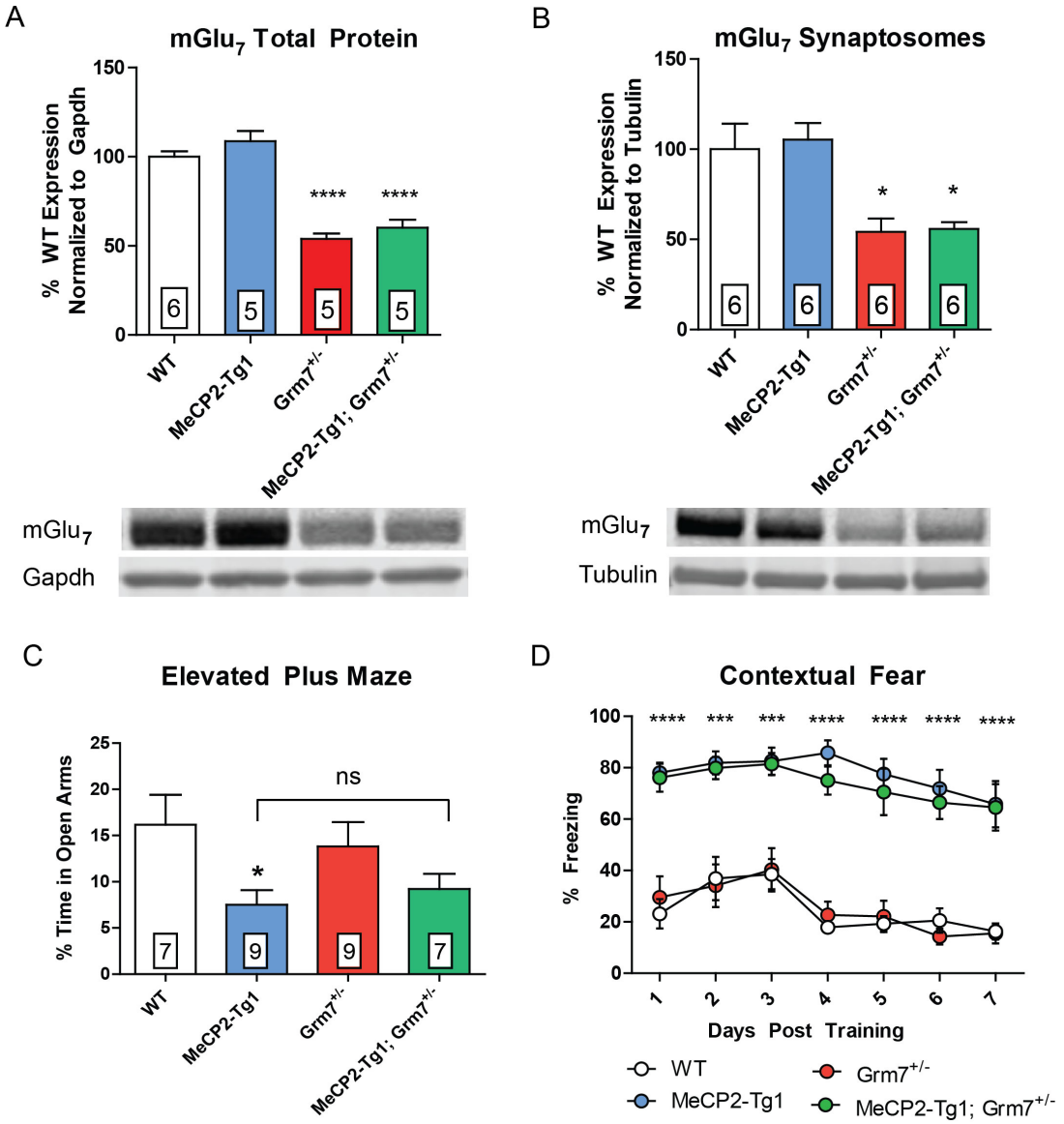

Figure 5. Genetic reduction of $mGlu_7$ does not affect anxiety or fear behavior in MeCP2-Tg1 mice.

A) $mGlu_7$ expression in total protein isolates from hippocampal tissue in *MeCP2-Tg1* mice compared relative to WT (WT 100.0 ± 3.1%, *MeCP2-Tg1* 108.6 ± 5.8%, *Grm7*$^{+/-}$ 54.0 ± 3.0%, *MeCP2-Tg1; Grm7*$^{+/-}$ 60.2 ± 4.5%, N = 5-6 mice per genotype, ****p < 0.0001, one-way ANOVA, Bonferroni comparisons relative to WT). B) $mGlu_7$ expression from synaptosomal isolates from hippocampal tissue (WT 100.0 ± 14.1, *MeCP2-Tg1* 105.3 ± 9.3, *Grm7*$^{+/-}$ 54.2 ± 7.3, *MeCP2-Tg1; Grm7*$^{+/-}$ 55.8 ± 3.7, N = 6 mice per genotype, *p < 0.05, one-way ANOVA, Bonferroni comparisons relative to WT). C) *MeCP2-Tg1* mice spend less time in the open arms of an elevated plus maze relative to WT mice, regardless of *Grm7* genotype (N = 7-9 mice per genotype, *p < 0.05, one-way ANOVA, Bonferroni comparisons). D) *MeCP2-Tg1* mice exhibit increased contextual fear freezing compared to those that do not, regardless of *Grm7* genotype (N = 7-10 mice per genotype, ***p < 0.001, ****p < 0.0001, two-way ANOVA, Bonferroni comparisons to WT).

Negative allosteric modulation of $mGlu_7$ activity does not affect anxiety-like behavior or contextual fear learning in *MeCP2-Tg1* mice.

As genetic reduction of $mGlu_7$ could have evoked developmental compensatory mechanisms, we next sought to confirm that acute negative modulation of $mGlu_7$ signaling pharmacologically had no effect on phenotypes in adult *MeCP2-Tg1* mice. To assess anxiety phenotypes, WT and *MeCP2-Tg1* mice were pre-treated with either vehicle or the $mGlu_7$ NAM ADX71743[135] and tested in the elevated plus maze assay. Similar to genetic reduction of $mGlu_7$, administration of ADX71743 had no effect on anxiety phenotypes in WT and *MeCP2-Tg1* mice (Figure 6A). To determine whether $mGlu_7$ negative modulation had any effect on learning and memory phenotypes, WT and *MeCP2-Tg1* mice were pretreated with a single dose of ADX71743 prior to fear conditioning and tested for contextual fear memory 24 hours later. Relative to vehicle-treated controls, *MeCP2-Tg1* mice treated with vehicle exhibited a significant increase in freezing when re-exposed to the context, and ADX71743 administration had no effect on freezing in *MeCP2-Tg1* mice (Figure 6B). Conversely, WT mice treated with ADX71743 exhibited significantly increased freezing relative to vehicle-treated controls and failed to extinguish the fear memory in a manner similar to *MeCP2-Tg1* mice (Figure 6C-D).

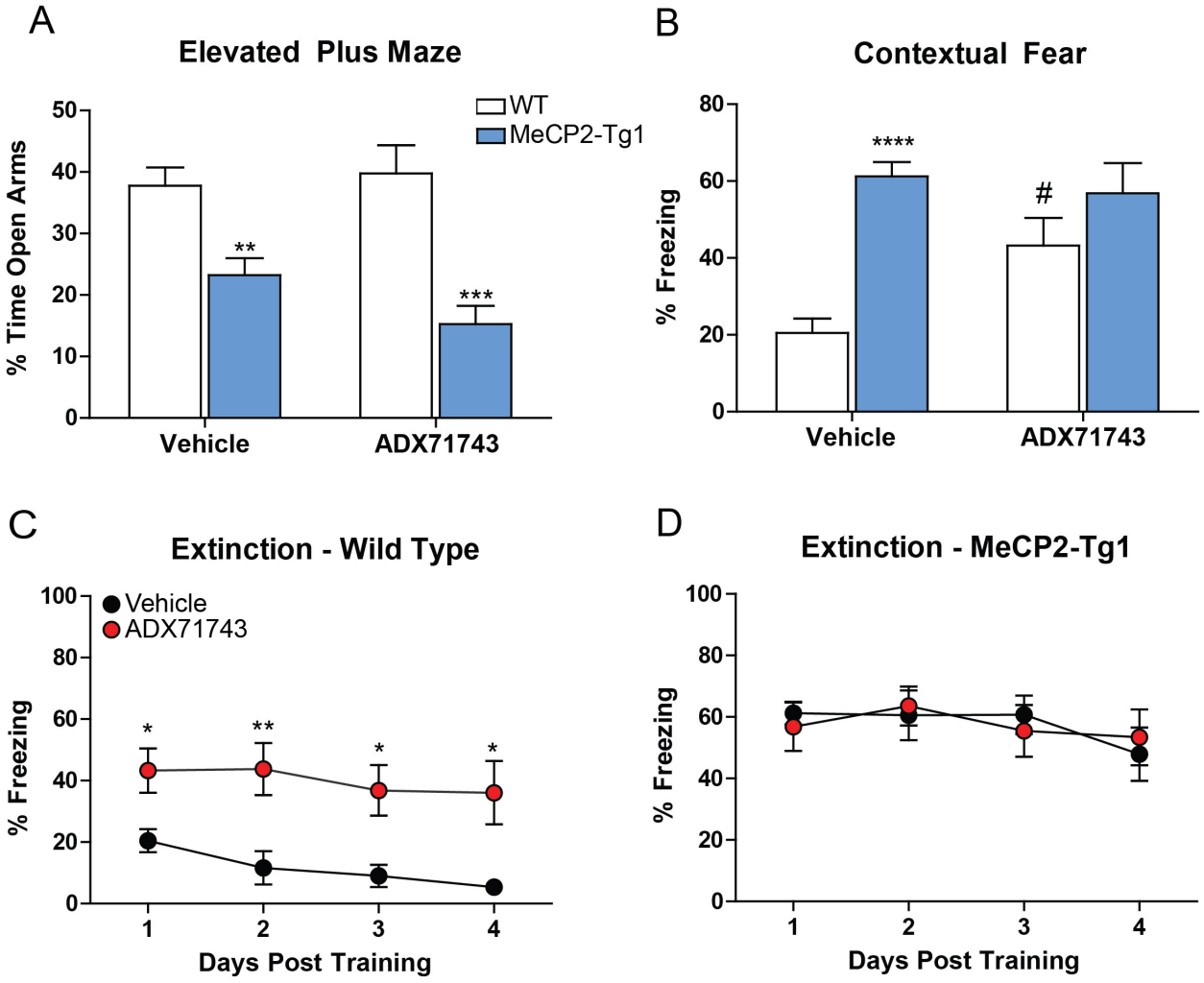

Figure 6. mGlu$_7$ negative allosteric modulation does not affect anxiety or fear behavior in MeCP2-Tg1 mice.

A) Vehicle-treated *MeCP2-Tg1* mice spent significantly less time in the open arms of the elevated plus maze relative to WT controls (WT: 37.8 ± 3.0% (N = 16) vs. *MeCP2-Tg1*: 23.2 ± 2.8% (N = 18), **p < 0.01), and ADX71743 (60 mg/kg) administration had no effect on this phenotype (WT: 39.8 ± 4.6% (N = 9) vs. *MeCP2-Tg1*: 15.3 ± 3.0%, (N = 7) ***p < 0.001). Two-way ANOVA with Bonferroni post hoc analysis. B) Relative to WT mice, *MeCP2-Tg1* mice treated with vehicle exhibited an enhanced contextual fear freezing response (WT: 20.5 ± 3.7% (N = 22) vs. *MeCP2-Tg1*: 61.2 ± 3.7% (N = 17), ****p < 0.0001). ADX71743 pretreatment had no effect in *MeCP2-Tg1* mice relative to the vehicle-treated mice of the same genotype (MeCP2-Tg1: 56.8 ± 7.9% (N = 11)); however, treatment with ADX71743 resulted in a significant increase in freezing in WT mice (WT: 43.3 ± 7.2% (N = 12), $^{\#}$p < 0.05, # denotes within genotype comparison. Two-way ANOVA with student's t-test post analysis). C-D) Wild-type mice treated with ADX71743 during training demonstrated a significantly attenuated ability to extinguish fear memory relative to vehicle-treated controls (*p < 0.05, **p < 0.01). ADX71743 administration had no effect on extinction in *MeCP2-Tg1* mice. Two-way ANOVA with Bonferroni post hoc analysis.

Discussion

To complement our $mGlu_7$ studies in RTT model mice, the experiments here aimed to evaluate the therapeutic potential of $mGlu_7$ receptor negative modulation in a mouse model of MDS. We previously reported that MeCP2 binding to the *GRM7* promoter activates gene transcription *in vitro*. In the brains of *Mecp2*$^{+/-}$ and *Mecp2*$^{-/y}$ model mice, $mGlu_7$ mRNA and protein expression were decreased in a brain-region specific manner[138]. Here, we tested the hypothesis that overexpression of MeCP2 *in vivo* would drive increased *GRM7* and $mGlu_7$ expression. Interestingly, the only significant change observed in samples from *MeCP2-Tg1* mice was an increased in total cellular $mGlu_7$ in the hippocampus. These findings suggest that the relationship between MeCP2 dysregulation and $mGlu_7$ expression may be more complex than initially appreciated and dependent on the brain region examined. It is possible that basal expression of $mGlu_7$ is maintained at, or near, maximal levels or that another process independent of MeCP2 is rate-limiting, such that MeCP2 overexpression no longer has an effect on $mGlu_7$ protein levels in some brain regions. Further studies will be needed to fully elucidate the molecular link between MeCP2, *GRM7* mRNA, and $mGlu_7$ protein expression.

Independent of receptor expression, we hypothesized that $mGlu_7$ genetic reduction or negative modulation could be an effective approach to reduce symptoms in *MeCP2-Tg1* mice due to the established role of $mGlu_7$ activation in LTP induction at SC-CA1 synapses[100]. However, despite extensive efforts, we were unable to replicate previous reports that LTP is augmented in slices from *MeCP2-Tg1* animals[167,169]. This could be due to differences in strain, age, genetic drift or technical/experimental differences. Interestingly, *Tau-Mecp2* mice exhibit decreased HFS-induced LTP at SC-CA1 despite exaggerated fear learning[170]. Together, these seemingly discordant results highlight that the effect of MeCP2 overexpression on LTP at SC-CA1 synapses appears to be complex and that, at least for this form of LTP, may not correlate with anxiety or fear memory phenotypes in mouse models of MeCP2 overexpression. In our experiments, one single administration of ADX71743 was given prior to fear conditioning to mimic our previous

experiments in RTT model mice; however, if the primary deficit in *MeCP2-Tg1* mice is memory extinction as opposed to acquisition, we do not exclude the possibility that compound administration on test days may be efficacious.

In summary, we tested the hypothesis that $mGlu_7$ expression is reciprocally regulated by MeCP2 such that negative modulation of $mGlu_7$ would be efficacious in a mouse model of *MDS*. However, $mGlu_7$ expression was increased only in the hippocampus of *MeCP2-Tg1* mice, and behavioral phenotypes were found to be insensitive to changes in $mGlu_7$ expression/activity. Interestingly, Lu et al. recently reported that mouse models of RTT and MDS share similar hippocampal circuit abnormalities including hypersynchronous firing[173]. Our findings further support the idea that mouse models of MDS are not simply anti-parallel to RTT models, but instead exhibit a unique pathophysiology that warrants further study.

Methods

Chemicals

ADX71743 and LSP4-2022 were synthesized in-house as described in 100. For *in vivo* experiments, ADX71743 was formulated using 10% Tween 20 as vehicle.

Animals

All animals used in the present study were group housed with food and water given *ad libitum* and maintained on a 12-hour light/dark cycle. Animals were cared for in accordance with the National Institutes of Health *Guide for the Care and Use of Laboratory Animals*. All studies were approved by the Institutional Animal Care and Use Committee for Vanderbilt University School of Medicine and took place during the light phase. *MeCP2-Tg1* breeders were obtained from The Jackson Laboratory (FVB-Tg(MECP2)1Hzo/J, stock no. 008679). Male mice were aged until 20-25 weeks of age for all experiments. *Grm7* knockout mice were cryorecovered from the

Mutant Mouse Regional Resource Center (B6.129P2-Grm7^{Tm1Dgen}/Mmnc) and maintained under identical conditions.

Quantitative Real-time PCR (QRT-PCR)

Cortex, hippocampus and striatum were microdissected from 20-week-old *MeCP2-Tg1* mice and WT littermates. Total RNA was prepared from tissue samples using TRIzol Reagent® (Invitrogen) in accordance with manufacturer's instructions. Total RNA from each brain region was DNase-treated with Roche Turbo^{TM} DNase kit, and cDNA from 2 µg total RNA was synthesized using the VILO^{TM} kit (Invitrogen). RT-qPCR on cDNA from 25 ng of initial RNA template was then run in triplicate using Taqman Fast® Reagent Mix (Life Technologies) and Life Technologies gene expression assays for *Grm7* (Mm0118924_m1), and *Gapdh* (Mm03302249_g1). C_t values for each sample were normalized to *Gapdh* expression and analyzed using the delta-delta C_t method as described in Gogliotti *et al.* 2016[174]. Values exceeding two times the standard deviation were classified as outliers. Each value was compared to the average delta-C_t value acquired for wild-type mice and calculated as percent-relative to the average control delta-C_t.

Total and Synaptosomal Protein Preparation

For total protein isolation, tissue samples from 20-week-old *MeCP2-Tg1* mice and WT littermates were homogenized using a hand-held motorized mortar and pestle in radioimmunoprecipitation assay buffer (RIPA) containing 10 mM Tris-HCL, 150 mM NaCl, 1 mM ethylenediaminetetraacetic acid (EDTA), 0.1% sodium dodecyl sulfate (SDS), 1% Triton^{TM} X-100, and 1% Deoxycholate. After homogenization, samples were spun for 20 minutes at 15,000 x g at 4 ºC. The supernatant was then transferred to new tubes and the protein concentration was determined using a bicinchoninic acid (BCA) protein assay (Pierce^{TM}). For synaptosome preparations, tissue was homogenized in 9 ml of ice-cold sucrose/HEPES (0.32 M sucrose, 4.2 mM HEPES, pH 7.4) using a Teflon-glass homogenizer (Wheaton Science Products). The

homogenate was centrifuged at 1,000 x g for 5 minutes at 4 °C and the resultant supernatant was centrifuged at 12,000 x g for 15 minutes at 4°C. The final pellets containing synaptosomes were re-suspended in RIPA buffer and protein concentration was determined by BCA assay.

SDS-Page and Western Blotting

Proteins (50 µg) were electrophoretically separated using a 4-20% SDS polyacrylamide gel and then transferred onto a nitrocellulose membrane (Bio-Rad). Membranes were blocked with Odyssey blocking buffer (LiCor) for one hour at room temperature. Membranes were probed with the following primary antibodies: rabbit anti-MeCP2 (1:1000, Millipore 07-013), rabbit anti-$mGlu_7$ antibody (1:1000, Millipore 07-239), mouse anti-Gapdh antibody (1:5000, ThermoFisher MA5-15738), and mouse anti-Tubulin antibody (1:500, Abcam ab44928) overnight at 4 °C. Membranes were washed three times with Tris-buffered Saline and Tween 20 (TBS-T, 25 mM Tris, 150 mM NaCl, 0.05% Tween 20) and then incubated with either a goat anti-rabbit-fluorescent secondary antibody (800, 1:5000, LiCor) or a goat anti-mouse fluorescent secondary antibody (680, 1:5000, LiCor). Fluorescence was then quantified using Image Studio Light software. Each value for MeCP2 and $mGlu_7$ protein expression was first normalized to the value calculated for Gapdh expression (total protein blots) or tubulin expression (synaptosome blots).

Extracellular Field Potential Recordings

Coronal brain slices were prepared from 20-week-old *MeCP2-Tg1* mice and WT littermates. Mice were anesthetized with isoflurane and decapitated. Brains were rapidly removed and submerged in ice-cold sucrose cutting buffer containing: 230 mM sucrose, 2.5 mM KCl, 8 mM $MgSO_4$, 0.5 mM $CaCl_2$, 1.25 mM NaH_2PO_4, 10 mM glucose, and 26 mM $NaHCO_3$ saturated with 95%/5% O_2/CO_2. A block of tissue containing hippocampus was trimmed, embedded in agarose, and coronal slices 400 µm thick were cut using a Compresstome™ VF-200 (Precisionary Instruments). Slices were transferred to a holding chamber containing N-methyl-D-glucamine (NMDG)-HEPES recovery solution (in mM, 93 NMDG, 2.5 KCl, 1.2 NaH_2PO_4, 30 $NaHCO_3$, 20

HEPES, 25 D-glucose, 5 sodium ascorbate, 2 thiourea, 3 sodium pyruvate, 10 $MgSO_4$, 0.5 $CaCl_2$, pH 7.3, 305 mOsm) for 15 minutes at 32 ºC. Slices were then transferred to a room temperature modified artificial cerebral spinal fluid (ACSF) containing (in mM) 126 NaCl, 1.25 NaH_2PO_4, 2.5 KCl, 10 D-glucose, 26 $NaHCO_3$, 2 $CaCl_2$ and 1 $MgSO_4$, and 600 µM sodium ascorbate for at least 1 hour. Subsequently, slices were transferred to a submersion recording chamber and continuously perfused (2 mL/min) with ACSF containing (in mM): 126 NaCl, 1.25 NaH_2PO_4, 2.5 KCl, 10 D-glucose, 26 $NaHCO_3$, 2 $CaCl_2$, 1 $MgSO_4$ heated to 32 °C. All solutions were continuously bubbled with 95%/5% O_2/CO_2.

A concentric bi-polar stimulating electrode was positioned near the CA3-CA1 border and paired-pulse field excitatory postsynaptic potentials (fEPSPs) were evoked (100 µs duration, every 20 sec) by placing a glass recording electrode in the stratum radiatum of CA1. Input-output curves were generated for each slice and the stimulation intensity was adjusted to 50% of the maximum response for subsequent experiments. Paired-pulse ratios (PPR) were calculated as the ratio between the slope of the second fEPSP divided by the slope of the first fEPSP. PPRs were calculated at several inter-stimulus intervals (ISI) ranging from 10-500 ms.

For LSP4-2022 and LTP experiments, slopes of three consecutive sweeps were averaged and normalized to the average slope during the baseline period. Data were digitized using a Multiclamp 700B, Digidata 1322A, and pClamp 10 software (Molecular Devices). For LSP4-2022 experiments, paired-pulse fEPSPs were generated with a 20 ms ISI at 0.05 Hz. After 10 minutes of stable baseline recordings, 100 µM LSP4-2022 was applied for 10 minutes followed by a 10-minute washout period. Long term potentiation (LTP) was induced by applying two trains of 100 Hz stimulation (HFS, 1 sec duration, 20 sec inter-train interval (ITI)) after a 15 minute baseline. fEPSPs were monitored for 60 minutes after HFS and percent LTP was quantified as the normalized slope during the last 5 minutes of recording.

Elevated Plus Maze

20-week-old *MeCP2-Tg1* mice and WT littermates were habituated to the testing room for 1 hour prior to the elevated plus maze test. Mice were placed on the elevated plus maze and allowed to explore freely for 5 minutes. Time spent exploring each arm was measured using AnyMaze tracking software. For ADX71743 experiments, mice were dosed intraperitoneally (i.p., 10 mL/kg) with 60 mg/kg ADX71743 or vehicle (10% Tween 80) 15 minutes prior to being placed in the maze.

Fear Conditioning

20-week-old *MeCP2-Tg1* mice and WT littermates were habituated to the testing room for 2 hrs on the day prior to training and the morning of training. On training day, mice were injected i.p. 15 minutes prior to conditioning with either vehicle (10% Tween 80) or 60 mg/kg ADX71743. Mice were then placed into an operant chamber with a shock grid (Med Associates Inc.) in the presence of a 10% vanilla odor cue. Following a 3-minute habituation period, mice were exposed to two 1 second, 0.7 mA foot shocks spaced 30 seconds apart. For experiments using the offspring of *MeCP2-Tg1* and *Grm7*$^{+/-}$ mice, only one shock was administered due to higher freezing observed in mice of that genetic background. Mice remained in the context for an additional 30 seconds after the second foot shock. Mice were placed back into the same shock chamber with a 10% vanilla odor cue and the percent of time spent freezing during a 3-minute testing period was assessed for up to 7 days after conditioning.

CHAPTER III. Characterization of *Grm7* knockout mice for behaviors relevant to NDDs

Preface

Work in this chapter is published in *Genes, Brain and Behavior.*[175] Electroencephalography (EEG) data acquisition and analysis was performed by myself, Robert Gould, Annalise McDonald, Hana Badivuku, Susmita Chennareddy and Hudson Robb. Annalise McDonald also performed the Western blot in Figure 11. Annah Moore was the second experimenter for the grip strength test, and Matt Jenkins blindly scored limb clapsing videos. All other behavioral and electrophysiology experiments were performed and analyzed by me. Aditi Buch assisted with some behavioral experiments and mouse colony maintenance.

Introduction

Glutamate, the main excitatory neurotransmitter in the brain, acts by binding to ionotropic and metabotropic receptors expressed at synapses. The metabotropic glutamate receptors (*GRM*, mGlu receptors) are a class of G protein-coupled receptors (GPCRs) that modulate synaptic transmission and play important roles in both short- and long-term plasticity. The mGlu receptors are divided into three groups based on their sequence homology, G protein coupling, and cellular localization: group I includes $mGlu_1$ and $mGlu_5$, group II includes $mGlu_2$ and $mGlu_3$, and group III includes $mGlu_4$, $mGlu_6$, $mGlu_7$ and $mGlu_8$[47]. Among the mGlu receptors, $mGlu_7$ is the most evolutionarily conserved and exhibits widespread expression across the mammalian brain[61]. $mGlu_7$ is expressed pre-synaptically on glutamatergic and GABAergic neurons and acts to inhibit neurotransmitter release both constitutively and in an activity-dependent manner[74,78,99].

Emerging clinical evidence has associated the *GRM7* locus with neurodevelopmental disorders. For example, homozygous point mutations in *GRM7* have been reported in several patients with severe neurological diseases that are characterized by developmental delay and epilepsy[31,32], while heterozygous mutations or deletions have been identified in patients with

autism spectrum disorder (ASD)[153–155] and attention deficit hyperactivity disorder (ADHD)[19]. Additionally, single-nucleotide polymorphisms have been associated with increased risk for ASD, ADHD, and schizophrenia[156,159,176,177].

We recently reported that $mGlu_7$ protein expression was significantly reduced in autopsy samples from patients with Rett syndrome (RTT)[138], suggesting that altered $mGlu_7$ expression can be a feature of monogenetic disorders in which the causative gene is not *GRM7*. In a mouse model of RTT, we found that potentiation of $mGlu_7$ activity with an allosteric modulator improved disease phenotypes[138]. This demonstrates that $mGlu_7$ could be a feasible target for therapeutic intervention; however, these previous studies relied on a combination of non-selective compounds since a truly selective activator or positive allosteric modulator for $mGlu_7$ is not yet available. Therefore, more work is needed to validate $mGlu_7$ as a therapeutic target in RTT and to evaluate whether $mGlu_7$ potentiation can also provide benefit in other models of neurodevelopmental disorders.

$mGlu_7$ activity contributes to many behaviors in rodents that are implicated in neurodevelopmental disorders, such as cognition, mood, and seizures (reviewed in 1); however, $mGlu_7$'s involvement in other areas, such as sociability, movement, and sleep remain relatively unexplored. Therefore, we sought to investigate the contribution of $mGlu_7$ to phenotypic domains considered relevant to symptoms observed in neurodevelopmental disorders by characterizing $mGlu_7$ heterozygous (*Grm7*$^{+/-}$) and knockout (*Grm7*$^{-/-}$) mice of both sexes. In the current manuscript, we expand upon previously reported phenotypes, including cognitive deficits and seizures, and report novel phenotypic differences in social behavior, repetitive limb clasping, motor coordination, sleep-wake architecture, and sensitivity to amphetamine. Together, these data demonstrate that $mGlu_7$ is well-positioned to modulate a wide range of behaviors that overlap with those that are characteristic of neurodevelopmental disorders in humans and suggest that targeting $mGlu_7$ activity may be a novel treatment strategy for symptoms within these behavioral domains.

Results

Grm7$^{-/-}$ and *Grm7*$^{+/-}$ mice exhibit abnormal social behavior

Social behavior is a major symptom domain disrupted in neurodevelopmental disease and a core diagnostic criterion for ASD. We tested social behavior in mice using a three-chamber interaction assay. *Grm7*$^{+/+}$, *Grm7*$^{+/-}$, and *Grm7*$^{-/-}$ littermates were placed in a three-chamber apparatus and allowed to explore freely. When given the choice to explore a novel mouse (Stranger 1) or an empty cup, all genotypes preferred to interact with the mouse (Figure 7A, ANOVA, chamber: $F_{(2,111)} = 76.6$, $p < 0.0001$, comparison of Stranger 1 to Empty: *Grm7*$^{+/+}$: $p = 0.0001$, *Grm7*$^{+/-}$: $p < 0.0001$, *Grm7*$^{-/-}$: $p < 0.0001$), suggesting that general sociability is unaffected in *Grm7*$^{-/-}$ mice. When given the choice to explore Stranger 1 versus a second novel mouse (Stranger 2), *Grm7*$^{+/+}$ and *Grm7*$^{+/-}$ mice demonstrated a clear preference for Stranger 2 (Figure 7B, ANOVA, chamber: $F_{(2,111)} = 47.7$, $p < 0.0001$, interaction: $F_{(4,111)} = 7.3$, $p < 0.0001$, comparison of Stranger 1 to Stranger 2: *Grm7*$^{+/+}$: $p = 0.0001$, *Grm7*$^{+/-}$: $p = 0.02$). However, *Grm7*$^{-/-}$ mice showed the opposite preference and spent significantly more time with Stranger 1 (Figure 7B, *Grm7*$^{-/-}$: $p = 0.02$). When data were analyzed to only include close interaction time, a preference for Stranger 1 over an empty cup was present for each genotype (Figure 7C, chamber: $F_{(1,74)} = 44.3$, $p < 0.0001$, comparison of Stranger 1 to Empty: *Grm7*$^{+/+}$: $p = 0.0005$, *Grm7*$^{+/-}$: $p = 0.0004$, *Grm7*$^{-/-}$: $p = 0.002$). A comparison of close interaction time between Stranger 1 and Stranger 2 revealed a significant preference for Stranger 2 in *Grm7*$^{+/+}$ controls only (Figure 7D, chamber: $F_{(1,74)} = 4.1$, $p = 0.046$, interaction: $F_{(2,74)} = 8.0$, $p = 0.0007$, comparison of Stranger 1 to Stranger 2: *Grm7*$^{+/+}$ $p = 0.006$).

To further test social recognition, a separate cohort of mice underwent a five-trial social recognition assay whereby each mouse was allowed to explore a novel mouse (Stranger 1) for four 2-minute trials with 10 minutes between each trial. During the fifth trial, the test mouse was introduced to a second novel mouse (Stranger 2). In this test, we observed no genotype

differences in social interaction time across trials (Figure 7E, ANOVA, trial: $F_{(3.1,84.6)} = 17.9$, $p < 0.0001$, genotype: $F_{(2,27)} = 0.4$, $p = 0.67$), and all genotypes showed a significantly increased interaction time between Trial 4 and Trial 5 (Figure 7F-H, paired t-tests, *Grm7*$^{+/+}$: $t_{(9)} = 2.8$, $p = 0.02$, *Grm7*$^{+/-}$: $t_{(10)} = 2.8$, $p = 0.018$, *Grm7*$^{-/-}$: $t_{(8)} = 4.2$, $p = 0.003$). Taken together, these data indicate that the loss of $mGlu_7$ does not affect general sociability or social recognition, but rather impacts social preference, motivation, or other factors underlying social behavior.

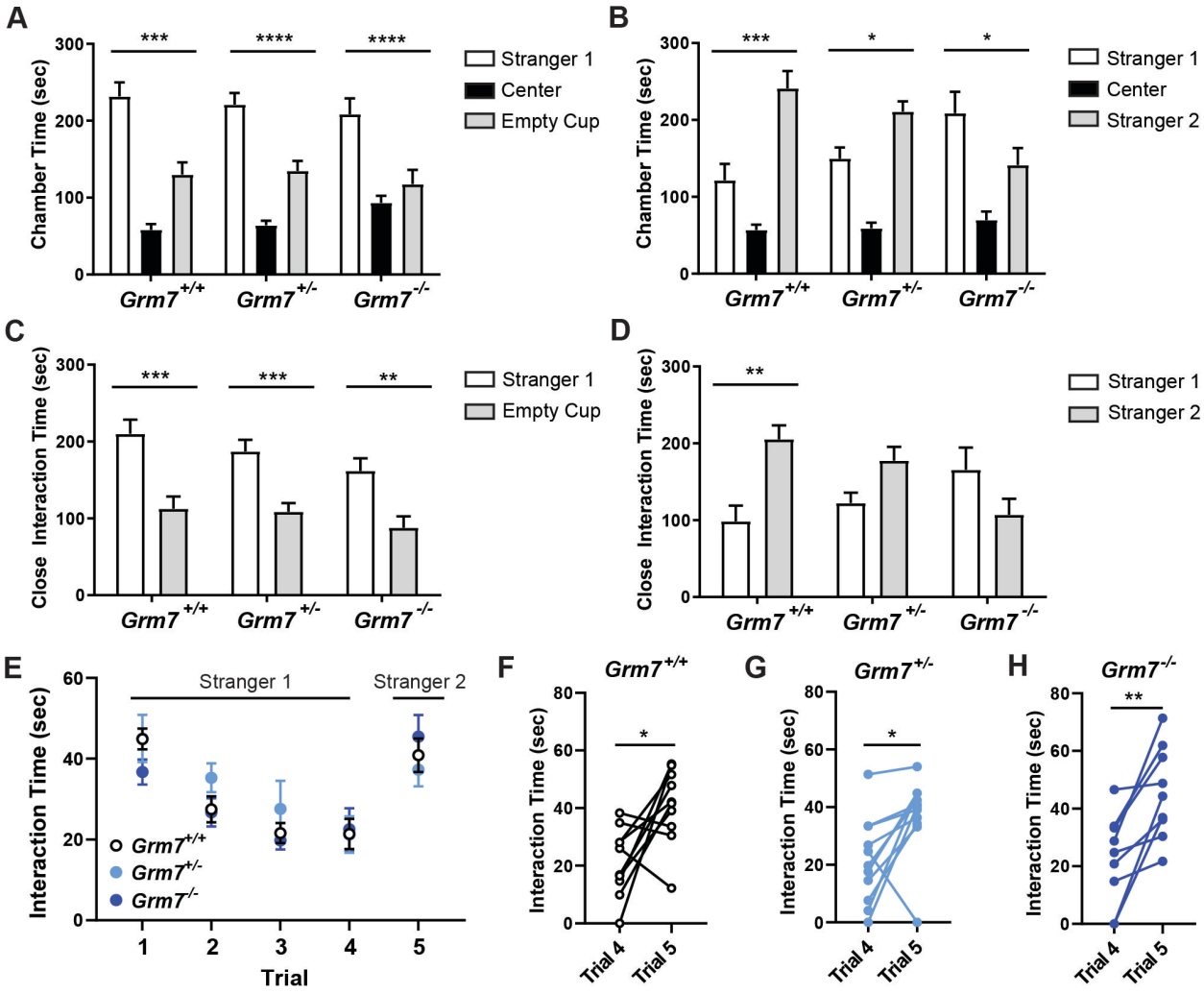

Figure 7. *Grm7*$^{-/-}$ and *Grm7*$^{+/-}$ mice exhibit abnormal social behavior.
(A) Quantification of time in the chamber with Stranger 1 relative to the chamber with the empty cup. (B) Quantification of time in the chamber with Stranger 2 relative to the chamber with Stranger 1. (C) Quantification of close interaction time with Stranger 1 and empty cup. (D) Quantification of close interaction time with Stranger 1 and Stranger 2. For panels A-D, N = 10 *Grm7*$^{+/+}$ (6 female, 4 male), 15 *Grm7*$^{+/-}$ (10 female, 6 male), 14 *Grm7*$^{-/-}$ (8 female, 6 male). (E) Five-trial social recognition assay. Quantification of interaction time over all trials. (F-H). Paired t-tests for each genotype comparing Trial 4 and Trial 5. For panels E-H, N = 10 *Grm7*$^{+/+}$ (5 female, 5 male), 11 *Grm7*$^{+/-}$ (5 female, 6 male), 9 *Grm7*$^{-/-}$ (5 female, 4 male). *p < 0.05, **p < 0.01, ***p < 0.001, ****p < 0.0001.

To control for potential changes in spontaneous locomotor behavior, we tested mice in the open field assay and found no differences between groups (Figure 8A, ANOVA, $F_{(2,57)} = 0.24$, $p = 0.78$); however, *Grm7*$^{-/-}$ mice spent significantly more time in the center of the open field (Figure 8B, ANOVA, $F_{(2,57)} = 9.4$, $p = 0.0003$, *Grm7*$^{+/+}$ vs. *Grm7*$^{-/-}$ $p = 0.03$) consistent with previously reports of diminished anxiety-like behavior in this model[134]. A similar phenotype was also observed in the elevated plus maze, whereby *Grm7*$^{-/-}$ mice spent significantly more time exploring the open arms of the maze (Figure 8C, ANOVA, $F_{(2,62)} = 6.0$, $p = 0.004$, *Grm7*$^{+/+}$ vs. *Grm7*$^{-/-}$ $p = 0.012$).

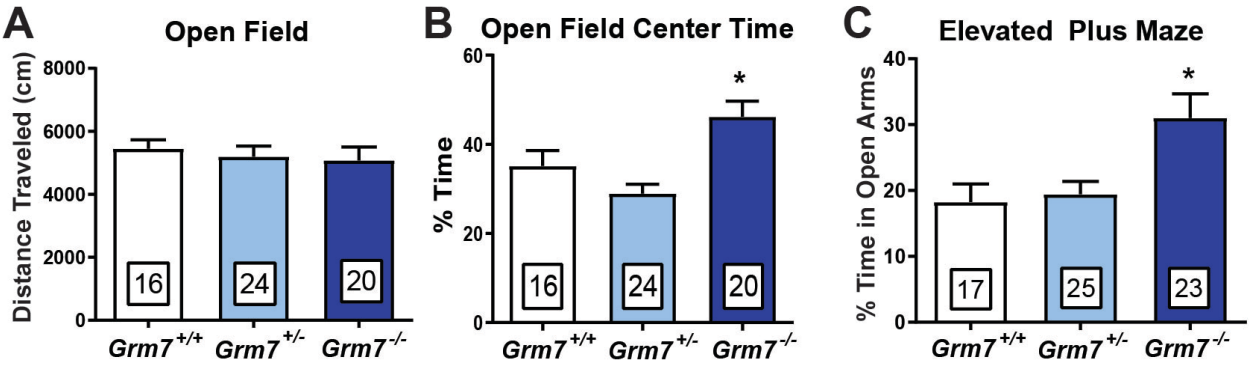

Figure 8. *Grm7*$^{-/-}$ mice have unaltered spontaneous locomotion but decreased anxiety-like behavior.
(A) Distance traveled in open field assay. (B) Time spent in center of open field. For panels A-B, N = 16 *Grm7*$^{+/+}$ (9 female, 7 male), 24 *Grm7*$^{+/-}$ (15 female, 9 male), 20 *Grm7*$^{-/-}$ (13 female, 7 male). (C) Time spent in open arms of elevated plus maze. N = 17 *Grm7*$^{+/+}$ (9 female, 8 male), 25 *Grm7*$^{+/-}$ (15 female, 10 male), 23 *Grm7*$^{-/-}$ (13 female, 10 male). *$p < 0.05$.

Grm7$^{-/-}$ mice have deficits in associative fear learning despite intact long-term potentiation in the hippocampus

Intellectual disability is a stand-alone diagnosis and a symptom domain that has high comorbidity with many neurodevelopmental disorders, including ASD[4]. To test associative learning, mice underwent a fear conditioning protocol that consisted of a three-minute habituation to a novel context, followed by two mild foot shocks paired to an auditory cue. Consistent with previous findings showing that pain sensitivity is unaffected in *Grm7*$^{-/-}$ mice[115], we did not observe

changes in shock threshold (data not shown), suggesting that differences in foot shock sensitivity do not confound behavioral responses in this task. During this conditioning session, *Grm7*$^{+/+}$ and *Grm7*$^{+/-}$ mice progressively froze more after each foot shock, while *Grm7*$^{-/-}$ mice exhibited a markedly decreased freezing response (Figure 9A, ANOVA, shock: $F_{(2,219)} = 24.3$, $p < 0.0001$, interaction: $F_{(4,219)} = 4.8$, $p = 0.001$, *Grm7*$^{+/+}$ vs. *Grm7*$^{-/-}$ shock 2: $p = 0.0004$). Twenty-four hours after conditioning, mice were placed back into the same context and freezing during a three-minute session was quantified. *Grm7*$^{-/-}$ mice froze significantly less than their littermates (Figure 9B, ANOVA, $F_{(2,73)} = 22.8$, $p < 0.0001$, *Grm7*$^{+/+}$ vs. *Grm7*$^{-/-}$: $p < 0.0001$). Four hours following the context test, mice were placed in a second novel context and the auditory cue was played. Again, *Grm7*$^{-/-}$ mice froze significantly less than their littermate controls (Figure 9C, ANOVA, $F_{(2,59)} = 9.9$, $p = 0.0002$, *Grm7*$^{+/+}$ vs. *Grm7*$^{-/-}$: $p = 0.025$).

Deficits in contextual fear learning can often be correlated with decreased synaptic plasticity within the hippocampus, as shown in rodent models of intellectual disability[101,103]. Pharmacological inhibition of $mGlu_7$ activity can block long-term potentiation (LTP) at Schaffer Collateral – CA1 (SC-CA1) synapses[100]; therefore, we tested the effect of $mGlu_7$ absence on this specific form of LTP. Following two trains of high frequency stimulation, field excitatory postsynaptic potentials (fEPSPs) in hippocampal slices from *Grm7*$^{-/-}$ mice remained potentiated from baseline for 60 minutes (Figure 9D), and the magnitude of LTP, quantified during the last five minutes of recording, was not significantly different across genotypes (Figure 9E, ANOVA, $F_{(2,40)} = 2.1$, $p = 0.13$).

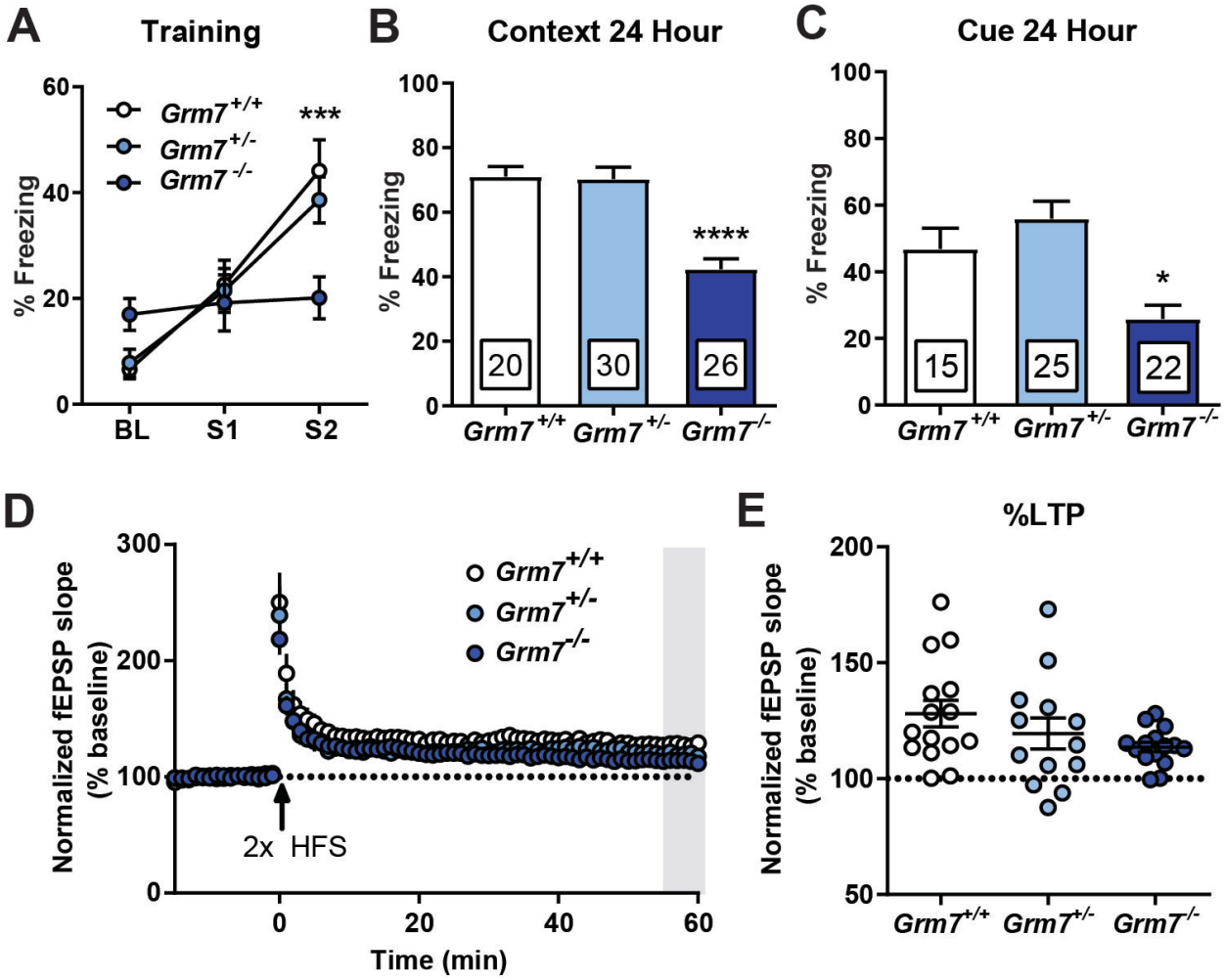

Figure 9. *Grm7*$^{-/-}$ mice have deficits in associative fear learning despite intact long-term potentiation at SC-CA1 synapses.

(A) Quantification of acute freezing during baseline (BL) and in response to foot shocks (S1 and S2) during fear conditioning. (B) Quantification of freezing behavior upon re-exposure to the conditioning context 24 hours post-conditioning. For A-B, N = 20 *Grm7*$^{+/+}$ (11 female, 9 male), 30 *Grm7*$^{+/-}$ (16 female, 14 male), 26 *Grm7*$^{-/-}$ (15 female, 11 male). (C) Quantification of freezing behavior in response to a one-minute auditory cue four hours after the context test. N = 15 *Grm7*$^{+/+}$ (9 female, 6 male), 25 *Grm7*$^{+/-}$ (13 female, 12 male), 22 *Grm7*$^{-/-}$ (12 female, 10 male). Five *Grm7*$^{+/+}$, five *Grm7*$^{+/-}$ and four *Grm7*$^{-/-}$ animals were excluded due to freezing > 20% prior to the tone. (D) Long-term potentiation at SC-CA1 synapses induced by two trains of high frequency stimulation (HFS, 100 Hz). N (total slices/total mice) = 15/9 *Grm7*$^{+/+}$ (10/6 female, 5/3 male), 13/8 *Grm7*$^{+/-}$ (6/4 female, 7/4 male), 15/8 *Grm7*$^{-/-}$ (8/4 female, 7/4 male). (E) Quantification of LTP magnitude during the last 5 minutes of recording (gray bar in D). *p < 0.05, ***p < 0.001, ****p < 0.0001.

Grm7$^{-/-}$ mice demonstrate a variety of deficits in motor coordination and strength

Motor stereotypies and impaired purposeful movement frequently occur in neurodevelopmental disorders; for example, repetitive hand wringing and gait abnormalities are core diagnostic criteria for RTT[139]. Although *Grm7*$^{-/-}$ mice did not differ in spontaneous locomotion as assessed in the open field (Figure 8A), they did exhibit motor abnormalities when challenged by paradigms that test strength and coordination. Upon weaning, we observed repetitive clasping of both the forepaws and hind paws in *Grm7*$^{-/-}$ mice when they were suspended by the tail. Clasping was captured on video and quantified by a blinded scorer at 5, 10, 15 and 20 weeks of age. Forepaw clasping in *Grm7*$^{-/-}$ mice was significantly increased at all ages and showed a significant interaction with age (Figure 10A, ANOVA, age: $F_{(3,148)} = 8.6$, $p < 0.0001$, genotype: $F_{(2,128)} = 123.1$, $p < 0.0001$, interaction: $F_{(6,148)} = 3.9$, $p = 0.01$, *Grm7*$^{+/+}$ vs *Grm7*$^{-/-}$ at all ages $p < 0.001$). Conversely, hind paw clasping was significantly increased at all ages, but did not change significantly with age (Figure 10B, ANOVA, age: $F_{(3,148)} = 1.4$, $p = 0.25$, genotype: $F_{(2,128)} = 150.6$, $p < 0.0001$, *Grm7*$^{+/+}$ vs *Grm7*$^{-/-}$ at all ages $p < 0.0001$). *Grm7*$^{-/-}$ mice also exhibited modest gait abnormalities when tested using a Treadscan system; specifically, the average swing and stride times of the front paws were significantly longer than littermate controls, while there was no difference in these parameters for the back paws between any group (Figure 10C, Swing: ANOVA, $F_{(2,33)} = 7.1$, $p = 0.003$, *Grm7*$^{+/+}$ vs *Grm7*$^{-/-}$ $p = 0.008$, Stride: ANOVA, $F_{(2,33)} = 6.5$, $p = 0.004$, *Grm7*$^{+/+}$ vs *Grm7*$^{-/-}$ $p = 0.01$; back paw data not shown). In a rotarod test, *Grm7*$^{-/-}$ mice fell from the accelerating rod significantly sooner than their littermates (Figure 10D, ANOVA, day: $F_{(2,186)} = 17.3$, $p < 0.0001$, genotype: $F_{(2,186)} = 25$, $p < 0.0001$, *Grm7*$^{+/+}$ vs *Grm7*$^{-/-}$ day 2: $p = 0.02$, day 3: $p = 0.003$). This effect did not correlate with impairments in motor learning (Figure 10E, ANOVA, day: $F_{(2,186)} = 21.4$, $p < 0.0001$, genotype: $F_{(2,186)} = 0.034$, $p = 0.96$,) or differences in weight (Figure 10F, correlation, *Grm7*$^{+/+}$: $r = -0.210$, *Grm7*$^{+/-}$: $r = 0.106$, *Grm7*$^{-/-}$: $r = 0.208$). *Grm7*$^{-/-}$ mice also exhibited reduced forepaw grip strength, which could contribute to their decreased

latency to fall from the rotarod (Figure 10G, ANOVA, $F_{(2,37)} = 6.4$, $p = 0.004$, *Grm7*$^{+/+}$ vs *Grm7*$^{-/-}$ $p = 0.02$).

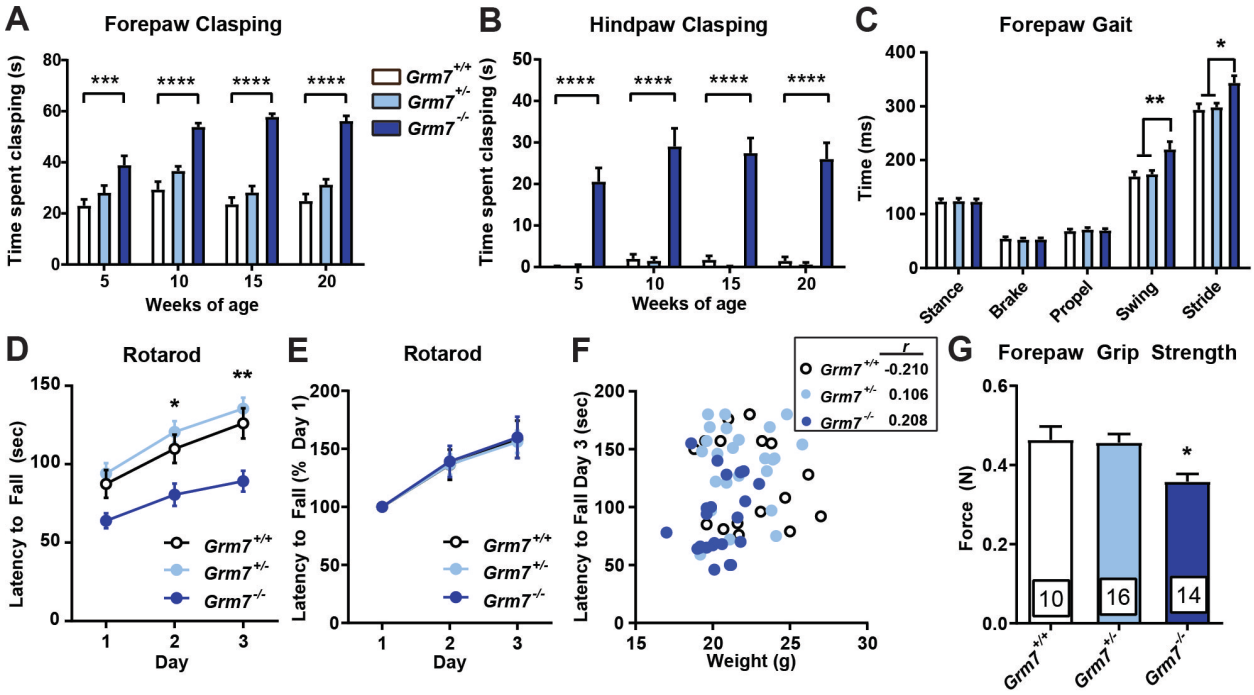

Figure 10. *Grm7*$^{-/-}$ mice exhibit repetitive paw clasping along with deficits in motor coordination and strength.

Quantification of forepaw (A) and hindpaw (B) clasping over time. N = 10 *Grm7*$^{+/+}$ (6 female, 4 male), 15 *Grm7*$^{+/-}$ (10 female, 6 male), 14 *Grm7*$^{-/-}$ (8 female, 6 male). (C) Forepaw gait parameters measured by Treadscan system. N = 10 *Grm7*$^{+/+}$ (5 female, 5 male), 14 *Grm7*$^{+/-}$ (5 female, 9 male), 12 *Grm7*$^{-/-}$ (7 female, 5 male). (D) Latency to fall from an accelerating rotarod over three days. (E) Latency to fall from rotarod normalized to Day 1. (F) Lack of correlation of latency to fall from rotarod on Day 3 with weight. *r* values shown in inset. For panels D-F, N = 17 *Grm7*$^{+/+}$ (9 female, 8 male), 25 *Grm7*$^{+/-}$ (15 female, 10 male), 24 *Grm7*$^{-/-}$ (13 female, 11 male). (G) Quantification of forepaw grip strength. N = 10 *Grm7*$^{+/+}$ (6 female, 4 male), 15 *Grm7*$^{+/-}$ (10 female, 6 male), 14 *Grm7*$^{-/-}$ (8 female, 6 male). *p < 0.05, **p < 0.01, ***p < 0.001, ****p < 0.0001.

Seizures in *Grm7*$^{-/-}$ mice can be induced by handling and involve hippocampal activation

Epilepsy is a common comorbidity in neurodevelopmental disorders that arises from excitatory/inhibitory imbalance that is often a result of deficits in synaptic development and function[178]. Over the course of testing, *Grm7*$^{-/-}$ mice and littermate controls were handled at least once per week, during which time we quantified the robust presence of behavioral seizures. These seizures were brief (< 1 minute), ranged from a Racine score of 3 to 5, and were observed in 64% of *Grm7*$^{-/-}$ mice (9/14 mice by 20 weeks of age), with a median age of onset of 15 weeks of age and were never observed in *Grm7*$^{+/+}$ or *Grm7*$^{+/-}$ littermates (Figure 11A). To evaluate the development of these seizures, a cohort of female *Grm7*$^{-/-}$ mice and *Grm7*$^{+/+}$ littermates was monitored by surface EEG from 8 to 20 weeks of age. No seizures were detectable during periods when the mice were left undisturbed; however, handling-induced generalized seizures were observed in 8/11 *Grm7*$^{-/-}$ mice and were detectable by EEG (Figure 11B). To further investigate which brain regions were involved in these seizures, we quantified c-Fos induction by Western blotting of protein isolated from brain tissue punches from the cortex, thalamus and hippocampus collected one hour following an observed seizure. Compared to *Grm7*$^{+/+}$ and *Grm7*$^{-/-}$ mice that did not experience a seizure, samples from *Grm7*$^{-/-}$ mice following a seizure revealed a large increase in c-Fos only in the hippocampus (Figure 11C-D, ANOVA, cortex: $F_{(2,6)} = 1.9$ $p = 0.22$, hippocampus: $F_{(2,6)} = 15.0$ $p = 0.005$, *Grm7*$^{+/+}$ vs *Grm7*$^{-/-}$ $p = 0.009$, thalamus $F_{(2,6)} = 1.3$ $p = 0.34$). This suggests that seizures in *Grm7*$^{-/-}$ mice likely involve limbic regions; however, the contribution of other brain regions cannot be excluded as our study only captured one time point.

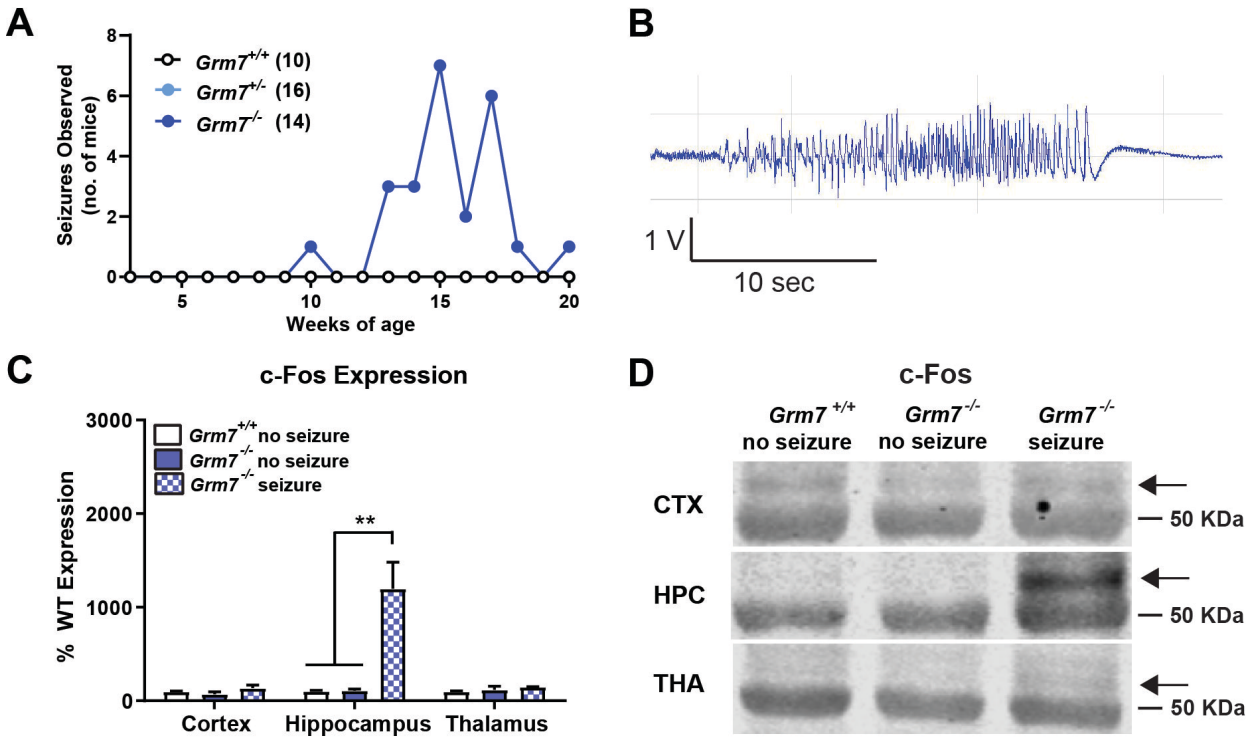

Figure 11. Seizures in *Grm7*$^{-/-}$ mice correlate with increased c-Fos expression in the hippocampus.

(A) Seizure observations over time, including seizures with Racine score greater or equal to 3. N = 10 *Grm7*$^{+/+}$ (6 female, 4 male), 15 *Grm7*$^{+/-}$ (10 female, 6 male), 14 *Grm7*$^{-/-}$ (8 female, 6 male). (B) Representative EEG trace of a seizure induced upon handling. (C) Quantification of c-Fos protein by Western blot in tissue samples collected one hour following handling. Regions analyzed: cortex (CTX), hippocampus (HPC), thalamus (THA). N = 3 male mice per group, 30 weeks of age. (D) Representative c-Fos blot photos. The arrow represents the band quantified in C. The band below is a nonspecific band that aligns with the 50 KDa ladder marker.

EEG analysis of *Grm7*$^{-/-}$ mice indicate alterations in sleep and blunted response to amphetamine

In addition to epileptiform activity, EEG analysis also allowed for characterization of sleep-wake architecture, which is commonly disrupted in neurodevelopmental disorders[179]. *Grm7*$^{-/-}$ mice (blue bars) exhibited increased percent time awake during both the light phase (Figure 12A, ANOVA, time: $F_{(2.9,51.4)} = 8.9$, $p < 0.0001$, genotype: $F_{(1,18)} = 9.5$, $p = 0.006$) and the dark phase (Figure 12B, ANOVA, genotype: $F_{(1,18)} = 17.6$, $p = 0.0005$), along with decreased percent time in NREM sleep during both phases (Light phase: Figure 12C, time: $F_{(2.5,45.7)} = 12.8$, $p < 0.0001$, genotype: $F_{(1,18)} = 6.0$, $p = 0.02$, Dark phase: Figure 12D ANOVA, genotype: $F_{(1,18)} = 20$, $p = 0.0003$, *Grm7*$^{+/+}$ vs. *Grm7*$^{-/-}$ 16 wk $p = 0.03$, 20 wk $p = 0.03$). There was a significant effect of time, but not genotype, on percent time in REM sleep during the light phase (Figure 12E, ANOVA, time: $F_{(2.2,39)} = 4.0$, $p = 0.02$, genotype: $F_{(1,18)} = 0.007$, $p = 0.93$). Bout analysis of REM sleep revealed a significant effect of time and genotype-time interaction on the number of bouts during the light phase (Figure 12G, ANOVA, time: $F_{(2.4,44)} = 8.4$, $p = 0.0004$, genotype: $F_{(1,18)} = 4.0$, $p = 0.06$, interaction: $F_{(3,54)} = 3.4$, $p = 0.02$). Average REM bout duration was significantly decreased during the light phase at 8 and 12 weeks of age (Figure 12H, ANOVA, time: $F_{(2.4,42.6)} = 3.2$, $p = 0.04$, genotype: $F_{(1,18)} = 16.1$, $p = 0.0008$, *Grm7*$^{+/+}$ vs. *Grm7*$^{-/-}$: 8 wk $p = 0.01$, 12 wk $p = 0.004$).

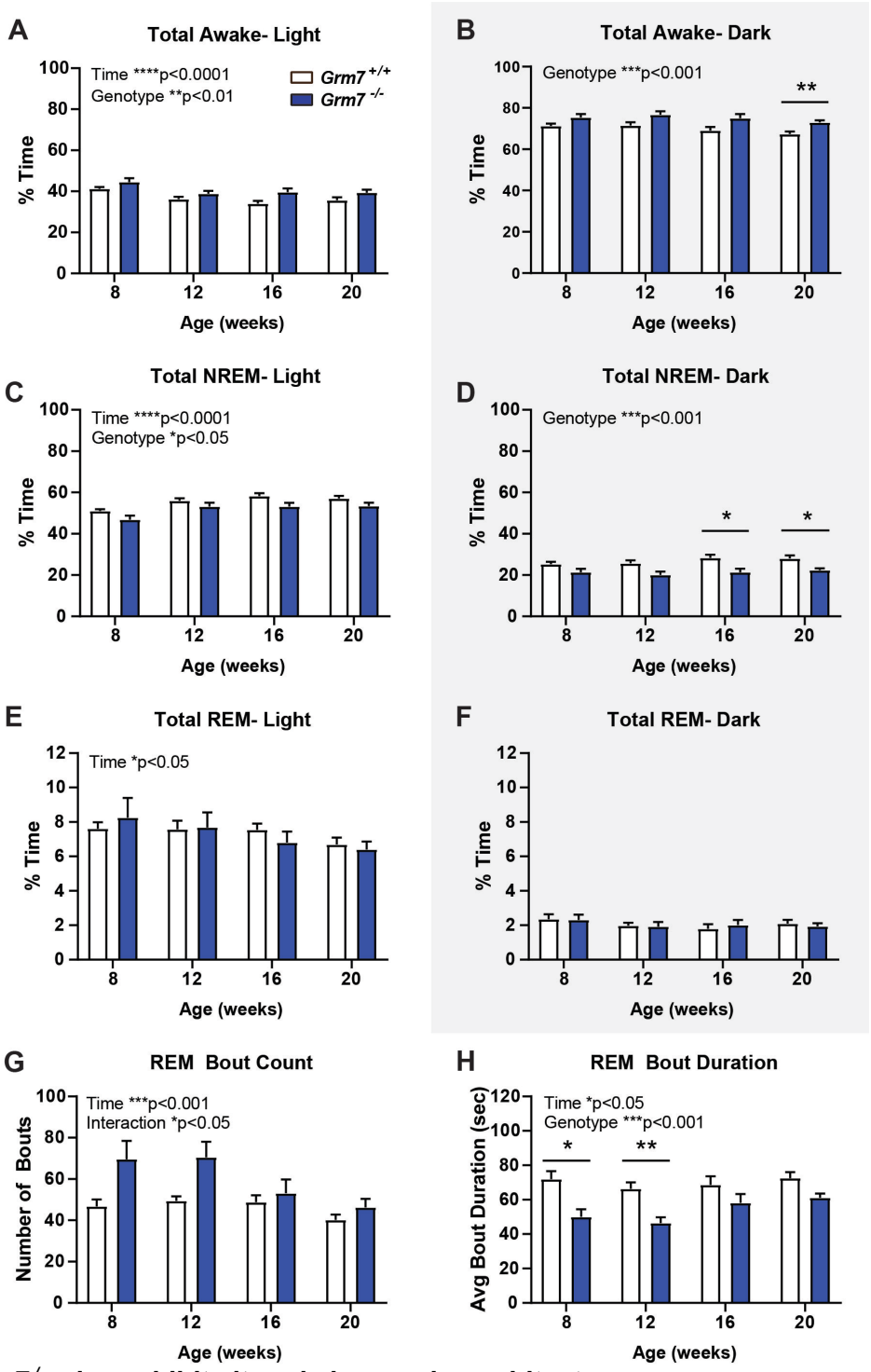

Figure 12. *Grm7*$^{-/-}$ mice exhibit altered sleep-wake architecture.

(A-B) Percent of time spent awake during (A) light and (B) dark phases. (C-D) Percent of time spent in NREM sleep during (C) light and (D) dark phases. (E-F) Percent of time spent in REM sleep during (E) light and (D) dark phases. (G) REM bout count and (H) bout duration during the light phase. For all panels, N = 9 female *Grm7*$^{+/+}$, 11 female *Grm7*$^{-/-}$. *p < 0.05, **p < 0.01, ***p < 0.001, ****p < 0.0001.

Quantitative EEG (qEEG) analysis did not indicate consistent age-dependent or genotype-dependent changes in relative spectral power across widely accepted bands (e.g. delta, theta, alpha; beta, gamma, data not shown); therefore, we hypothesized that, similar to handling-induced seizures, differences may emerge following stimulation. We examined the effects of amphetamine on brain function in this cohort because *GRM7* polymorphisms have been associated with response to methylphenidate in ADHD patients[161,180]. Following a single dose, we observed a significantly reduced effect of amphetamine on activity counts in *Grm7*$^{-/-}$ mice (Figure 13A, ANOVA, time: $F_{(17,198)} = 15.9$, $p < 0.0001$, genotype: $F_{(1,198)} = 47.2$, $p < 0.0001$, interaction: $F_{(17,198)} = 4.5$, $p < 0.0001$, min 50: $p = 0.046$, min 60-90: $p < 0.0001$, min 100: $p = 0.036$). This was comorbid with a significantly blunted effect of amphetamine on high gamma power (50-80 Hz) in *Grm7*$^{-/-}$ mice (Figure 13B, ANOVA, time: $F_{(17,185)} = 7.4$, $p < 0.0001$, genotype: $F_{(1,185)} = 16.1$, $p < 0.0001$, interaction: $F_{(17,185)} = 1.9$, $p = 0.02$, min 40: $p = 0.002$, min 50: $p = 0.02$) along with effects on low gamma power (30-50 Hz) (Figure 13C, ANOVA, time: $F_{(17,185)} = 2.7$, $p = 0.0004$, genotype: $F_{(1,185)} = 19.3$, $p < 0.0001$) and delta power (0.5-4 Hz) (Figure 13D, ANOVA, time: $F_{(17,185)} = 2.9$, $p = 0.0002$, genotype: $F_{(1,185)} = 67.0$, $p < 0.0001$, interaction: $F_{(17,185)} = 2.7$, $p = 0.0006$, min 40-80: $p < 0.01$). There were no significant changes in other frequency bands (data not shown).

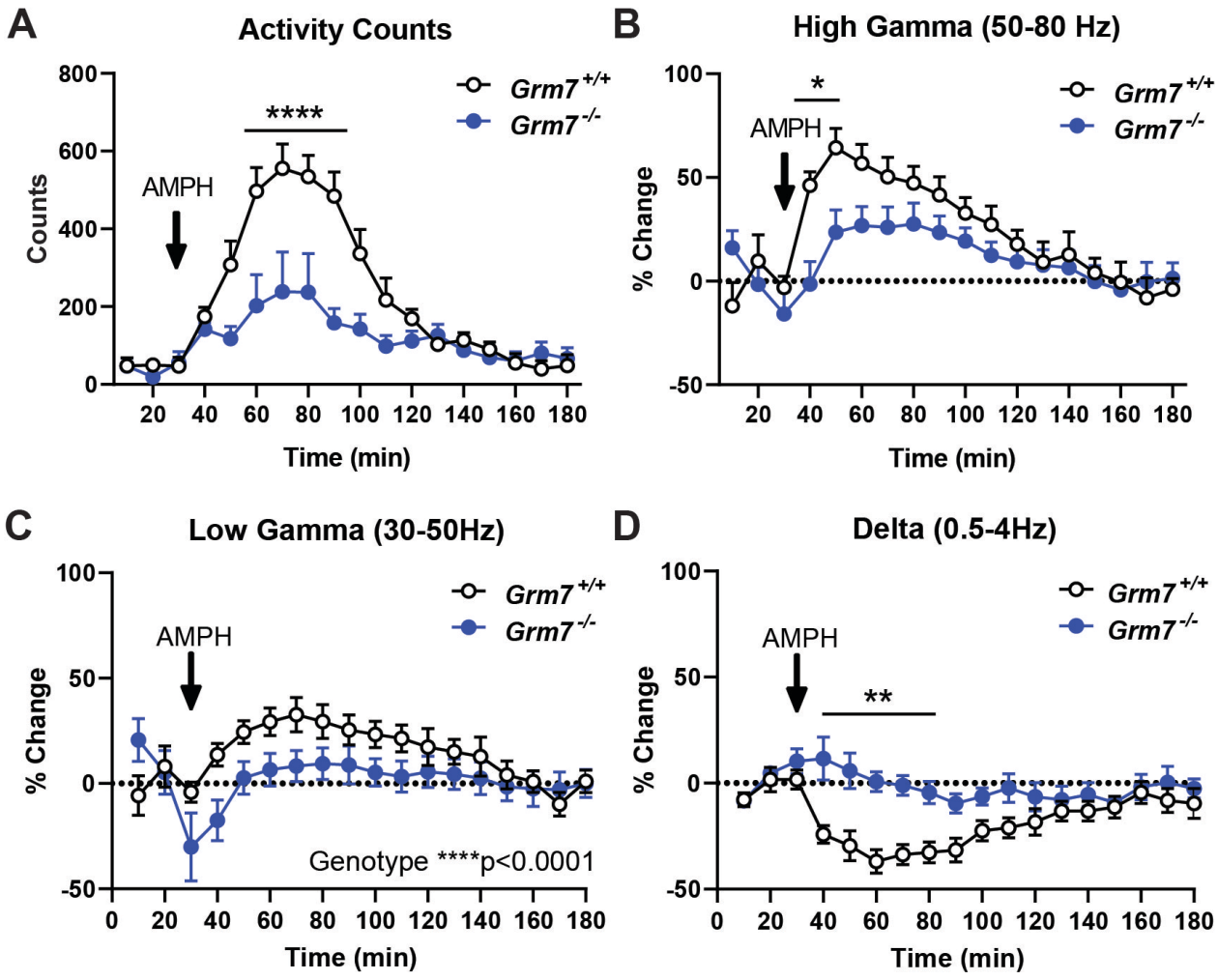

Figure 13. The response to amphetamine is blunted in *Grm7*$^{-/-}$ mice compared to controls.

Quantification of (A) activity counts, (B) high gamma power, (C) low gamma power and (D) delta power following subcutaneous administration of 2.25 mg/kg amphetamine. For all panels, N = 6 female *Grm7*$^{+/+}$, 7 female *Grm7*$^{-/-}$. *p < 0.05, **p < 0.01, ****p < 0.0001.

Discussion

Our data reveal a wide range of disrupted phenotypes in *Grm7*$^{-/-}$ mice, some of which replicate and expand upon published findings, while others have not been previously reported. A major novel finding is the disruption of social behavior in the three-chamber assay. Masugi-Tokita et al. recently showed that $mGlu_7$ in the bed nucleus of the stria terminalis is essential for inter-male aggression, and that male *Grm7*$^{-/-}$ mice show less frequent anogenital sniffing and more frequent grooming of an intruder[181,182]. In female mice, Gryksa et al showed that *Grm7*$^{-/-}$ animals exhibit decreased maternal aggression and increased maternal care[183]. Additionally, the $mGlu_7$ negative allosteric modulator (NAM) MMPIP was reported to decrease social interaction time in rats[119]. Our data suggest that loss of $mGlu_7$ also impairs social preference, motivation or another aspect of behavior in the three-chamber assay, but not the ability to recognize and interact with a new mouse. Both *Grm7*$^{-/-}$ and *Grm7*$^{+/-}$ mice exhibited a lack of preference when only close interaction was analyzed; interestingly, this is the only phenotype that we observed in heterozygous mice. As social deficits are a core symptom of ASD and common in other neurodevelopmental disorders, $mGlu_7$'s role in social behaviors and its underlying neural circuits merits further investigation.

The existing literature on *Grm7*$^{-/-}$ mice has focused primarily on anxiety, depression and emotional learning. Specifically, loss of $mGlu_7$ has been shown to produce phenotypes predictive of anti-depressive and anxiolytic effects in rodent models,[134] and *Grm7*$^{-/-}$ mice have been characterized extensively in paradigms of fear and aversion learning in which they show a clear deficit[115–117]. Here, we corroborate these findings in a fear conditioning assay where we observed decreased associative memory in response to both context and cue. However, cued fear results should be interpreted with caution as variants in *GRM7* have been linked to age-related hearing loss in human populations[184], and this association remains unstudied in mice.

LTP at SC-CA1 synapses is one form of synaptic plasticity that has been correlated with cognitive deficits across a range of neurological diseases, including neurodevelopmental

disorders. $mGlu_7$ activation is required for LTP at SC-CA1 synapses through its ability to reduce GABAergic inhibition onto CA1 pyramidal cells[100]. Application of an $mGlu_7$ NAM can completely block LTP; however, a previous study reported no change in LTP at SC-CA1 synapses in *Grm7*$^{-/-}$ mice despite a significant decrease in potentiation directly following 100Hz stimulation[107]. Our results confirm that long-term potentiation is not significantly altered by *Grm7* genotype, suggesting that compensatory mechanisms may occur with global deletion of $mGlu_7$.

To our knowledge, the motor phenotypes we observed in *Grm7*$^{-/-}$ mice have not been previously published. Rotarod performance and grip strength were characterized in *Grm7*$^{-/-}$ mice at 8-10 weeks of age by Callaerts-Vegh et al.[118]; in contrast, our testing was performed on animals that were greater than 10 weeks of age. Motor deficits in *Grm7*$^{-/-}$ mice may develop only at older ages and are likely aggravated by the onset of seizures. Only one time-point was tested for rotarod, gait and grip strength; therefore, it will be important to investigate the developmental onset of these phenotypes in future studies. The repetitive clasping phenotype was apparent at 5 weeks of age and persisted through the entire testing period, indicating that at least some aspects of motor function are impacted early in life. Hindlimb clasping and gait abnormalities are commonly seen in many models of neurological disorders, including mouse models of RTT where it has been used widely as a measure of disease progression[174]. $mGlu_7$ is expressed on excitatory corticostriatal projections along with inhibitory striatopallidal and striatonigral projections[185]; however, the functional role of $mGlu_7$ in these circuits is poorly defined at present.

As $mGlu_7$ is a presynaptic regulator of glutamate release, its activation would be predicted to provide negative feedback in the event of high glutamate levels. Consistent with this idea, we routinely observed behavioral seizures in *Grm7*$^{-/-}$ mice. Spontaneous seizures in response to sensory stimuli, along with heightened excitability of area CA1 in hippocampal slices, has been previously reported[68]. Our data further support that these seizures involve the hippocampus and are only detectable following a stimulus, in this case, handling. Interestingly, the seizures we observed are very similar to those reported in mice lacking the protein Elfn1 (extracellular-leucine-

rich repeat fibronectin domain 1), which were triggered by moving mice to a clean, empty cage and ranged on the Racine scale from a score of 2-5[17,131]. Elfn1 is a postsynaptic protein that promotes constitutive $mGlu_7$ activation and downstream inhibition of release probability onto somatostatin interneurons in the hippocampus and cortex[78,98]. The convulsive seizures observed in *Grm7*$^{-/-}$ and *Elfn1*$^{-/-}$ mice differ from those reported in mice after specific disruption of the interaction between $mGlu_7$ and Protein Interacting with C Kinase (PICK1). Disruption of the $mGlu_7$-PICK1 interaction leads to absence seizures that correlate with increased c-Fos expression with the thalamocortical circuit without changes in the hippocampus[129]. Constitutive activity of $mGlu_7$ provides tonic inhibition at thalamic synapses, an effect that is dependent on $mGlu_7$ interaction with PICK1[77]. Altogether, these data suggest that $mGlu_7$ may play distinct roles in seizure activity depending on seizure type, brain region involved, and the expression of $mGlu_7$-interacting proteins. $mGlu_7$ activation would be predicted to reduce seizures, as demonstrated by a recent report that the $mGlu_7$ agonist LSP2-9166 exhibits efficacy in two distinct models of chemically-induced epilepsy[186].

We also report alterations in sleep architecture in female *Grm7*$^{-/-}$ mice assessed by EEG across time from 8 to 20 weeks of age. The balance of glutamate and GABA function is known to regulate sleep[187], and normal sleep is critical for memory consolidation[188]. Reduced NREM sleep and altered REM bout patterns in *Grm7*$^{-/-}$ mice suggest abnormal sleep fragmentation, which has been specifically linked with deficits in contextual fear consolidation[189]. We did not observe any significant changes in qEEG spectra in *Grm7*$^{-/-}$ mice relative to their littermates when left undisturbed in their home cage. This is consistent with a previous publication that reported no differences in baseline qEEG but found increased hippocampal theta power in *Grm7*$^{-/-}$ mice during a working memory task[150]. It is important to note that this EEG study was restricted to female mice due to interest in $mGlu_7$ as a potential target for Rett syndrome, where the relevant clinical population is predominantly female.

We also observed that *Grm7*$^{-/-}$ mice exhibited a significantly blunted response to amphetamine, which increased gamma power and lowered delta power in *Grm7*$^{+/+}$ animals. Oscillations in the gamma range are regulated by a balance in glutamate and GABA function[190,191], evolve throughout development[192] and are thought to contribute to cognitive functions[193]. Amphetamines have been shown to strongly modulate gamma activity in attention-associated regions in adults with ADHD[194], and, interestingly, there have been reports that polymorphisms in *GRM7* correlate with response to methylphenidate in ADHD patients[161,180]. We also observed a blunted effect of amphetamine on locomotor activity, which is consistent with the reported decrease in amphetamine-induced hyperlocomotion by the $mGlu_7$ NAM ADX71743[135]. These data could have implications for disease states such as ADHD and schizophrenia where abnormal dopaminergic signaling and aberrant gamma power is well established[191,195]. In further support of the $mGlu_7$-ELFN1 interaction, pathogenic mutations in the *ELFN1* gene have been identified in patients with ADHD and *Elfn1* knockout mice also have a reduced sensitivity to amphetamine[17,131].

In summary, we report a wide range of altered phenotypes in *Grm7*$^{-/-}$ mice, many of which mirror those commonly observed in mouse models of neurodevelopmental disorders. We recently reported preclinical efficacy of $mGlu_7$ potentiation in a RTT mouse model[138]. One limitation of our previous work was the use of a non-selective compound that potentiates the activity of all group III mGlu receptors. The phenotypes reported here overlap extensively with those reported in RTT models (reviewed in 196), providing further support for $mGlu_7$ as a bona fide therapeutic target for RTT. Moreover, these data provide rationale for studying $mGlu_7$ in the context of neurodevelopmental disorders broadly and for investigating the therapeutic potential of compounds that increase $mGlu_7$ activity.

Methods

Animals

All animals used in this study were group housed with food and water given *ad libitum* and maintained on a 12 hour light/dark cycle. Animals were cared for in accordance with the National Institutes of Health *Guide for the Care and Use of Laboratory Animals*. All studies were approved by the Institutional Animal Care and Use Committee for Vanderbilt University School of Medicine and took place during the light phase with the exception of EEG recordings. *Grm7* knockout mice were cryorecovered from the Mutant Mouse Regional Resource Center (B6.129P2-Grm7^{Tm1Dgen}/Mmnc). All mice were generated from heterozygous breeding pairs.

Protein Isolation and Western Blotting

In experiments to measure c-Fos protein expression following generalized seizures, 30-week old male mice were handled and tissue was collected 1 hour following seizure observation. Mice were anesthetized with isoflurane and decapitated. Tissue from the dorsal hippocampus, surrounding cortex and thalamus was dissected from a 1 mm coronal slice. Tissue samples were homogenized using a hand-held motorized mortar and pestle in radioimmunoprecipitation assay buffer (RIPA, Sigma). After homogenization, samples were spun for 20 minutes at 15,000 x g at 4 ºC. The supernatant was saved and protein concentration was determined using a bicinchoninic acid (BCA) protein assay (Pierce^{TM}). Proteins (50 µg) were electrophoretically separated using a 4-20% SDS polyacrylamide gel and then transferred onto a nitrocellulose membrane (Bio-Rad). Membranes were blocked with Odyssey blocking buffer (LiCor) for one hour at room temperature and probed with primary antibodies to c-Fos (1:1000, Millipore ABE457) and tubulin (1:5000, Abcam ab44928) overnight at 4°C. Membranes were washed three times with Tris-buffered saline plus Tween 20 (TBS-T, 25 mM Tris, 150 mM NaCl, 0.05% Tween 20) and then incubated with goat anti-rabbit fluorescent secondary antibody (800CW, 1:5000, LiCor) and goat anti-mouse fluorescent secondary antibody (680CW, 1:5000, LiCor). Blots were washed again and imaged

with an Odyssey scanner and fluorescence was quantified using Image Studio Light software. Each value for c-Fos was normalized to the value calculated for tubulin.

Long-term Potentiation Recordings

Coronal brain slices were prepared from 8-10 week old mice. Mice were anesthetized with isoflurane and decapitated. Brains were rapidly removed and submerged in ice-cold sucrose cutting buffer containing: 230 mM sucrose, 2.5 mM KCl, 8 mM $MgSO_4$, 0.5 mM $CaCl_2$, 1.25 mM NaH_2PO_4, 10 mM glucose, and 26 mM $NaHCO_3$ saturated with 95%/5% O_2/CO_2. A block of tissue containing hippocampus was trimmed, embedded in agarose, and coronal slices 400 µm thick were cut using a Compresstome^{TM} VF-200 (Precisionary Instruments). Slices were transferred to a holding chamber containing *N*-methyl-D-glucamine (NMDG)-HEPES recovery solution (in mM, 93 NMDG, 2.5 KCl, 1.2 NaH_2PO_4, 30 $NaHCO_3$, 20 HEPES, 25 D-glucose, 5 sodium ascorbate, 2 thiourea, 3 sodium pyruvate, 10 $MgSO_4$, 0.5 $CaCl_2$, pH 7.3, 305 mOsm) for 15 minutes at 32ºC. Slices were then transferred to room temperature artificial cerebral spinal fluid (ACSF) containing (in mM) 126 NaCl, 1.25 NaH_2PO_4, 2.5 KCl, 10 D-glucose, 26 $NaHCO_3$, 2 $CaCl_2$ and 1 $MgSO_4$, supplemented with 600 µM sodium ascorbate for at least 1 hour. Subsequently, slices were transferred to a submersion recording chamber and continuously perfused (2 mL/min) with ACSF heated to 30-32°C. All solutions were continuously bubbled with 95%/5% O_2/CO_2.

A concentric bi-polar stimulating electrode was positioned near the CA3-CA1 border and paired-pulse field excitatory postsynaptic potentials (fEPSPs) were evoked (100 µs duration, every 20 sec) and recorded with a glass electrode placed within the stratum radiatum of CA1. Input-output curves were generated for each slice and the stimulation intensity was adjusted to 50% of the maximum response for subsequent experiments. For LTP experiments, slopes of three consecutive sweeps were averaged and normalized to the average slope during the baseline period. Data were digitized using a Multiclamp 700B, Digidata 1322A, and pClamp 10 software (Molecular Devices). Long term potentiation (LTP) was induced by applying two trains of 100 Hz

stimulation (HFS, 1 sec duration, 20 sec inter-train interval (ITI)) after a 15 minute baseline. fEPSPs were monitored for 60 minutes after HFS and percent LTP was quantified as the average normalized slope during the last 5 minutes of recording.

Phenotyping

Both male and female mice were used in phenotyping experiments. No significant sex differences were observed; therefore, data were combined. Mice underwent the following testing schedule with a minimum of 5 days of time between each test: open field (6 wk), elevated plus maze (7wk), three-chamber social interaction (8 wk), fear conditioning (9-10 wk), motor assays (> 10 wks). A separate cohort of mice was used for the five-trial social recognition assay at 15-20 weeks of age. Limb clasping videos were taken at 5, 10, 15 and 20 weeks of age. For all tests, mice were habituated to the testing room for a minimum of 1 hour.

Open field: Mice were placed in an activity chamber measuring 27 by 27 cm for 60 minutes where X, Y, and Z beam breaks were monitored by Activity Monitor software (MedAssociates Inc). The total distance traveled and time spent in the center of the chamber was quantified by this software.

Elevated plus maze: Mice were placed on the elevated plus maze and allowed to explore freely for 5 minutes under full light. Time spent exploring each arm was measured using AnyMaze tracking software.

Three-chamber social interaction: Mice were place in a three-chamber apparatus in which the test mouse was free to explore each chamber. Mice were habituated to the chamber for 5 minutes while two empty wire cups were present (Phase 1). A novel mouse of the same strain and sex (Stranger 1) was placed under one wire cup and the test mouse was left to explore freely for 7 minutes (Phase 2). A second novel mouse of the same strain and sex from a different cage as Stranger 1 (Stranger 2) was then placed under the remaining empty cup and the test mouse was allowed to explore for an additional 7 minutes (Phase 3). The location of Stranger 1 was

alternated in a randomized fashion between test mice, but remained constant between Phase 2 and Phase 3 within each trial. The time spent in each chamber was quantified by AnyMaze tracking software.

Five trial social recognition assay: Mice were placed in a 16 by 16 inch box with an empty wire cup placed in the center and allowed to habituate for 10 minutes. A novel mouse (Stranger 1) of the same strain and sex was placed under the wire cup and a two-minute trial was videotaped. Following a 10-minute interval, Stranger 1 was introduced to the wire cup for another two-minute trial. This was repeated for a total of four trials with Stranger 1. For the fifth trial, a second novel mouse of the same strain and sex from a different cage as Stranger 1 (Stranger 2) was placed under the wire cup and a 2-minute trial was videotaped. For each trial, direct interaction of the test mouse with the wire cup was scored manually by a blinded observer.

Fear conditioning: On training day, mice were placed into an operant chamber with a shock grid (Med Associates, Inc.) in the presence of a 10% vanilla odor cue. Following a three-minute habituation period, two tone-shock pairings were administered consisting of a 30 second tone ending with a one second, 0.7 mA foot shock. Each tone-shock pairing was spaced 30 seconds apart and mice remained in the context for an additional 30 seconds after the second foot shock. On the next day, mice were tested for contextual fear memory by placing each animal back into the same chamber with a 10% vanilla odor cue for three minutes. Time spent freezing during a three-minute testing period was quantified using Video Freeze software. Four hours later, cued fear memory was assessed by placing the mice in a novel context (10% almond, no light). Following one minute of habituation in the novel context, the same auditory cue from conditioning was played for one minute. Freezing during each minute was quantified, and mice that froze > 20% prior to the tone were excluded.

Limb clasping: For each time point assessed, mice were suspended by the tail and video-recorded for 1 minute. Time spent clasping the fore and hindlimbs was quantified by a blinded scorer. For the forepaws, the timer was started when the paws were clearly clasped together and

stopped when they were apart. The time was also counted when a noticeable repetitive “clapping” motion of the forepaws was observed. For the hindpaws, the timer was started when one or both hind limbs began to knuckle in, and the timer was stopped the paws came apart at any point. Time was counted if one paw remained knuckled in while the other came away. For both front and hind paws, the timer was stopped when the back of the mouse was turned to the camera.

Gait analysis: Following a brief training session, mice were video-taped running at a speed of 18 cm/sec on the Treadscan gait analysis system. Discrete video clips of fluid gait were identified by the Treadscan software and manually checked by the experimenter. A foot model was built from *Grm7*$^{+/+}$ mice and used to process gait dynamics in accordance with the manufacturer’s instructions.

Rotarod: Mice were placed on an accelerating rotarod (4 to 40 rpm over three minutes) and the latency to fall from the apparatus was recorded with a cut off of 180 seconds. Mice underwent three trials per day with a rest period of 30-60 minutes between each trial. Data from each day were averaged.

Grip strength: Mice were suspended by the tail and allowed to place their forepaws on a wire grid angled at 45^{o} and attached to a force transducer (SD Instruments). Mice were then pulled by the tail until they let go of the apparatus and the maximal force was recorded. This assay was performed by two separate experimenters and the values for each mouse were averaged.

Seizure evaluation: Mice were handled at least once weekly by being picked up by the tail and placed back into their home cage. Seizure severity was described using the Racine scale defined as: 1 = mouth and/or facial movements, increased digging; 2 = head nodding; 3 = forelimb clonus and tonic tail; 4 = rearing and/or tonic body; 5 = generalized seizure with motor convulsions.

Electroencephalography

Surgery: At 5-6 weeks of age, female *Grm7*$^{+/+}$ and *Grm7*$^{-/-}$ mice were surgically implanted under isoflurane anesthesia with a telemetric transmitter (HD-X02; Data Sciences International [DSI], Minneapolis, MN) for recording EEG, electromyography (EMG), and motor activity as previously described[197–199]. Transmitters were implanted subcutaneously just off the midline of the dorsal flank of each mouse under aseptic conditions. Transmitter leads were tunneled subcutaneously to the skull. Holes were drilled in the skull and exposed wires were placed directly in contact with the dura and secured via dental cement (Butler Schein, USA). One lead was placed at +1mm AP, -2mm ML and the other was placed at -3mm AP, +2mm ML. An additional set of leads was placed bilaterally in the nuchal muscle for EMG recording. Animals were individually housed following surgery for the duration of the study and allowed to recover for a minimum of one week prior to the first EEG recording.

Recordings: Uninterrupted EEG recordings occurred every four weeks between 8 and 20 weeks of age. Approximately 12 hr before each EEG study began, mice were moved into the recording room for habituation. EEG and EMG were recorded from the home cage of each animal continuously for 48 hr beginning at the onset of the light cycle on the day of each study. Telemetric EEG and EMG waveform data were collected using Ponemah software (DSI). Data were continuously sampled at a rate of 250 Hz and transmitted via a receiver (RPC-1; DSI) placed below the cage of each mouse to a computer for off-line analysis. For the amphetamine challenge, a 30 min baseline EEG recording was obtained prior to subcutaneous administration of 2.25 mg/kg amphetamine (3 mg/kg amphetamine sulfate) followed by an additional 2.5 hrs of EEG recording.

Sleep staging and analysis: Trained observers, blinded to condition (age, genotype or pharmacological challenge) scored each five-second epoch using Neuroscore 3.0 software to determine sleep/wake stages, including wake, non-rapid eye movement (NREM) or rapid eye movement (REM) sleep based on accepted characteristic oscillatory patterns as previously

published by our group[197–199]. The amount of time in each stage (wake, NREM, REM) during each 12-hr period (light, dark), along with bout numbers and duration, were quantified. Power spectra were computed in 1Hz bins from 0.5 to 80 Hz using a Fast Fourier Transform with a Hamming window and overlap ratio of 0.5 for each mouse in 5-sec epochs. Spectral power was examined across the entire spectrum within discrete states (e.g. Wake, NREM or REM). We examined power within pre-defined frequency ranges (Delta [0.5-4Hz], Theta [4-8 Hz], Alpha [8-13 Hz], Beta [13-30 Hz], Low Gamma [30-50 Hz], and High Gamma [50-80 Hz]) by averaging the power from all 5-sec epochs within that state to yield the state-dependent relative power spectrum in either 12 hr light or 12 hr dark periods as previously described[199]. To examine effects of amphetamine on EEG, spectral power within the frequency bands defined above were averaged across the 30 min baseline period; power during waking epochs only was then binned in 10 min bins and expressed as a percent change from the 30-minute baseline. Activity counts were quantified and expressed in 10 min bins.

Statistical Analysis

All data shown represent mean ± SEM. Statistical significance between groups was determined by an unpaired t-test, paired t-test or ANOVA with Bonferroni comparisons where appropriate. For each figure, the number of animals of each sex per group is indicated in the figure legend. In all cases, p-values are indicated as *$p < 0.05$, **$p < 0.01$, ***$p < 0.001$, ****$p < 0.0001$.

CHAPTER IV. Identification and functional characterization of the *GRM7* point mutation c.461T>C, p.I154T in patients with developmental delay and epilepsy

Preface

Work in this chapter has been submitted to *JCI Insight* and is currently under revision. All clinical data was provided by Aqeela Al-Hashim and Manar Samman. Aditi Buch performed the Western blots in Figure 19 and assisted with behavioral experiments. Hana Badivuku assisted with genotyping and the experiments in Figure 16D-E. All other experiments were performed and analyzed by me. The $mGlu_7$-I154T mouse line generated by the Vanderbilt Genome Editing Resource, and I performed the validation of this line.

Introduction

The metabotropic glutamate (mGlu) receptors are a class of G protein-coupled receptors that bind glutamate, the major excitatory neurotransmitter, and activate intracellular signaling pathways that modulate synaptic transmission and plasticity[47]. The metabotropic glutamate receptor subtype 7 ($mGlu_7$) is a presynaptic $G_{i/o}$-coupled receptor with widespread expression on glutamatergic and GABAergic neurons and its activation leads to both constitutive and activity-dependent inhibition of neurotransmitter release[74,78,99]. In recent years, whole exome sequencing studies have identified rare deletions and variants in *GRM7*, the human gene encoding $mGlu_7$, in patients with neurodevelopmental disorders. Heterozygous deletions and point mutations have been reported in patients with autism spectrum disorder[153–155] and attention deficit hyperactivity disorder[19], while homozygous point mutations have been found in rare cases of severe developmental delay, microcephaly and epilepsy[31,32,200]. However, the consequence of these mutations on $mGlu_7$ receptor function and a causal role in disease pathogenesis has not yet been determined.

Here, we present new clinical cases of two sisters with severe developmental delay and epilepsy confirmed to be homozygous for a *GRM7* variant c.461T>C p.Ile154Thr ($mGlu_7$-I154T).

This variant was first identified by whole exome sequencing in two brothers in 2016, and detailed clinical information was recently published.[31,200] Functional studies of the $mGlu_7$-I154T mutant protein in HEK293A cells and knock-in mice reveal that this single amino acid change is sufficient to significantly reduce $mGlu_7$ protein levels and produce a range of neurological phenotypes in mice, thus providing further support for *GRM7* as a causative gene in neurodevelopmental disorders.

Results

Identification of the *GRM7* c.461T>C, p.Ile154Thr variant in a family from Saudi Arabia

We have identified a family from Saudi Arabia in which the recessive *GRM7* variant c.461T>C p.Ile154Thr segregates with severe developmental delay. Two female siblings from a consanguineous marriage presented with similar clinical features including intellectual disability, microcephaly, epilepsy, motor stereotypes, and motor impairment with early onset hypotonia that progressed into peripheral hypertonia and spasticity. Both pregnancies were uneventful with no antenatal or post-natal complications.

The eldest daughter, now age 9, (individual II.4, Figure 14A) developed hemi-convulsive focal seizures at 20 days of age, which were treated with phenobarbital for several months. Once treatment was stopped, she remained seizure free until the age of 7 years when she developed nocturnal myoclonic seizures. These nocturnal seizures have since been controlled by levetiracetam. This patient exhibited global developmental delay from birth. She sat at 4 years and walked at 7 years of age. She is nonverbal and unable to comprehend or follow simple commands. She exhibited stereotyped clasping hand movements and head nodding at an earlier age, but these features have recently resolved.

The other daughter, now age 4, (individual II.5, Figure 14A) experienced her first seizure at 4 months of age. Her seizures were myoclonic and focal clonic in nature and have since been controlled by treatment with levetiracetam. This patient sat at the age of 2.5 years and is not yet

ambulatory. She developed head nodding behavior that is similar to that of her sister. Both siblings displayed abnormal electroencephalograms (EEG), which showed frequent multifocal epileptiform discharges over the centro-parietal region enhanced by sleep. Magnetic resonance imaging (MRI) demonstrated diffuse brain atrophy, thin corpus callosum, patchy T2 hyperintensities in subcortical and deep periventricular white matter consistent with hypomyelination (individual II.4, Figure 14B).

Whole exome sequencing (WES) was performed for the eldest sibling (Figure 14A, individual II.4) and did not identify any variants in genes known to cause neurodevelopmental disorder or epilepsy at that time. A candidate variant was identified in *GRM7*, c.461T>C; p.Ile154Thr. This variant segregated appropriately after Sanger sequencing of all immediate family members: the two affected siblings were homozygous for this variant while the remainder of the family were heterozygous carriers (Figure 14C). The heterozygous carriers are asymptomatic with no history of any neurological or psychiatric illness. This mutation has also been identified in another family in Saudi Arabia with brothers with similar neurodevelopmental symtpoms,[31,200] and one additional heterozygous case is noted in the gnomAD database in an individual of European descent (Version 3, https://gnomad.broadinstitute.org).

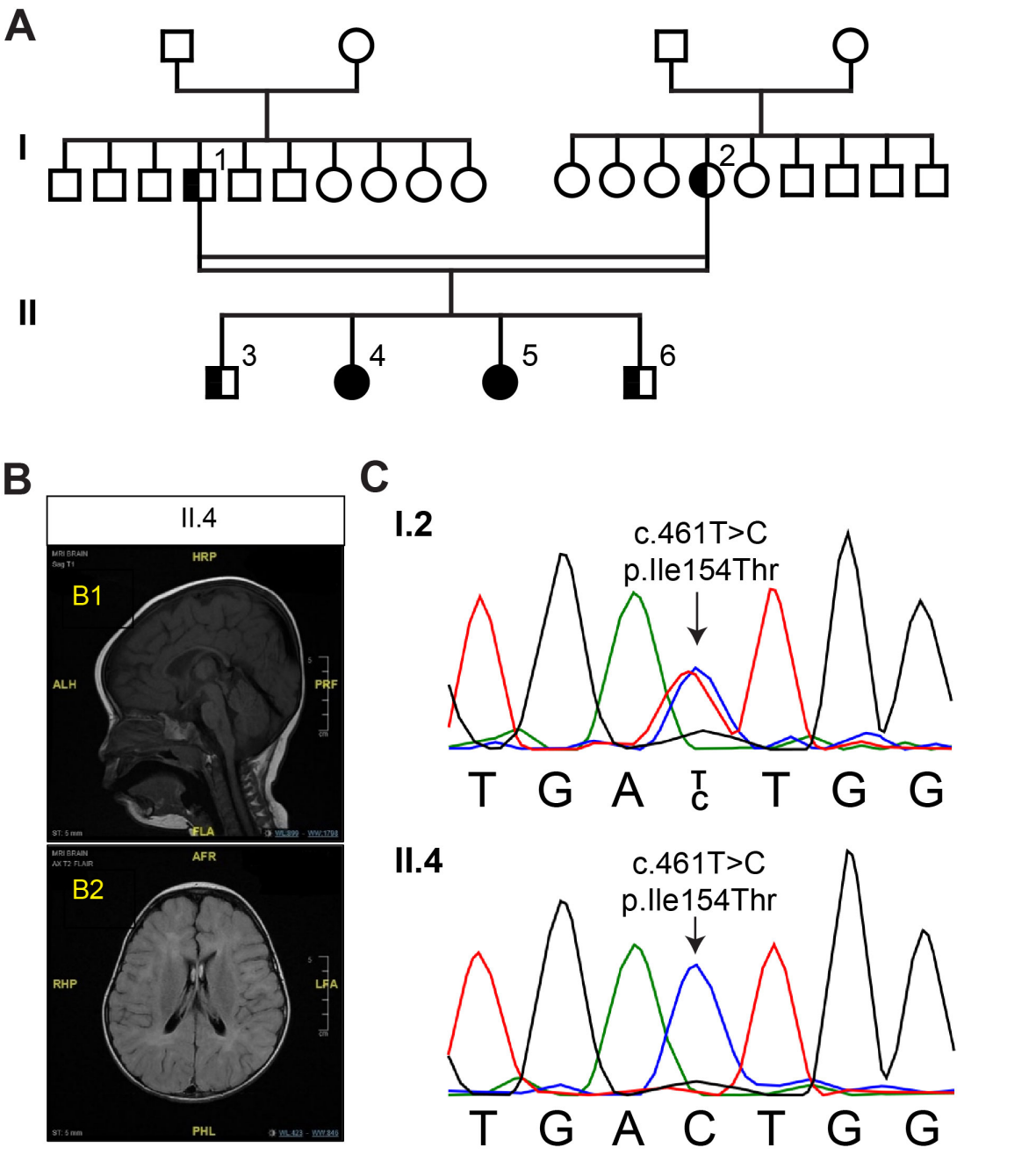

Figure 14. The *GRM7* c.461T>C, p.Ile154Thr variant segregates with neurodevelopmental disorder and epilepsy.

A) Family pedigree demonstrating affected subjects. II.4 and II.5 are proband; I.1, I.2, II.3 and II.6 are all unaffected. B) MRI images of affected individual II.4. B1 is a sagittal T1 image demonstrating the finding of thin corpus callosum. B2 is an axial FLAIR image demonstrating diffuse brain atrophy with multiple patchy T2 hyperintensity in both cerebral hemispheres in subcortical and deep periventricular regions. C) Sanger sequencing of the *GRM7* gene from unaffected individual I.2 showing the heterozygous variant and the affected individual II.4 showing the homozygous variant.

We next sought to characterize the functional consequence of the *GRM7* c.461T>C; p.Ile154Thr variant (here on referred to as $mGlu_7$-I154T) to confirm that this mutation is sufficient to cause disease. Interestingly, *Grm7* knockout mice display several phenotypes that mirror those reported in the patients above. These include learning deficits, seizures, motor impairments and stereotyped paw clasping[175]. Based on this phenotypic overlap, we hypothesized that the $mGlu_7$-I154T substitution would lead to loss of receptor function.

The I154T mutation impairs the dimerization of $mGlu_7$ via its extracellular domain

The mGlu receptors are obligate dimers, and each monomer of the dimer contains a large extracellular domain (ECD), a 7-transmembrane domain, and a C-terminal cytoplasmic tail. The ligand-binding domain is within the ECD and is comprised of an upper lobe (LB1) and a lower lobe (LB2). This domain assumes an open-open inactive state and a closed-closed active state upon glutamate binding[50]. Isoleucine 154 is positioned within a hydrophobic region of LB1, notably distant from the glutamate binding pocket (Figure 15A). When compared to the amino acid sequence of other mGlu subtypes, this isoleucine residue is highly conserved (Figure 15B). Several studies have implicated LB1 as an important interface for receptor dimerization in the inactive state[53,54], and it has been previously shown that the ECD domains of $mGlu_1$, $mGlu_4$ and $mGlu_5$ are secreted into media as a disulfide-bonded dimer when expressed in cell culture[201–204]. To test whether the I154T mutation might disrupt receptor dimerization, we assessed the ability of a soluble ECD to dimerize upon introduction of the I154T mutation. We expressed HA-tagged ECDs (HA-ECD-WT and HA-ECD-I154T) in HEK293A cells and collected both whole cell lysate and culture media. In the absence of a reducing agent, HA-ECD-WT from cell lysate appeared as both a dimer and monomer by Western blot, but was present in only a dimeric form in the culture media (Figure 15C). HA-ECD-I154T appeared as a monomer in cell lysate, but was barely detectable as a dimer in either cell lysate or media (Figure 15C). Dimer bands were fully reduced

to a monomeric form upon addition of dithiothreitol (DTT) (Figure 15D). These results suggest that I154T disrupts the covalent dimerization, trafficking, and/or secretion of the $mGlu_7$ ECD.

We next tested whether HA-ECD-I154T could be trafficked to the cell surface through dimerization with a full-length WT receptor. Previously studies have demonstrated that the soluble mGlu ECDs can be retained on the cell surface only when co-expressed with a full-length receptor, and this has been utilized as a measure of mGlu dimerization[70,204]. To further test the effect of I154T on ECD dimerization and trafficking, we expressed HA-ECD-WT and HA-ECD-I154T constructs either alone or in combination with a full-length MYC-$mGlu_7$-WT protein and measured surface expression of the N-terminal epitope tag by on-cell ELISA (Figure 15E). When expressed alone, HA-ECD-WT or HA-ECD-I154T had comparable intracellular expression (Figure 15F), but were not detectable on the cell surface (Figure 15G). When expressed with the full length MYC-$mGlu_7$-WT construct, we detected a significant increase in HA surface staining for HA-ECD-WT cells but not for HA-ECD-I154T cells (Figure 15G). Surface expression of the full length MYC-$mGlu_7$-WT remained constant in these experiments (Figure 15H). These results further confirm that I154T disrupts receptor dimerization and trafficking.

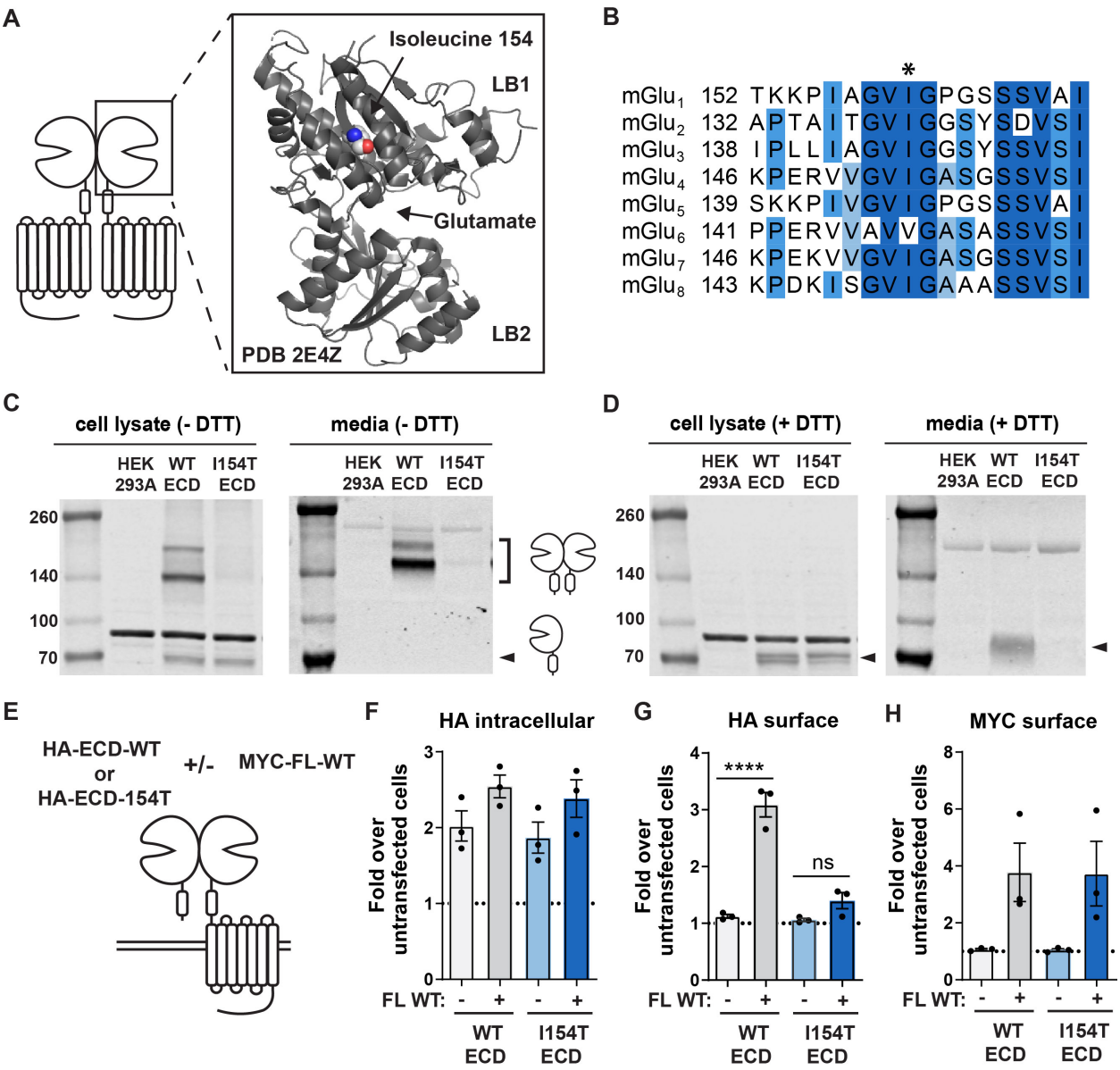

Figure 15. The I154T substitution disrupts the interaction of two ECDs within an mGlu$_7$ dimer.

A) Location of isoleucine 154 in the structure of the mGlu$_7$ ECD. PBD 2E4Z. B) Protein sequence alignment of all eight human mGlu receptor subtypes. Darker shades of blue indicate increased conservation. C) Western blot of total protein lysates and media from cells expressing HA-ECD-WT and HA-ECD-I154T constructs in the absence of DTT. D) Western blot of total protein lysates and media from cells expressing HA-ECD-WT and HA-ECD-I154T constructs in the presence of DTT. E) Experimental design for cell surface ELISA experiments. FL = full length. F-H) Quantification of F) intracellular HA signal, G) surface HA signal, and H) surface MYC signal. N = 3 independent experiments with 3 technical replicates each. One-way ANOVA with Tukey multiple comparisons. ****p < 0.0001.

$mGlu_7$-I154T receptors exhibit reduced surface trafficking and are degraded by the proteasome

When expressed as a full-length receptor in HEK293A cells, HA-$mGlu_7$-I154T exhibited a striking reduction in total protein expression quantified by Western blot, along with altered banding patterns (Figure 16A). In the presence of DTT, HA-$mGlu_7$-WT appeared primarily as a dimeric band with two additional monomeric bands. Expression levels of the dimer and upper monomer band were significantly reduced in cells transfected with HA-$mGlu_7$-I154T, while expression of the lower monomer band was increased (Figure 16B). The monomer to dimer ratio in these blots was significantly increased for HA-$mGlu_7$-I154T (Figure 16C), consistent with weakened dimerization. Park et al. recently showed that the lower monomer band observed in heterologous cells represents an immature form of $mGlu_7$ that is sensitive to endoglycosidase H (EndoH), whereas the upper monomer and dimer bands represent forms of $mGlu_7$ with mature glycosylation that are resistant to EndoH but sensitive to peptide:N-glycosidase F (PNGaseF)[205]. To confirm this in our hands, we treated cell lysates with peptide:N-PNGase F and EndoH. As expected, PNGase F, which removes almost all N-linked glycosylation, reduced the size of all $mGlu_7$ bands (Figure 16D) and only the lower monomer band was sensitive to EndoH in both WT and I154T cells (Figure 16E). Since this band represents an immature form of $mGlu_7$ present in the endoplasmic reticulum (ER) or early Golgi apparatus and given that mGlu receptors are known to dimerize in the ER[202], we hypothesized that I154T receptors are degraded by the proteasome through ER-associated degradation[206]. Consistent with this hypothesis, treatment with the proteasome inhibitor MG-132 (10 μM) for 4 hours led to a significant increase in the expression of HA-$mGlu_7$-I154T dimer and monomer bands while having no significant effect on HA-$mGlu_7$-WT expression (Figure 16F-H).

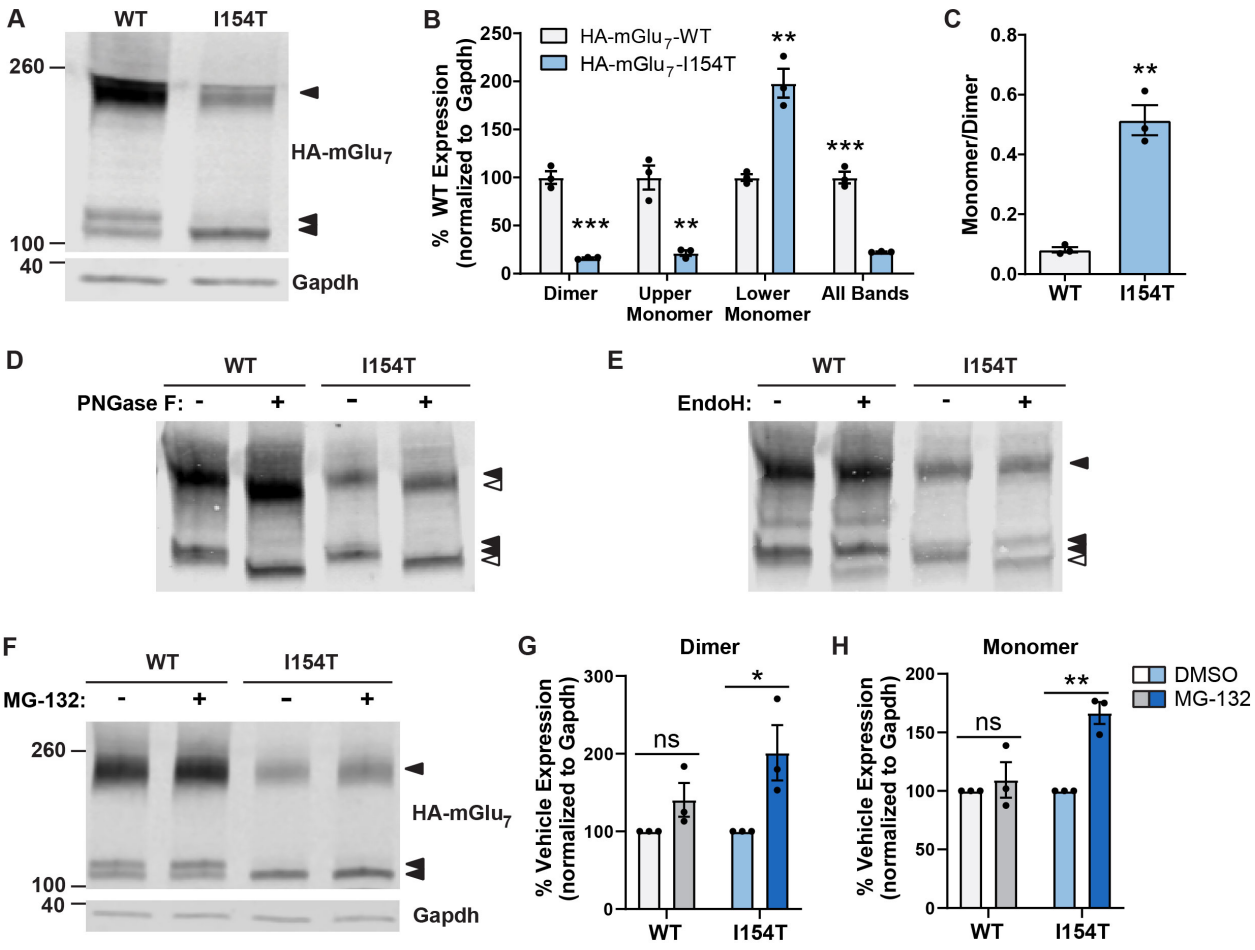

Figure 16. HA-mGlu$_7$-I154T receptors exhibit reduced surface trafficking in HEK293A cells and are degraded by the proteasome.

A) Western blot of total protein lysate from HEK293A cells expressing HA-mGlu$_7$-WT or HA-mGlu$_7$-I154T. B) Quantification of different immunoreactive bands representing mGlu$_7$. C) Quantification of dimer to monomer ratio. For B-C, N = 3 biological replicates. Student's t-tests. **p < 0.01, ***p < 0.001. D) Western blot in the presence or absence of PNGase F treatment. E) Western blot in the presence or absence of EndoH treatment. For panels D-E, open arrows indicate bands resulting from deglycosylation. N = 3 independent experiments. F) Western blot of cell lysates following a 4-hour treatment with 10 μM MG-132 or vehicle (DMSO). G-H) Quantification of mGlu$_7$ dimer (G) and monomer (H) bands following MG-132 treatment. N = 3 independent experiments. Two-way ANOVA with Sidak's multiple comparisons. *p < 0.05, **p < 0.01.

mGlu$_7$-I154T receptors are expressed on the cell surface and have retained function

We next sought to determine the level of surface expression of mGlu$_7$-I154T receptors. We measured cell surface expression by on-cell ELISA and found a significant reduction in surface HA staining in cells transfected with HA-mGlu$_7$-I154T (Figure 17A). When normalized to permeabilized wells, HA-mGlu$_7$-I154T cells also exhibited a decreased surface to intracellular ratio, consistent with a deficit in forward trafficking (Figure 17B). Since a population of surface HA-mGlu$_7$-I154T receptors was detectable, we next tested the functionality of HA-mGlu-I154T receptors using a thallium flux assay (described in 207). Cells stabling expressing HA-mGlu$_7$-WT, along with G protein-coupled inwardly rectifying potassium (GIRK) channels, exhibited a concentration-dependent response to the agonist L-AP4 (Figure 17C). HA-mGlu$_7$-I154T cells responded to agonist application, but the maximum response was significantly reduced (Figure 17C, D). These data demonstrate that HA-mGlu$_7$-I154T receptors have the potential to become activated upon pharmacological stimulation if they are properly trafficked to the cell surface.

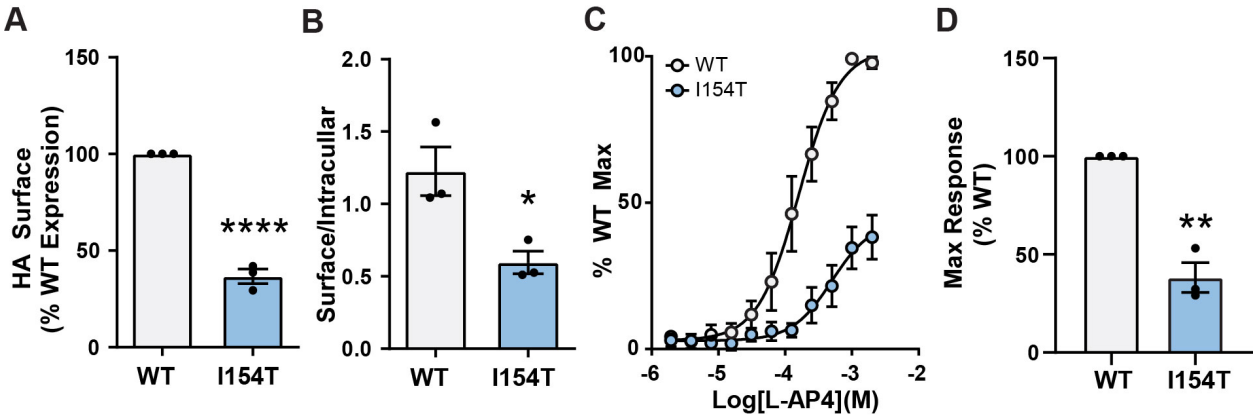

Figure 17. mGlu$_7$-I154T receptors are expressed on the cell surface and are functional.

A) Quantification of surface HA signal in HEK293A cells expressing HA-mGlu$_7$-WT or HA-mGlu$_7$-I154T as measured by cell surface ELISA. B) Quantification of surface to intracellular ratio for HA signal in cell surface ELISA experiments. For A-B, N = 3 individual experiments with 3 technical replicates each. Student's t-tests. *$p < 0.05$, ****$p < 0.0001$. C) Concentration response curves of cells expressing HA-mGlu$_7$-WT and HA-mGlu$_7$-I154T in the thallium flux assay. D) Quantification of maximum response in thallium flux assay. Student's t-test. **$p < 0.01$. For C-D, N = 3 independent experiments with 2 technical replicates each.

mGlu$_7$-I154T expression is reduced *in vivo* at the post-transcriptional level

To determine the main effect of mGlu$_7$-I154T *in vivo,* we generated a knock-in mouse model using CRISPR/Cas9 technology to introduce the I154T mutation in the endogenous mouse *Grm7* gene (Figure 18).

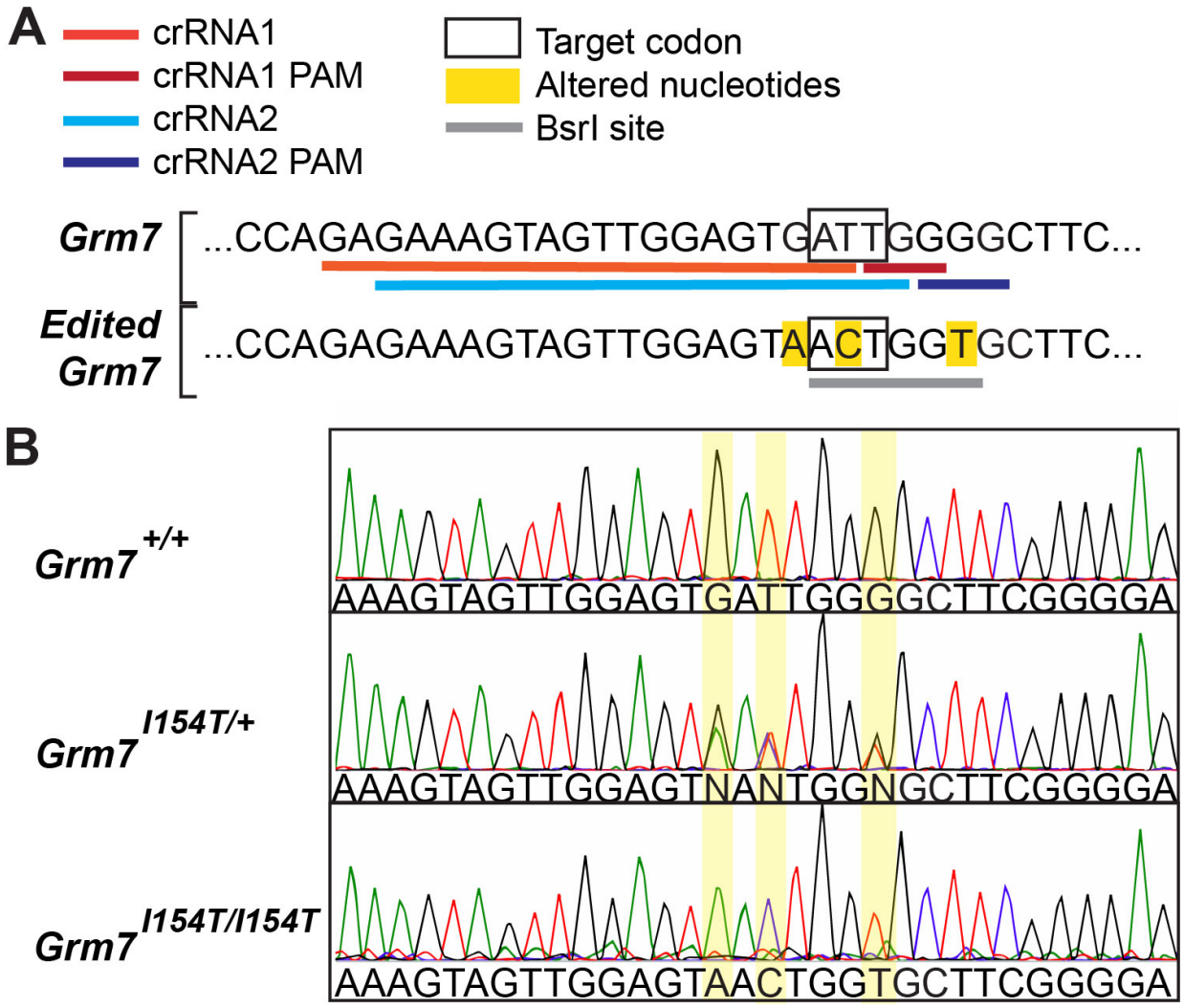

Figure 18. Generation of mGlu$_7$-I154T knock-in mouse by CRIPSR/Cas9.
A) Diagram of editing strategy targeting exon 1 of mouse *Grm7*. B) Representative Sanger sequencing results to confirm the presence of the expected single base substitutions

Western blots of total protein lysate isolated from brain tissue of wildtype (*Grm7*$^{+/+}$), heterozygous (*Grm7*$^{I154T/+}$) and homozygous (*Grm7*$^{I154T/I154T}$) littermates revealed a ~50% reduction in $mGlu_7$ protein expression in *Grm7*$^{I154T/+}$ mice and little to no expression in *Grm7*$^{I154T/I154T}$ mice across three brain regions (Figure 19A-C). In mouse tissue, only one monomeric band was detectable; this band was resistant to EndoH treatment in controls (Figure 20) and was weakly detectable in *Grm7*$^{I154T/I154T}$ mice (Figure 19C). Quantification of *Grm7* mRNA transcripts from each brain region by qRT-PCR revealed no difference between genotypes (Figure 19D), confirming that $mGlu_7$-I154T is degraded at the post-transcriptional level *in vivo*.

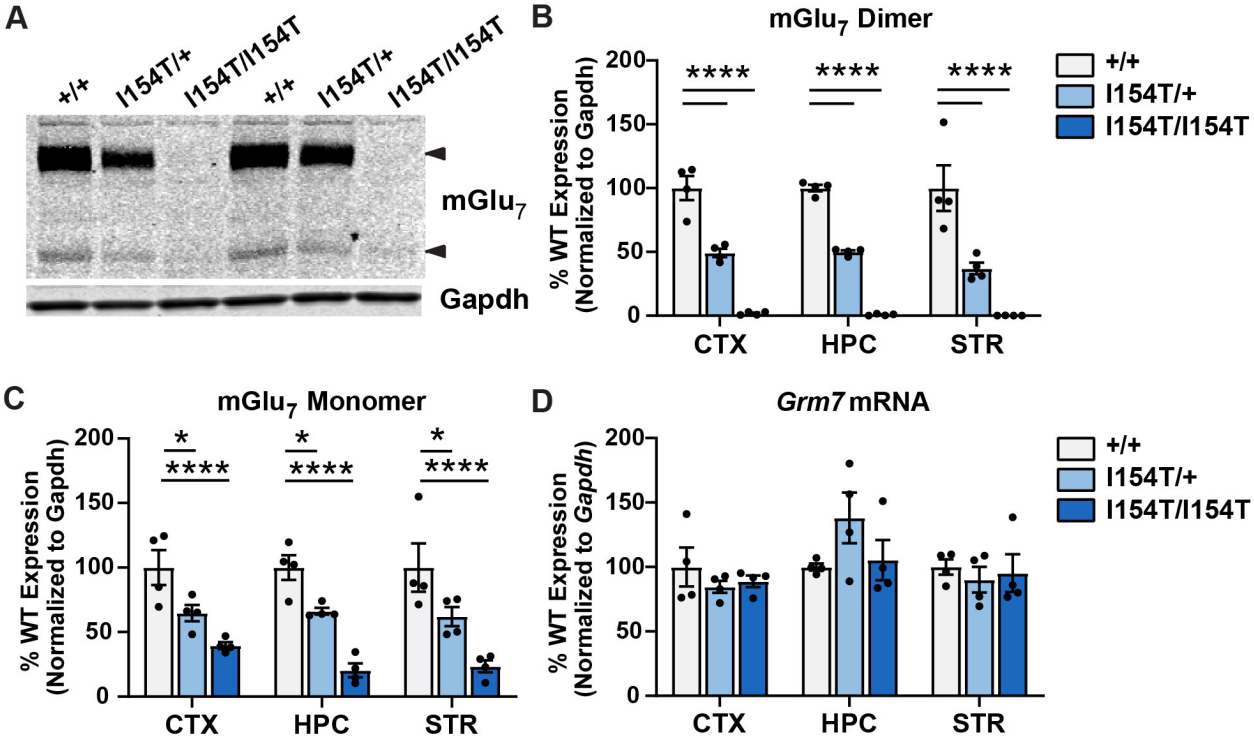

Figure 19. $mGlu_7$-I154T expression is reduced in vivo at the post-transcriptional level.

A) Western blot of total protein lysate from cortex of *Grm7*$^{+/+}$ (+/+), *Grm7*$^{I154T/+}$ (I154T/+) and *Grm7*$^{I154T/I154T}$ (I154T/I154T) mice. Arrows indicate $mGlu_7$ bands. B-C) Quantification of the $mGlu_7$ dimer band (B) and monomer band (C) across three brain regions. CTX = cortex, HPC = hippocampus, STR = striatum. Two-way ANOVA with Dunnett's comparisons to *Grm7*$^{+/+}$. *p < 0.05, ***p < 0.001, ****p < 0.0001. D) *Grm7* mRNA transcript expression across each brain region. No significant difference by two-way ANOVA. For all panels, N = 4 mice per genotype (2 male, 2 female).

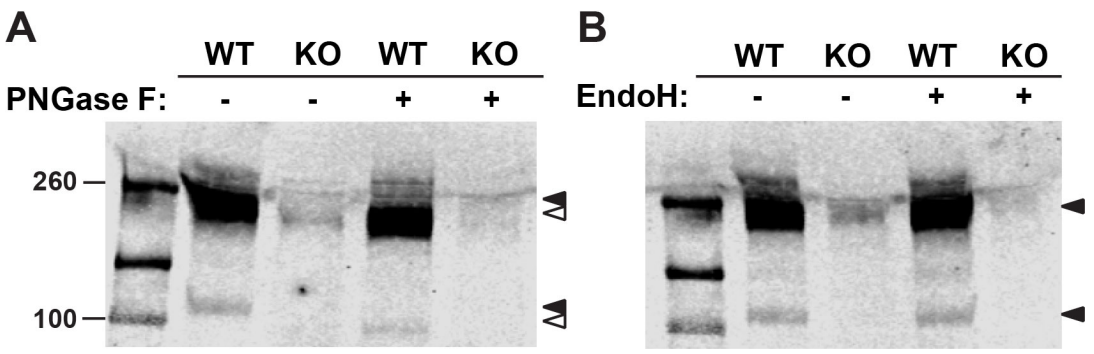

Figure 20. $mGlu_7$ detected from mouse tissue is N-glycosylated but resistant to EndoH. Western blot of total protein lysate from mouse hippocampus in the presence or absence of A) PNGase F treatment or B) EndoH treatment. Open arrows indicate bands resulting from deglycosylation. Tissue from *Grm7*$^{-/-}$ (KO) mice was included to confirm antibody specificity.

Mice homozygous for $mGlu_7$-I154T exhibit deficits in motor coordination and associative learning in addition to seizures

We next evaluated $mGlu_7$-I154T knock-in mice for phenotypes analogous to the clinical presentation of the patients described above and consistent with those reported in *Grm7* knockout animals. We found that *Grm7*$^{I154T/I154T}$ mice exhibited a small but significant reduction in body weight (Figure 21A). Spontaneous locomotion in an open field test was not different between genotypes (Figure 21B). Despite no gross changes in locomotion, *Grm7*$^{I154T/I154T}$ mice exhibited decreased performance on the accelerating rotarod task (Figure 21C) and developed a limb clasping phenotype (Figure 21D). We also tested associative memory by contextual fear conditioning and found that *Grm7*$^{I154T/I154T}$ mice exhibited significantly decreased freezing when re-exposed to the conditioning context 24 hours after training (Figure 21E). General health was assessed weekly until 20 weeks of age, and during this routine handling, convulsive seizures were observed in 8/23 *Grm7*$^{I154T/I154T}$ mice and never observed in littermates. These seizures were similar in nature to what we previously observed in *Grm7* knockout mice[175].

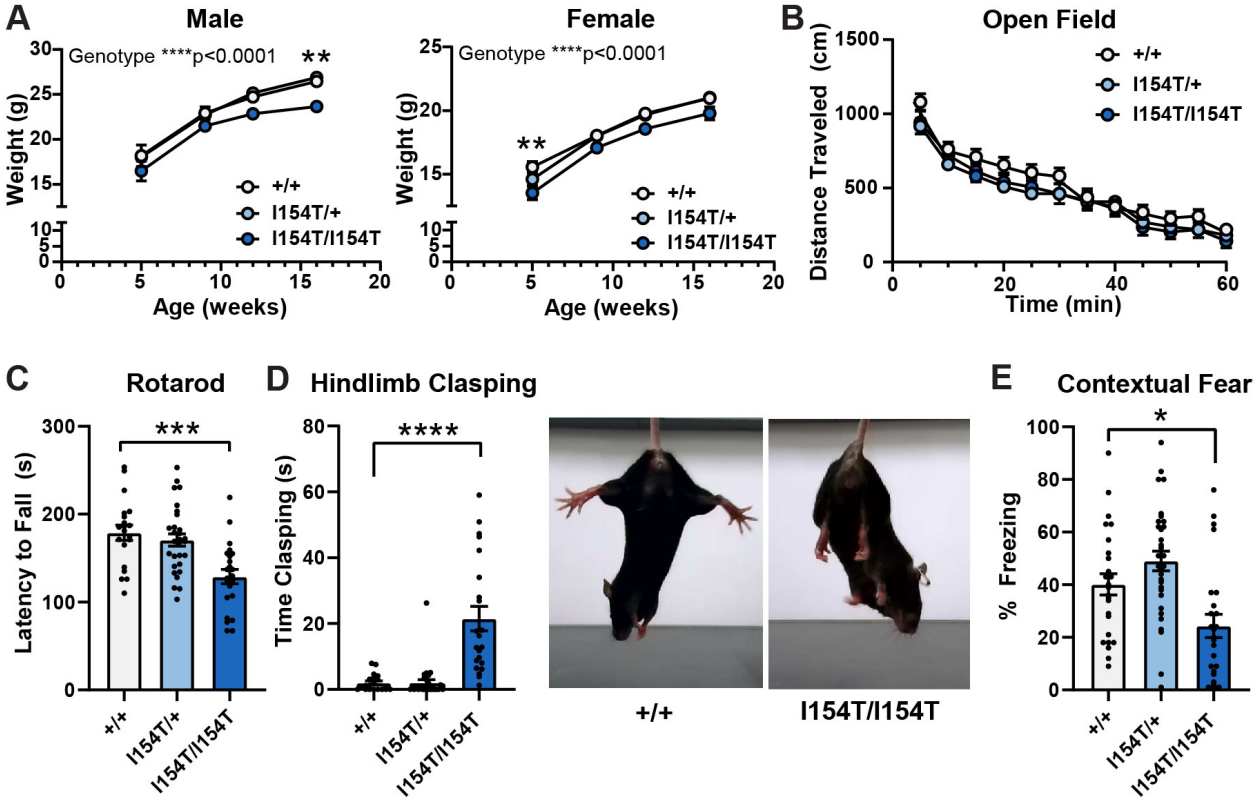

Figure 21. Mice homozygous for mGlu$_7$-I154T exhibit deficits in motor coordination and associative learning.

A-B) Weight over time of male and female mice. Genotypes are as follows: *Grm7*$^{+/+}$ (WT), *Grm7*$^{I154T/+}$ (I154T/+) and *Grm7*$^{I154T/I154T}$ (I154T/I154T). N = 6-11 mice per genotype for each sex. Two-way ANOVA with Dunnett's comparisons to *Grm7*$^{+/+}$. **p < 0.01, ****p < 0.0001. B) Spontaneous activity over time in an open field. C) Latency to fall from an accelerating rotarod. D) Quantification of hindlimb clasping. Representative photos shown at right. E) Percent freezing in a contextual fear assay 24 hours following training. For B-E, N = 20-32 mice per genotype (males and females combined). One-way ANOVA with Dunnett's comparisons to *Grm7*$^{+/+}$. *p < 0.05, ***p < 0.001, ****p < 0.001.

Discussion

Here we present new clinical findings in parallel with the first functional characterization of a disease-associated mutation affecting the $mGlu_7$ receptor. Recently, biallelic mutations in *GRM7* were reported in 11 patients from six unrelated families, two of whom have the same mutation described here[200]. All affected children were reported to exhibit global developmental delay, intellectual disability, epilepsy, and microcephaly. The phenotype of the individuals presented here matches what has been published[31,200]. Their seizures have responded well to antiepileptic drugs, which is similar to patients with the same variant, but contrasts with six patients with other variants who exhibited drug-resistant epilepsy[200]. We also noted transient stereotypic movements in the form of head nodding and hand clasping. Stereotypic hand clasping is well recognized as a hallmark of the neurodevelopmental disorder Rett syndrome (RTT). Interestingly, $mGlu_7$ has been proposed as a novel target for Rett syndrome due to decreased $mGlu_7$ expression in RTT autopsy tissue and $mGlu_7$'s role in promoting synaptic plasticity[138]. Activation of $mGlu_7$ can regulate release of glutamate and GABA, both of which have been shown to contribute to RTT-related phenotypes[149,208,209]. Taken together with the fact that *Grm7* knockout mice recapitulate phenotypes often observed in neurodevelopmental disorders[175], it was likely that *GRM7* clinical variants would lead to loss-of-function of the $mGlu_7$ receptor. However, this hypothesis had not been directly tested and so we sought to determine the functional consequence of the $mGlu_7$-I154T mutation.

Our data demonstrate that the I154T substitution reduces receptor dimerization, impairs cell surface trafficking, and ultimately leads to a significant decrease in total receptor expression. Isoleucine 154 is situated in the core of the LB1 domain, which harbors residues that are important for resting state dimerization of mGlu receptors[53,54]. mGlus are also known to dimerize in the ER[202], resulting in the possibility that weakened dimerization and/or stability may lead to ER retention of $mGlu_7$-I154T. Interestingly, mutations affecting the N-terminal domain of $mGlu_6$ have been shown to accumulate in the ER[210]. In support of this hypothesis, we observed an

accumulation of an EndoH-sensitive band in HEK293A cells expressing HA-mGlu$_7$-I154T representing an early glycosylated form of the receptor. We also observed an increase in mGlu$_7$-I154T expression in cells treated with a proteasome inhibitor, but no significant effect on mGlu$_7$-WT receptors with our treatment conditions. These findings suggest that mGlu$_7$-I154T receptors are degraded in part by the proteasome, which is the final step of the ER-associated degradation pathway. It should be noted that degradation of mGlu$_7$ by the proteasome has also been shown to occur following agonist-induced receptor internalization, a distinct process from ER-associated degradation[90], and that fully de-glycosylated mGlu$_7$ is degraded by the autophagolysosomal degradation pathway[205]. The mechanisms that regulate ER export and early trafficking of mGlu$_7$ are currently poorly understood, and the relative importance of dimerization and N-glycosylation remain to be determined.

In mice homozygous for the I154T mutation, mGlu$_7$ protein expression was nearly absent, suggesting that mGlu$_7$ is more tightly regulated in neurons compared to HEK293A cells. We observed no change in *Grm7* mRNA transcript levels in brain tissue, confirming that the mGlu$_7$-I154T receptor is degraded at the post-transcriptional level *in vivo*. Altogether, these data demonstrate that mGlu$_7$ protein expression is highly regulated by quality-control mechanisms that recognize and degrade mGlu$_7$-I154T receptors, and that the ECD plays a critical role in protein expression and trafficking. Consistent with an almost complete lack of mGlu$_7$ protein expression, *Grm7*$^{I154T/I154T}$ mice exhibit similar phenotypes as those reported in global mGlu$_7$ knockout mice, including deficits in motor coordination, impaired contextual fear memory and seizures[68,115,175]. Importantly, these phenotypes parallel the clinical description of patients that are homozygous for this variant.

Despite having about 50% protein expression, heterozygous *Grm7*$^{I154T/+}$ animals appear phenotypically normal, similar to our previous finding that *Grm7*$^{+/-}$ mice were no different from their wildtype littermates[175]. The lack of phenotype in *Grm7*$^{I154T/+}$ mice suggests that I154T receptors do not have a significant dominant negative effect on WT mGlu$_7$ receptors or other

mGlu receptor subtypes *in vivo*. We predict that in the heterozygous state, I154T receptors are degraded early in biosynthesis and that essentially all expressed $mGlu_7$ protein is wildtype. The heterozygous carriers in the family presented here were asymptomatic; however, heterozygous deletions in *GRM7* have been reported in patients with ASD and ADHD[19,154]. Therefore, heterozygous *GRM7* mutations may be associated with disease only in the presence of other genetic or environmental factors. Altogether, the clinical, biochemical and mouse model data presented here establish that the recessive $mGlu_7$-I154T variant can cause a neurodevelopmental syndrome in humans by essentially producing the same effect as gene deletion. Future studies, both clinical and preclinical, should address how modest reductions in $mGlu_7$ expression may increase the risk of disorders such as ASD and ADHD.

In future studies, it will also be important to test whether other clinical *GRM7* mutations lead to loss-of-function and delineate whether this loss is due to reduced receptor expression or function. If some variants lead to altered function with retained expression, there may be an opportunity for therapeutic intervention by treatment with compounds that modulate the activity of $mGlu_7$, such as positive allosteric modulators. In the case of $mGlu_7$-I154T, it appears that a therapeutic strategy would need to be aimed at increasing receptor stability, trafficking and/or expression due to the extremely low expression observed in our mouse model. In order to design such compounds, a better understanding of the mechanisms that regulate $mGlu_7$ trafficking and expression is needed. The retained function of I154T receptors in heterologous cells (Figure 17C-D) provides proof-of-concept that this approach could be successful.

Another interesting outcome from this work is an association between $mGlu_7$ and myelination. Patients with homozygous *GRM7* variants exhibited characteristic neuroimaging features of cerebral atrophy and a thin corpus callosum, the latter of which reflects a paucity of white matter and a hypomyelinated state[200]. This consistent finding of brain hypomyelination is the first evidence to our knowledge that $mGlu_7$ signaling may play a role in myelin formation and/or maintenance. The presence of ionotropic and metabotropic glutamate receptors on

oligodendrocytes and their precursor cells has been established in previous studies, and it is known that glutamatergic signaling can contribute to excitotoxicity of these cells under pathological conditions[211,212]. $mGlu_3$ and $mGlu_5$ receptors are expressed in oligodendrocyte precursor cells[213], and $mGlu_4$ receptors have been shown to promote oligodendrocyte maturation and survival[214]. $mGlu_7$ has recently been shown to be expressed in both oligodendrocytes and precursor cells in mouse neocortex[70,215]. The role of $mGlu_7$ in these cell types will be an interesting topic for future studies. Activation of neuronal $mGlu_7$ would be expected to mitigate excessive glutamate release and may protect oligodendroctyes from excitotoxicity; however, this hypothesis remains to be tested.

In summary, the clinical and functional data presented here demonstrates that a homozygous point mutation in the $mGlu_7$ receptor is sufficient to cause disease phenotypes through a loss of receptor expression. Therefore, loss-of-function mutations in *GRM7* should be considered as a potential underlying cause for patients with unexplained developmental delay and epilepsy.

Methods

Whole Exome Sequencing

Whole exome sequencing was performed for the index case (individual II.4, Figure 1A). DNA libraries were constructed using the Agilent SureSelect kit (Version 5). Quality control for insert size and library representation was performed using Agilent Bio-analyzer and qPCR, respectively. Sequencing was undertaken using an Illumina HiSeq 4000 to an average depth of coverage of 75x-150x with automated adapter trimming of the fastq sequences. DNA alignment, variant identification and quality filtering were undertaken using commercially available algorithms (XNG (DNASTAR v13.0a-d/v14.0 - Madison, USA) using default parameters). Human reference assemblies were aligned against GRCh37.p13 with variant annotation using dbNSFPv.2.9.0 and dbSNP146 databases.

Non-synonymous homozygous/hemizygous variant (SNP/indel) selection was performed using preliminary filtering parameters including a minimum depth of coverage of 20x, pNotRef ≥ 0.9 (internal probability calculation from MAQ (Mapping and Alignment Quality algorithm) that the variant is not the reference), Q call (Phred base quality score) ≥ 20 and a PhyloP100way_veterbrate score ≥ 2.5. Variants were triaged by their absence from publicly available databases including dbSNP146/1000G/ESP6500. Candidates were then manually curated by having a requirement for allele and/or genotype frequency of less than 1% as compared with an in-house exome database (n = 2564 (Build version 3 – 2020)). Variants with PhyloP100way_veterbrate scores lower than 2.5 still had a requirement to meet the allele and/or genotype frequency of less than 1% using the in-house database in order to be considered further.

All variant sites were manually curated using SeqMan Pro (next generation sequencing alignment visualization software) in order to confirm the presence of the variant and to minimize the risk of PCR strand bias with respect to either the forward (F) or reverse (R) strands (maximum ratio of 9:1 for either F/R or R/F). Non-synonymous heterozygous, frameshift and splice site

donor/acceptor variants were screened using similar methodologies outlined above. Genomic, mRNA and protein coding variant locations were obtained using Mutalyzer v2.0.22 (Human Genome Variation Society (HGVS) nomenclature version 2.0). Variants, their associated genes/biological pathways were correlated to clinical phenotypes using publicly available databases (e.g. OMIM; Pubmed; HGMD).

Comprehensive analysis of exome sequencing data was implemented to detect potentially damaging variants and candidate variants were classified and reported by board-certified geneticists following HGVS nomenclature and American College of Medical Genetics guidelines, whereas no variants were identified in other known disease genes. For the index case (individual II.4), a homozygous missense variant was identified in the GRM7 gene: NM_000844.4(GRM7): c.461T>C (p.I154T), classified as damaging by SIFT, and probably damaging by PolyPhen-2, with a CADD score of 28.900, genotype quality 60, call quality 60, and a read depth of 161. The variant in GRM7 gene was classified as likely pathogenic in ClinVar. Sanger confirmation for the other affected case and segregation analysis for family members was performed, see Figure 1.

Cell Culture, Expression Constructs, and Transfection

HEK293A cells were cultured in growth media containing DMEM with 10% fetal bovine serum, 20 mM HEPES, 1 mM sodium pyruvate, 2 mM GlutaMAX, 0.1 mM nonessential amino acids, and antibiotic/antimycotic. For Figure 2C-D, cells were grown in OptiMEM with reduced serum (2% FBS) and cell culture media was concentrated using Amicon Ultra centrifugal filters (Millipore, 50kDa cut off). HA-mGlu$_7$-WT was custom designed using the cDNA sequence for the human mGlu$_7$a isoform (NM_000844.4) and synthesized as a gBlock fragment (Integrated DNA Technologies). The HA tag was inserted after the N-terminal signal peptide MVQLRKLLRVLTLMKFPCCVLEVLLCALAAAARG. This DNA fragment was cloned into

the pIRESpuro3 expression vector (Clontech) using the EcoRI and NotI sites. For the MYC-mGlu$_7$-WT construct, a second gBlock with a MYC tagged substituted for the HA tagged was subcloned into the HA-mGlu$_7$-WT vector using the EcoRI site and an internal Bsu36I site. Similarly, a gBlock containing the c.461T>C p.Ile154Thr mutation was synthesized and subcloned using the EcoRI site and the Bsu36I site to generate HA-mGlu$_7$-I154T. To generate HA-ECD-WT and HA-ECD-I154T, a gBlock containing the mutation c.1757G>A p.W586* was subcloned using the Bsu36I site and the NotI site. All experiments were performed from HEK293A cells transfected with plasmid DNA using Fugene6 (3 µg DNA for about 2x10^6 cells unless otherwise stated) or from polyclonal lines selected with puromycin from an initial 3 µg transfection.

Cell Surface ELISA

For Figure 2D-H, HEK293A cells were transfected with 2 µg of HA-ECD-WT or HA-ECD-I154T alone or in addition to 1 µg MYC-mGlu$_7$-WT. Twenty-four hours after transfection, cells were trypsinized and plated onto a 96-well plate coated with poly-D-lysine at a density of 100,000 cells per well. Twenty-four hours after plating, media was aspirated and cells were washed with PBS before fixation with 4% paraformaldehyde for 15 minutes. Cells were washed again with PBS and then incubated with 0.5% Triton X-100 for 10 minutes for permeabilization. For surface expression, wells continued to incubate in PBS without detergent. Following permeabilization, cells were washed with PBS and incubated with Odyssey blocking buffer (LI-COR) for 1 hour at room temperature. Wells were then incubated overnight at 4^{o}C with primary antibodies to either the HA tag (1:5000, Abcam ab9110) or MYC tag (1:1000, Cell Signaling Technologies 71D10 product no. 2278) diluted in blocking buffer. Primary antibody was removed and cells were washed three times with Tris-buffered saline plus Tween 20 (TBST, 25 mM Tris, 150 mM NaCl, 0.05% Tween 20). Cells were then incubated for 1 hour at room temperature with fluorescent

secondary antibody (800CW, 1:5000, LI-COR) and DRAQ5 (1:1000, Invitrogen) diluted in blocking buffer. Cells were washed 3 times with TBST and the plate was allowed to dry at room temperature before imaging with an Odyssey scanner. For each well, signal was quantified with Image Studio Light software. The signal from the 800 channel (HA or MYC-tag) was normalized to the signal from the 700 channel (DRAQ5) to account for cell number.

Protein Isolation

To collect brain tissue, mice were anesthetized with isoflurane and decapitated. Brains were quickly removed and microdissected to isolate whole cortex, hippocampus, and striatum. Tissue was frozen on dry ice and stored at -80^{o}C until processing. Cells were washed with ice-cold PBS, harvested by scraping, pelleted and stored at -80^{o}C. To isolate total protein, samples were resuspended in radioimmunoprecipitation assay buffer (RIPA, Sigma), homogenized with a hand-held motorized mortal and pestle and allowed to incubate on ice for 30 minutes with occasional vortexing. Samples were then spun for 20 minutes at 15,000 x g at 4 ºC. The supernatant was saved and protein concentration was determined using a bicinchoninic acid (BCA) protein assay (Pierce^{TM}).

Western Blotting

Samples were prepared by combining total protein lysate (20 µg from cells, 50 µg from brain tissue) with 4X Odyssey loading dye (LI-COR) in the presence or absence of 250mM dithiothreitol (DTT). For glycosidase experiments, whole cell lysates were treated with PNGase F (Promega) or EndoH (New England Biolabs) according to the manufacturer's instructions. Samples were electrophoretically separated using a 4-20% SDS polyacrylamide gel and then transferred onto a nitrocellulose membrane (Bio-Rad). Membranes were blocked with Odyssey blocking buffer (LiCor) for one hour at room temperature and probed with primary antibodies against the HA tag (1:5000, Abcam ab9110), $mGlu_7$ (1:1000, Millipore 07-239) or Gapdh (1:5000, ThermoFisher MA5-15738). Membranes were washed three times with TBST and then incubated

with goat anti-rabbit- fluorescent secondary antibody (800CW, 1:5000, LI-COR) and goat anti-mouse fluorescent secondary antibody (680CW, 1:5000, LI-COR). Blots were imaged with an Odyssey scanner and fluorescence was quantified using Image Studio Light software.

Thallium Flux Assay

Polyclonal cell lines stably expressing HA-mGlu$_7$-WT or HA-mGlu$_7$-I154T along with GIRK1/2 channels were generated by transfecting 3 µg of each mGlu$_7$ constructs into an existing HEK/GIRK cell line as described in reference 207 and selected for mGlu$_7$ with puromycin. Polyclonal lines were maintained in growth media containing 1:1 DMEM:F12 with 10% fetal bovine serum, 20 mM HEPES, 1 mM sodium pyruvate, 2 mM GlutaMAX, 0.1 mM nonessential amino acids, antibiotic/antimycotic, 700 µg/ml G418 (for maintaining GIRK1/2) and 600 ng/ml puromycin (for maintaining mGlu$_7$). Thallium flux assays were performed according to methods described[207], with minor modifications. The day prior to the experiment, cells were plated in an amine-coated 384-well plate (Corning 356719) at a density of 15,000 cells per well in assay media containing DMEM with 10% fetal bovine serum, 20 mM HEPES, 1 mM sodium pyruvate and antibiotic/antimycotic. For dye loading, media was exchanged with Assay Buffer (Hanks Balanced Salt Solution (HBSS) containing 20 mM HEPES, pH 7.4) using an ELX405 microplate washer (BioTek), leaving 20 µL/well, followed by addition of 20 µL/well 2× FluoZin-2 AM (330 nM final) indicator dye (Life Technologies, prepared as a DMSO stock and mixed in a 1:1 ratio with pluronic acid F-127) in Assay Buffer. After a 50-minute incubation at room temperature, dye was exchanged with Assay Buffer, leaving 20 µL/well. Thallium flux was measured at room temperature using a Functional Drug Screening System 7000 (FDSS 7000, Hamamatsu). Baseline readings were taken (2 images at 1 Hz; excitation, 470 ± 20 nm; emission, 540 ± 30 nm), and positive allosteric modulators (2X) were added in a 20 µL volume and incubated for 140 s before the addition of 10 µL of Thallium Buffer with agonist (5X). Data were collected for an additional 2.5 min and analyzed using Excel (Microsoft Corp, Redmond, WA) as previously

described[207], and the concentration–response curves were fitted to a four-parameter logistic equation to determine potency estimates using GraphPad Prism (La Jolla, CA).

RNA Isolation and qRT-PCR

Tissue samples were homogenized by mortar and pestle and total RNA was prepared using Trizol Reagent (Life Technologies) in accordance with the manufacturer's instructions. Total RNA was treated with DNase and cleaned using the RNeasy kit (Qiagen). Complementary DNA was synthesized using the Superscript VILO cDNA synthesis kit (Invitrogen). A no reverse-transcriptase control was run for each sample. QRT-PCR was then performed with PowerSYBR Green PCR master mix (Applied Biosystems) using cDNA representing 25ng of starting RNA and primers targeting *Grm7* and *Gapdh*. Primer sequences are as follows: *Grm7* 5'-CTCGACCAGATCAACAGCGA-3' and 5'-CAGGAGCCGTGGATGCATAA-3', *Gapdh* 5'-AGGTCGGTGTGAACGGATTTG-3' and 5'-GGGGTCGTTGATGGCAACA-3'. Cycle threshold (Ct) values for each sample were normalized to *Gapdh* expression and analyzed using the ΔΔCt method.

Generation of mGlu$_7$-I154T Knock-in Mice

Mice expressing the p.Ile154Thr mutation in the endogenous *Grm7* gene were generated on a C57BL/6J background by the Vanderbilt Genome Editing Resource. Two overlapping crRNAs were designed targeting the mutation site within exon 1 of *Grm7*. The crRNAs were microinjected into embryos along with CRISPR-Cas9 ribonucleoprotein complex and a 180bp single stranded DNA donor sequence for homology-directed repair. This donor template was designed to incorporate a single base substitution at position 461 to create the Ile154Thr mutation (ATT to ACT), along with two silent mutations at Val153 (GTG to GTA) and Gly155 (GGG to GGT). The I154T mutation introduced a new BsrI restriction site, which was used for genotyping. Founder mice were screened by PCR amplification followed by BsrI digestion (New England Biolabs). See Table S2 for sequences of crRNAs, repair template, and primers.

Table 2. Sequences of reagents used to generate and genotype $mGlu_7$-I154T mice

crRNA1	GAGAAAGTAGTTGGAGTGAT
crRNA2	GAAAGTAGTTGGAGTGATTG
ssDNA repair template Red text indicates bases that differ from WT *Grm7*	GCGCTTATCCAGAAGGACACCTCCGACGTGCGTTGCACC AACGGAGAGCCCCCGGTTTTCGTCAAGCCAGAGAAAGTA GTTGGAGTAACTGGT GCTTCGGGGAGCTCCGTCTCCATCATGGTAGCCAACATC TTGAGGCTTTTCCAGgtagggggcgctccctttggggaggagcattc
Primers for PCR and sequencing	AGATCAACAGCGATCCCAAC
	CATGAAGTCCAAACCAGCTTTT

Founder mice positive for cleavage were further confirmed by Sanger sequencing. One male founder was bred to a female C57BL/6J mouse (Jackson Laboratories) to confirm germline transmission. One heterozygous male offspring from the resulting litter (generation N1) was sequenced to confirm the absence of off-target editing within the region of the repair template. This male mouse was backcrossed once again to female C57BL/6J mice (Jackson Laboratories). Heterozygous mice from the resulting generation (N2) were used as breeders to generate the colony. Littermate controls were used in all experiments.

Animal Behavior

All animals used in this study were group housed with food and water given *ad libitum* and maintained on a 12-hour light/dark cycle with tests occurring during the light phase. Both male and female mice were used in phenotyping experiments. No significant sex differences were observed; therefore, data were combined. Mice underwent the following testing schedule starting at 6-7 weeks of age with a minimum of 3 days of time between each test: open field, rotarod, fear

conditioning, hindlimb clasping. For all tests, mice were habituated to the testing room for a minimum of 1 hour.

Open field: Mice were placed in an activity chamber measuring 27 by 27 cm for 60 minutes where X, Y, and Z beam breaks were monitored by Activity Monitor software (MedAssociates Inc). The total distance traveled was quantified by this software.

Rotarod: Mice were placed on an accelerating rotarod (4 to 40 rpm over 5 minutes) and the latency to fall from the apparatus or complete two rotations without regaining control was recorded with a cut off of 300 seconds.

Limb clasping: Mice were suspended by the tail and video-recorded for 1 minute. Time spent clasping the hindlimbs were quantified by a blinded reviewer. The timer was started when one or both hind limbs began to knuckle in, and the timer was stopped if the paws came apart at any point. Time was counted if one paw remained knuckled in while the other came away. Time was stopped when the mouse's back was turned to the camera.

Fear conditioning: On training day, mice were placed into an operant chamber with a shock grid (Med Associates, Inc.) in the presence of a 10% vanilla odor cue. Following a three-minute habituation period, two tone-shock pairings were administered consisting of a 30 second tone ending with a one second, 0.7 mA foot shock. Each tone-shock pairing was spaced 30 seconds apart and mice remained in the context for an additional 30 seconds after the second foot shock. On the next day, mice were tested for contextual fear memory by placing each animal back into the same chamber with a 10% vanilla odor cue for three minutes. Time spent freezing during a three-minute testing period was quantified using Video Freeze software.

Statistical Analysis

All data shown represent mean ± SEM. The tests used to determine statistical significance are noted in each figure legend. In all cases, p-values are indicated as *$p < 0.05$, **$p < 0.01$, ***$p < 0.001$, ****$p < 0.0001$.

Study Approval

All clinical data has been shared with informed consent of the patients' family with approval from the Institutional Review Board (IRB) at King Fahad Medical City (IRB number 16-324). All animal studies were approved by the Institutional Animal Care and Use Committee for Vanderbilt University School of Medicine. Animals were cared for in accordance with the National Institutes of Health *Guide for the Care and Use of Laboratory Animals.*

CHAPTER V. Conclusions and Future Directions

Summary

Taken together, the results described herein support the hypothesis that decreased $mGlu_7$ expression and function can contribute to neurodevelopmental disease in a broad sense. Previous work by Gogliotti et al. had established that $mGlu_7$ expression is decreased in autopsy samples from patients with Rett syndrome and demonstrated that potentiation of $mGlu_7$ activity with an allosteric modulator was able to improve several phenotypes in Rett syndrome model mice[138]. To our knowledge, this was the first study to investigate $mGlu_7$ in a model of neurodevelopmental disease. This work thus sought to investigate the role of $mGlu_7$ in other NDDs, which was supported by genetic associations between *GRM7* and diagnoses of ASD, ADHD, ID and epilepsy in clinical populations.

In **Chapter II**, we evaluated $mGlu_7$ as a therapeutic target in a mouse model of *MECP2* Duplication syndrome to complement our previous work in Rett syndrome models. Gogliotti et al. had previously demonstrated that MeCP2 could drive expression of the *GRM7* promoter *in vitro*[138]. From this, we initially hypothesized that $mGlu_7$ transcription and expression would be increased in the context of *MECP2* overexpression. Contrary to this hypothesis, we did not observe an increase in *Grm7* mRNA expression in a mouse model of *MECP2* Duplication syndrome. While we did measure a small increase in total $mGlu_7$ protein expression in the hippocampus, it did not result in increased synaptic expression or function of $mGlu_7$ at SC-CA1 synapses. Furthermore, genetic reduction of $mGlu_7$ expression and negative allosteric modulation had no effect on phenotypes of *MECP2* Duplication syndrome model mice. This work suggests that MeCP2 does not regulate $mGlu_7$ in a bidirectional manner and rather that $mGlu_7$ expression may be impacted by loss of MeCP2 at the post-transcriptional or post-translational level. The exact mechanism by which MeCP2 loss leads to reduced $mGlu_7$ protein expression remains an open question for future studies.

Since the expression of many genes is disrupted in Rett syndrome, an ongoing effort in the field is to identify which alterations directly contribute to the manifestation of disease phenotypes. The fact that $mGlu_7$ potentiation was able to improve several phenotypes in Rett syndrome model mice suggested that decreased $mGlu_7$ expression may contribute to the development of these phenotypes. Alternatively, $mGlu_7$ could be positioned such that potentiation of its activity can compensate for other deficits regardless of its level of expression. To determine whether decreased $mGlu_7$ function contributes to phenotypes associated with Rett syndrome, we hypothesized that loss of $mGlu_7$ expression would be sufficient to recapitulate such phenotypes without MeCP2 disruption. In **Chapter III**, we tested this hypothesis through careful characterization of global $mGlu_7$ knockout mice. We identified novel alterations in social behavior, motor coordination, and sleep while expanding upon previously reported phenotypes. We found that *Grm7*$^{-/-}$ mice exhibited significant phenotypic overlap with models of Rett syndrome as summarized in Figure 22. Heterozygous mice were indistinguishable from wildtype littermates indicating that full loss of $mGlu_7$ protein is needed to produce neurodevelopmental phenotypes. Altogether, this work demonstrates that loss of $mGlu_7$ function can disrupt a wide range of behaviors that are relevant to NDDs and further validates $mGlu_7$ as a potential therapeutic target for Rett syndrome and related disorders.

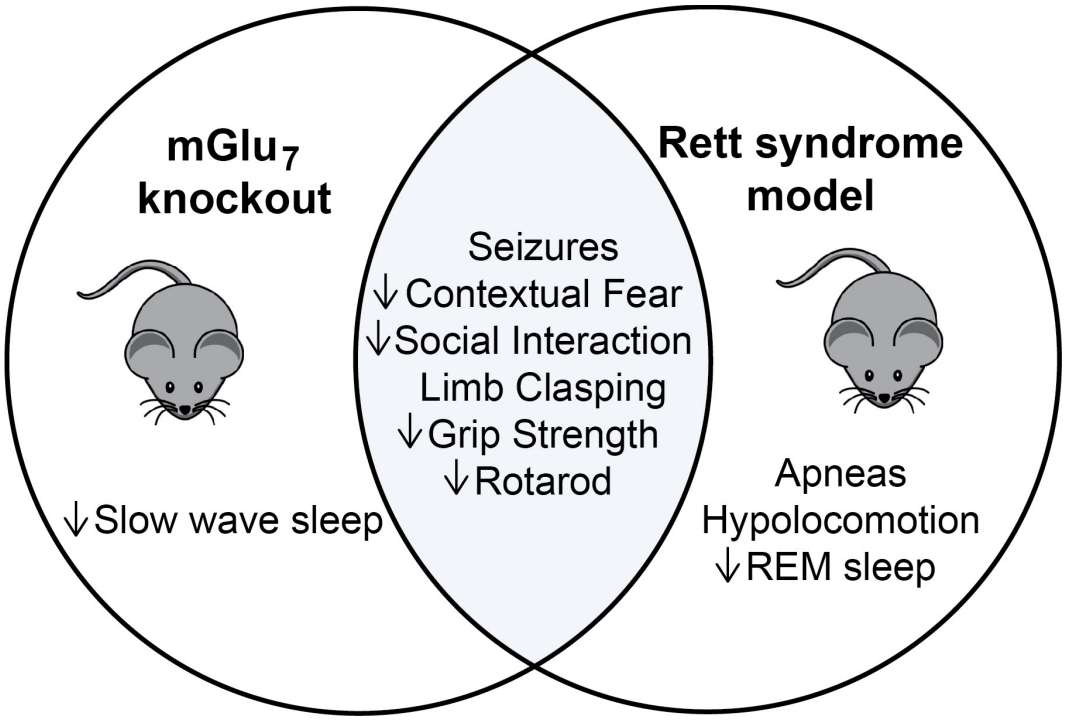

Figure 22. Venn diagram summarizing the phenotypic overlap between $mGlu_7$ knockout mice and Rett syndrome model mice.

Recent whole exome sequencing studies have identified *GRM7* gene disruptions in patients with NDDs. Heterozygous deletions and point mutations have been reported in patients with ASD and ADHD, while homozygous mutations have been identified in patients with severe developmental delay and epilepsy (summarized with references in Table 1). Despite these clinical reports, the functional effect of *GRM7* point mutations on $mGlu_7$ expression and/or function had not been determined. In **Chapter IV**, we described two new patients with the recessive $mGlu_7$-I154T point mutation and demonstrated that this mutation leads to reduced receptor dimerization, trafficking and expression *in vitro*. We then generated the $mGlu_7$-I154T mutant mouse model, which expressed little to no $mGlu_7$ protein and recapitulated phenotypes previously observed in the global $mGlu_7$ knockout mouse. This work provides proof-of-concept that *GRM7* can be a disease-causing gene in the human population and highlights the importance of $mGlu_7$'s ligand-binding domain for dimerization and expression.

Future Directions

Do other *GRM7* point mutations lead to loss-of-function?

In April 2020, Marafi et al. reported three additional families with recessive *GRM7* point mutations associated with severe neurodevelopmental disease[200]. This leads to a total of 13 children from 7 distinct families (including the family reported in **Chapter IV**) with inherited *GRM7* mutations. These mutations are summarized in Figure 23.

A

GRM7 Variant	Amino Acid Change	Protein Domain	Zygosity	Location	No. Affected
461T>C	I154T	ECD	Homozygous	Saudi Arabia	4
1757G>A	W586*	ECD	Homozygous	Syria	2
1972C>T + 2024C>A	R658W + T675K	TMD	Compound Heterozygous	USA	2
1973G>A	R658Q	TMD	Homozygous	UAE	3
1975C>T	R659*	TMD	Homozygous	Turkey	1
2671G>A	E891K	CTD	Homozygous	Turkey	1

B

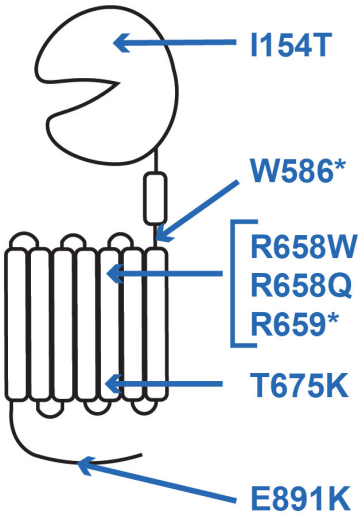

Figure 23. Summary of clinical *GRM7* point mutations.
A) Summary of patients with inherited *GRM7* point mutations reported by Marafi et al. and those described in **Chapter IV**. B) Location of mutations within the $mGlu_7$ protein.

All of the patients listed in Figure 23A exhibited global developmental delay, intellectual disability and seizures within the first year of life[200]. The striking phenotypic similarity between these cases points to a shared mechanism of action. Based on our findings with the I154T mutation in **Chapter IV**, one might hypothesize that all of these mutations lead to reduced expression. It is also possible that receptor activation and signaling, rather than expression, are disrupted by these mutations. While the I154T mutation affects the ligand-binding domain of $mGlu_7$, the other mutations are located in either the transmembrane domain (TMD) or C-terminal domain (CTD) (Figure 23B). The TMDs of mGlu receptors are not a major dimerization interface

in the resting state, but rather interact and rearrange during receptor activation[54]. The mutations within the TMD could disrupt receptor activation, or conversely, lead to a constitutively active receptor. Early death was reported in patients homozygous for R658Q and R569*, which may indicate potential dominant negative affects beyond simple loss of expression/function. The E891K mutation in the CTD is positioned near the interaction sites of intracellular proteins, such as calmodulin and PICK1, that are involved in signaling and stabilization of $mGlu_7$ surface expression[58]. The CTD is also important for the targeting of $mGlu_7$ to axons[216]. Thus, the E891K mutation could potentially have a variety of effects on $mGlu_7$ expression and function. It will also be important to consider effects of $mGlu_7$ mutants on other mGlu subtypes given that $mGlu_7$ can form heterodimers with other group II and group III mGlu receptors[69,70]. Further characterization of *GRM7* variants is expected to reveal new insights into $mGlu_7$ biology, which could inform the development of therapies aimed at increasing $mGlu_7$ expression and/or normalizing its function.

How does loss of $mGlu_7$ expression and/or activity lead to neurodevelopmental phenotypes?

Characterization of global $mGlu_7$ knockout mice and $mGlu_7$-I154T mice demonstrated that $mGlu_7$ is clearly involved in many NDD-related phenotypes; however, there is much work to be done to understand *how* $mGlu_7$ contributes to these behavioral domains in normal and pathological conditions. $mGlu_7$ has been shown to be involved in LTP in the hippocampus[96,100] and the amygdala[112,114], which correlate with the receptor's role in cognition and anxiety, respectively. Constitutive activity of $mGlu_7$ through its PDZ domain regulates activity of thalamic synapses in a way that prevents pathological oscillations and absence-like seizures[77]; however, our data in **Chapter III** suggest that convulsive seizures observed in *Grm7*$^{-/-}$ mice involve the hippocampus. Therefore, $mGlu_7$ activity may protect against seizure activity in multiple brain regions with potentially distinct mechanisms. Beyond these few studies, little work has focused

on understanding how $mGlu_7$ activity regulates other brain circuits despite its widespread expression in the CNS.

The striatum is one area that may have important implications for NDDs as it has been proposed as a central node for autism-associated behaviors[217]. As part of the basal ganglia, the striatum acts to link incoming sensory information to regulated motor output. The striatum can be subdivided into the dorsal striatum and the ventral striatum, also referred to as the nucleus accumbens. The dorsal striatum is involved in action selection and cognitive flexibility while the nucleus accumbens mediates reward processing and goal-directed behaviors. Dysfunction of these areas has been proposed to contribute to repetitive behaviors/interests and abnormal social behaviors, respectively, which are core features of ASD[217]. This idea is supported by work in several genetic mouse models of ASD. As one example, Shank3 knockout mice, a model for Phelan-McDermid syndrome, displays deficits in social behavior, over grooming, and large reductions in cortico-striatal transmission[218]. Additionally, MeCP2 has been shown to inhibit repetitive behaviors through regulation of Sapap3 expression in the striatum[219]. $mGlu_7$ is expressed on excitatory corticostriatal projections along with inhibitory striatopallidal and striatonigral projections[185]; however, the functional role of $mGlu_7$ in these circuits remains uncharacterized. It is plausible that loss of striatal $mGlu_7$ contributes to the social abnormalities observed in *Grm7*$^{-/-}$ mice in **Chapter III** and the motor phenotypes (hindlimb clasping and decreased rotarod performance) observed in both *Grm7*$^{-/-}$ and $mGlu_7$-I154T mice **(Chapters III and IV)**. It should be noted that social behavior was not tested in $mGlu_7$-I154T mice. Future experiments could test this hypothesis using region- and/or cell-specific knockout of $mGlu_7$.

Another novel finding from this work is the reduced sensitivity to amphetamine observed in *Grm7*$^{-/-}$ mice **(Chapter III)**. The underlying mechanism of this effect remains unknown and may have important implications for ADHD in which stimulants like amphetamine are the first line of treatment. Indeed, a single nucleotide polymorphism in *GRM7* in a non-coding region has been associated with response to methylphenidate in ADHD patients[161,180]. Amphetamine acts through

reversal of the dopamine transporter (DAT) to increase extracellular concentrations of dopamine and norepinephrine. Increased dopamine release in the nucleus accumbens is required for both the rewarding and locomotor effects of amphetamine[220]. One previous study showed that local administration the allosteric $mGlu_7$ agonist AMN082 into the nucleus accumbens was able to block the rewarding effects of cocaine, which blocks DAT and increases extracellular dopamine similarly to amphetamine. This behavioral effect of AMN082 occurred via a non-dopaminergic mechanism that involved decreased GABA and increased glutamate in the nucleus accumbens[221]. However, these results should be interpreted with caution because a metabolite of AMN082 has since been shown to be a DAT inhibitor[222]. Complimentary approaches are thus needed to understand how $mGlu_7$ activity interacts with the dopamine signaling in the nucleus accumbens. It would be interesting to investigate whether similar alterations in GABA/glutamate are present in $mGlu_7$ knockout animals and to test whether specific loss of $mGlu_7$ in the nucleus accumbens is sufficient to reduce sensitivity to amphetamine.

Are the effects of $mGlu_7$ loss-of-function reversible?

Neurodevelopment is an extremely complex process during which the brain is particularly vulnerable to environmental insults and genetic mutations. Abnormal development can result in long-term changes in brain circuit organization, cell-type composition and gross anatomy of certain brain regions. Because of this, NDDs have been traditionally viewed as incurable; however, it has become increasingly accepted that there is a significant window for symptomatic improvement if underlying cellular and molecular pathologies are normalized, even in adulthood[223]. This is partly because many genes linked to NDDs play important roles during both development and adulthood. In the case of Rett syndrome, Guy et al. demonstrated that restoration of Mecp2 expression in adult mice was able to significantly improve disease phenotypes observed in Mecp2 null mice[147]. Since this proof-of-concept of the reversibility of Rett syndrome, many groups have demonstrated efficacy of various pharmacological interventions in

adult Mecp2 null mice (reviewed in 224). Similar genetic and pharmacologic rescue of cellular and behavioral phenotypes has been reported in other models of NDDs, including Fragile X syndrome and Angelman syndrome[223].

$mGlu_7$ has been almost exclusively studied in mature neurons and the adult brain, and only one study thus far has investigated $mGlu_7$ in early neurodevelopment. Xia et al. showed that knockdown of $mGlu_7$ expression increased the proliferation of neuronal progenitor cells, decreased the differentiation of neurons and led to abnormal neuronal morphology[225]. Patients with homozygous *GRM7* mutations exhibit abnormal MRI features including cerebral atrophy, hypomyelination and thinning of the corpus callosum[200]. These findings suggest that $mGlu_7$ may play a role in the maturation of neurons and myelin-associated cell types; however, further experiments are needed to characterize the role of $mGlu_7$ in early development.

Given that $mGlu_7$ has a variety of important roles in the adult brain, we hypothesize that at least some of the deficits observed in *Grm7*$^{-/-}$ and $mGlu_7$-I154T mice are reversible. Future experiments could test this through re-expression of $mGlu_7$ protein at various time-points during development with a conditional *Grm7* allele and a tamoxifen-inducible Cre recombinase. If behavioral phenotypes can be rescued in adult mice, this provides further rationale to develop pharmacological interventions for diseases with reduced $mGlu_7$ expression or function. PAMs with activity at $mGlu_7$ would be useful to boost $mGlu_7$ activity in contexts where at least some $mGlu_7$ surface expression is maintained. Molecules that can increase the expression and surface trafficking of $mGlu_7$ receptors would be particularly useful as well and could be used in combination with PAMs for a synergistic effect. However, no compounds that selectively increase the expression/trafficking of mGlu receptors have been reported to date.

Which subpopulation of NDDs would benefit from an $mGlu_7$-targeted therapy?

The work described herein demonstrates that total absence of $mGlu_7$ expression is sufficient to produce phenotypes consistent with NDDs in mice and, in rare cases, *GRM7* mutations can be the primary cause of severe disease in humans. This raises the possibility that reduced $mGlu_7$ expression might a contributor to disease in cases where *GRM7* disruptions are not the primary cause, such as Rett syndrome. Our current work in Rett syndrome has been limited to Mecp2 null mice, while Rett syndrome in humans is typically caused by a range of *MECP2* point mutations[164]. One future direction is to profile $mGlu_7$ expression in point mutant models of Rett syndrome to test whether decreased $mGlu_7$ expression is a shared feature or distinct to certain *MECP2* mutation types. Then, it will be important to test whether decreased $mGlu_7$ protein expression is a prerequisite for efficacy of $mGlu_7$ PAMs. This will enable a personalized medicine approach to identify those patients who will be predicted to respond best to treatment.

Heterozygous deletions in *GRM7* have also been associated with ASD, ADHD and global developmental delay (Table 1). Interestingly, $Grm7^{+/-}$ and heterozygous $mGlu_7$-I154T mice did not display any altered behavior indicating that $mGlu_7$ expression must be extremely low, if not altogether absent, before phenotypes become detectible. This could be a species difference between mice and humans; however, it is important to note that the heterozygous carriers in the family described in **Chapter IV** were asymptomatic and Marafi et al. made no mention of neuropsychiatric diagnoses in heterozygous carriers from the other families carrying *GRM7* variants. Therefore, heterozygous *GRM7* mutations may be associated with disease only in the presence of other genetic or environmental factors. Future studies, both clinical and preclinical, should address how modest reductions in $mGlu_7$ expression may increase the risk of neuropsychiatric disease or modify other diagnoses. Diseases like ASD and ADHD are notoriously heterogeneous; thus, a better understanding of the contexts in which reduced $mGlu_7$

expression can contribute to these diseases may provide new insights into disease pathology and potential treatments.

Concluding Remarks

This dissertation represents a significant step forward in understanding the role of $mGlu_7$ in NDDs. We have established that decreased $mGlu_7$ expression is a feature of Rett syndrome and that total loss of $mGlu_7$ expression is sufficient to recapitulate NDD-associated phenotypes in mice and humans. This leads to a proposed model in which intermediate reductions in $mGlu_7$ expression could modify or increase the risk of other diseases, such as ASD or ADHD, but this hypothesis will require further testing (Figure 24). As a GPCR, $mGlu_7$ represents a highly druggable target for therapeutic intervention. Understanding how *GRM7* variants contribute to disease and how $mGlu_7$ receptor function regulates circuits relevant to NDDs will be important next steps to validate $mGlu_7$ as a therapeutic target.

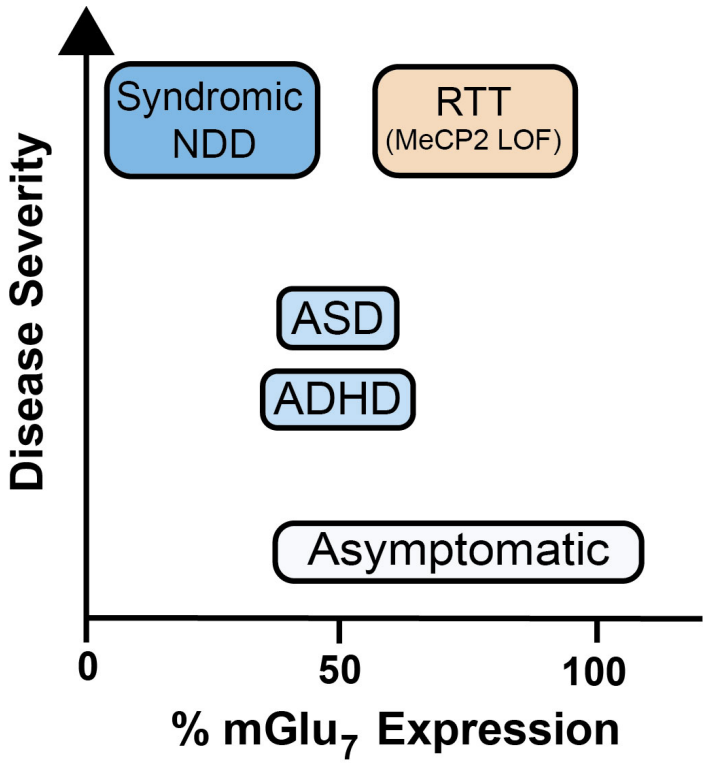

Figure 24. Proposed model of how $mGlu_7$ expression correlates with NDD severity.
NDD= Neurodevelopmental disorder, RTT = Rett syndrome, LOF = loss of function.

REFERENCES

1. Fisher NM, Seto M, Lindsley CW, Niswender CM. Metabotropic Glutamate Receptor 7: A New Therapeutic Target in Neurodevelopmental Disorders. *Front Mol Neurosci*. 2018;11. doi:10.3389/fnmol.2018.00387
2. Zablotsky B, Black LI, Maenner MJ, et al. Prevalence and trends of developmental disabilities among children in the United States: 2009–2017. *Pediatrics*. 2019;144(4). doi:10.1542/peds.2019-0811
3. *Diagnostic and Statistical Manual of Mental Disorders : DSM-5.*; 2013.
4. Christensen DL, Baio J, Braun KVN, et al. Prevalence and Characteristics of Autism Spectrum Disorder Among Children Aged 8 Years — Autism and Developmental Disabilities Monitoring Network, 11 Sites, United States, 2012. *MMWR Surveill Summ*. 2016;65(3):1-23. doi:10.15585/mmwr.ss6503a1
5. Doshi-Velez F, Ge Y, Kohane I. Comorbidity clusters in autism spectrum disorders: An electronic health record time-series analysis. *Pediatrics*. 2014;133(1). doi:10.1542/peds.2013-0819
6. Mannion A, Leader G. Comorbidity in autism spectrum disorder: A literature review. *Res Autism Spectr Disord*. 2013;7(12):1595-1616. doi:10.1016/j.rasd.2013.09.006
7. Lord C, Elsabbagh M, Baird G, Veenstra-Vanderweele J. Autism spectrum disorder. *Lancet*. 2018;392(10146):508-520. doi:10.1016/S0140-6736(18)31129-2
8. Lyall K, Croen L, Daniels J, et al. The Changing Epidemiology of Autism Spectrum Disorders. *Annu Rev Public Health*. 2017;38:81-102. doi:10.1146/annurev-publhealth-031816-044318
9. Tick B, Bolton P, Happé F, Rutter M, Rijsdijk F. Heritability of autism spectrum

disorders: A meta-analysis of twin studies. *J Child Psychol Psychiatry Allied Discip*. 2016;57(5):585-595. doi:10.1111/jcpp.12499

10. Wiśniowiecka-Kowalnik B, Nowakowska BA. Genetics and epigenetics of autism spectrum disorder—current evidence in the field. *J Appl Genet*. 2019;60(1):37-47. doi:10.1007/s13353-018-00480-w
11. Satterstrom FK, Kosmicki JA, Wang J, et al. Large-Scale Exome Sequencing Study Implicates Both Developmental and Functional Changes in the Neurobiology of Autism. *Cell*. 2020;180(3):568-584.e23. doi:10.1016/j.cell.2019.12.036
12. Thomas R, Sanders S, Doust J, Beller E, Glasziou P. Prevalence of attention-deficit/hyperactivity disorder: A systematic review and meta-analysis. *Pediatrics*. 2015;135(4):e994-e1001. doi:10.1542/peds.2014-3482
13. Fayyad J, De Graaf R, Kessler R, et al. Cross-national prevalence and correlates of adult attention-deficit hyperactivity disorder. *Br J Psychiatry*. 2007;190(MAY):402-409. doi:10.1192/bjp.bp.106.034389
14. Posner J, Polanczyk G V., Sonuga-Barke E. Attention-deficit hyperactivity disorder. *Lancet*. 2020;395(10222):450-462. doi:10.1016/S0140-6736(19)33004-1
15. Larsson H, Anckarsater H, Råstam M, Chang Z, Lichtenstein P. Childhood attention-deficit hyperactivity disorder as an extreme of a continuous trait: A quantitative genetic study of 8,500 twin pairs. *J Child Psychol Psychiatry Allied Discip*. 2012;53(1):73-80. doi:10.1111/j.1469-7610.2011.02467.x
16. Faraone S V., Larsson H. Genetics of attention deficit hyperactivity disorder. *Mol Psychiatry*. 2019;24(4):562-575. doi:10.1038/s41380-018-0070-0
17. Tomioka NH, Yasuda H, Miyamoto H, et al. Elfn1 recruits presynaptic mGluR7 in

trans and its loss results in seizures. *Nat Commun*. 2014;5(1):4501. doi:10.1038/ncomms5501

18. Gizer IR, Ficks C, Waldman ID. Candidate gene studies of ADHD: A meta-analytic review. *Hum Genet*. 2009;126(1):51-90. doi:10.1007/s00439-009-0694-x
19. Elia J, Glessner JT, Wang K, et al. Genome-wide copy number variation study associates metabotropic glutamate receptor gene networks with attention deficit hyperactivity disorder. *Nat Genet*. 2012;44(1):78-84. doi:10.1038/ng.1013
20. Akutagava-Martins GC, Salatino-Oliveira A, Genro JP, et al. Glutamatergic copy number variants and their role in attention-deficit/hyperactivity disorder. *Am J Med Genet Part B Neuropsychiatr Genet*. 2014;165(6):502-509. doi:10.1002/ajmg.b.32253
21. Cheng J, Liu A, Shi MY, Yan Z. Disrupted glutamatergic transmission in prefrontal cortex contributes to behavioral abnormality in an animal model of ADHD. *Neuropsychopharmacology*. 2017;42(10):2096-2104. doi:10.1038/npp.2017.30
22. Maltezos S, Horder J, Coghlan S, et al. Glutamate/glutamine and neuronal integrity in adults with ADHD: A proton MRS study. *Transl Psychiatry*. 2014;4(3):373. doi:10.1038/tp.2014.11
23. Mégarbané A, Ravel A, Mircher C, et al. The 50th anniversary of the discovery of trisomy 21: The past, present, and future of research and treatment of Down syndrome. *Genet Med*. 2009;11(9):611-616. doi:10.1097/GIM.0b013e3181b2e34c
24. Pieretti M, Zhang F, Fu YH, et al. Absence of expression of the FMR-1 gene in fragile X syndrome. *Cell*. 1991;66(4):817-822. doi:10.1016/0092-8674(91)90125-I
25. Lubs HA, Stevenson RE, Schwartz CE. Fragile X and X-linked intellectual disability:

Four decades of discovery. *Am J Hum Genet*. 2012;90(4):579-590. doi:10.1016/j.ajhg.2012.02.018

26. Vissers LELM, Gilissen C, Veltman JA. Genetic studies in intellectual disability and related disorders. *Nat Rev Genet*. 2016;17(1):9-18. doi:10.1038/nrg3999
27. Fitzgerald TW, Gerety SS, Jones WD, et al. Large-scale discovery of novel genetic causes of developmental disorders. *Nature*. 2015;519(7542):223-228. doi:10.1038/nature14135
28. McRae JF, Clayton S, Fitzgerald TW, et al. Prevalence and architecture of de novo mutations in developmental disorders. *Nature*. 2017;542(7642):433-438. doi:10.1038/nature21062
29. Martin HC, Jones WD, McIntyre R, et al. Quantifying the contribution of recessive coding variation to developmental disorders. *Science (80-)*. 2018;362(6419):1161-1164. doi:10.1126/science.aar6731
30. Musante L, Ropers HH. Genetics of recessive cognitive disorders. *Trends Genet*. 2014;30(1):32-39. doi:10.1016/j.tig.2013.09.008
31. Charng WL, Karaca E, Coban Akdemir Z, et al. Exome sequencing in mostly consanguineous Arab families with neurologic disease provides a high potential molecular diagnosis rate. *BMC Med Genomics*. 2016;9(1). doi:10.1186/s12920-016-0208-3
32. Reuter MS, Tawamie H, Buchert R, et al. Diagnostic yield and novel candidate genes by exome sequencing in 152 consanguineous families with neurodevelopmental disorders. *JAMA Psychiatry*. 2017;74(3):293-299. doi:10.1001/jamapsychiatry.2016.3798

33. Verpelli C, Galimberti I, Gomez-Mancilla B, Sala C. Molecular basis for prospective pharmacological treatment strategies in intellectual disability syndromes. *Dev Neurobiol*. 2014;74(2):197-206. doi:10.1002/dneu.22093

34. Fisher RS, Cross JH, French JA, et al. Operational classification of seizure types by the International League Against Epilepsy: Position Paper of the ILAE Commission for Classification and Terminology. *Epilepsia*. 2017;58(4):522-530. doi:10.1111/epi.13670

35. Amiet C, Gourfinkel-An I, Bouzamondo A, et al. Epilepsy in Autism is Associated with Intellectual Disability and Gender: Evidence from a Meta-Analysis. *Biol Psychiatry*. 2008;64(7):577-582. doi:10.1016/j.biopsych.2008.04.030

36. Covanis A. Epileptic encephalopathies (including severe epilepsy syndromes). *Epilepsia*. 2012;53(SUPPL. 4):114-126. doi:10.1111/j.1528-1167.2012.03621.x

37. Thomas RH, Berkovic SF. The hidden genetics of epilepsy - A clinically important new paradigm. *Nat Rev Neurol*. 2014;10(5):283-292. doi:10.1038/nrneurol.2014.62

38. Steinlein OK, Mulley JC, Propping P, et al. A missense mutation in the neuronal nicotinic acetylcholine receptor α4 subunit is associated with autosomal dominant nocturnal frontal lobe epilepsy. *Nat Genet*. 1995;11(2):201-203. doi:10.1038/ng1095-201

39. Kalachikov S, Evgrafov O, Ross B, et al. Mutations in LGI1 cause autosomal-dominant partial epilepsy with auditory features. *Nat Genet*. 2002;30(3):335-341. doi:10.1038/ng832

40. Barcia G, Fleming MR, Deligniere A, et al. De novo gain-of-function KCNT1 channel mutations cause malignant migrating partial seizures of infancy. *Nat Genet*.

2012;44(11):1255-1259. doi:10.1038/ng.2441

41. Wang J, Lin ZJ, Liu L, et al. Epilepsy-associated genes. *Seizure*. 2017;44:11-20. doi:10.1016/j.seizure.2016.11.030

42. Rogawski MA, Löscher W. The neurobiology of antiepileptic drugs. *Nat Rev Neurosci*. 2004;5(7):553-564. doi:10.1038/nrn1430

43. Brodie MJ, Barry SJE, Bamagous GA, Norrie JD, Kwan P. Patterns of treatment response in newly diagnosed epilepsy. *Neurology*. 2012;78(20):1548-1554. doi:10.1212/WNL.0b013e3182563b19

44. Lutas A, Yellen G. The ketogenic diet: Metabolic influences on brain excitability and epilepsy. *Trends Neurosci*. 2013;36(1):32-40. doi:10.1016/j.tins.2012.11.005

45. Helbig I, Ellis CA. Personalized medicine in genetic epilepsies – possibilities, challenges, and new frontiers. *Neuropharmacology*. 2020;172:107970. doi:10.1016/j.neuropharm.2020.107970

46. Reiner A, Levitz J. Glutamatergic Signaling in the Central Nervous System: Ionotropic and Metabotropic Receptors in Concert. *Neuron*. 2018;98(6):1080-1098. doi:10.1016/j.neuron.2018.05.018

47. Niswender CM, Conn PJ. Metabotropic Glutamate Receptors: Physiology, Pharmacology, and Disease. *Annu Rev Pharmacol Toxicol*. 2010;50(1):295-322. doi:10.1146/annurev.pharmtox.011008.145533

48. Pin JP, Kniazeff J, Liu J, et al. Allosteric functioning of dimeric class C G-protein-coupled receptors. *FEBS J*. 2005;272(12):2947-2955. doi:10.1111/j.1742-4658.2005.04728.x

49. El Moustaine D, Granier S, Doumazane E, et al. Distinct roles of metabotropic

glutamate receptor dimerization in agonist activation and G-protein coupling. *Proc Natl Acad Sci U S A*. 2012;109(40):16342-16347. doi:10.1073/pnas.1205838109

50. Kunishima N, Shimada Y, Tsuji Y, et al. Structural basis of glutamate recognition by a dimeric metabotropic glutamate receptor. *Nature*. 2000;407(6807):971-977. doi:10.1038/35039564

51. Pin JP, Galvez T, Prézeau L. Evolution, structure, and activation mechanism of family 3/C G-protein-coupled receptors. *Pharmacol Ther*. 2003;98(3):325-354. doi:10.1016/S0163-7258(03)00038-X

52. Jingami H, Nakanishi S, Morikawa K. Structure of the metabotropic glutamate receptor. *Curr Opin Neurobiol*. 2003;13(3):271-278. doi:10.1016/S0959-4388(03)00067-9

53. Levitz J, Habrian C, Bharill S, Fu Z, Vafabakhsh R, Isacoff EY. Mechanism of Assembly and Cooperativity of Homomeric and Heteromeric Metabotropic Glutamate Receptors. *Neuron*. 2016;92(1):143-159. doi:10.1016/j.neuron.2016.08.036

54. Koehl A, Hu H, Feng D, et al. Structural insights into the activation of metabotropic glutamate receptors. *Nature*. January 2019:1. doi:10.1038/s41586-019-0881-4

55. Kniazeff J, Bessis AS, Maurel D, Ansanay H, Prézeau L, Pin JP. Closed state of both binding domains of homodimeric mGlu receptors is required for full activity. *Nat Struct Mol Biol*. 2004;11(8):706-713. doi:10.1038/nsmb794

56. Rondard P, Liu J, Huang S, et al. Coupling of agonist binding to effector domain activation in metabotropic glutamate-like receptors. *J Biol Chem*. 2006;281(34):24653-24661. doi:10.1074/jbc.M602277200

57. Yates AD, Achuthan P, Akanni W, et al. Ensembl 2020. *Nucleic Acids Res*. 2020. doi:10.1093/nar/gkz966

58. Dev KK, Nakanishi S, Henley JM. Regulation of mglu7 receptors by proteins that interact with the intracellular C-terminus. *Trends Pharmacol Sci*. 2001;22(7):355-361. doi:10.1016/S0165-6147(00)01684-9

59. El Far O, Airas J, Wischmeyer E, Nehring RB, Karschin A, Betz H. Interaction of the C-terminal tail region of the metabotropic glutamate receptor 7 with the protein kinase C substrate PICK1. *Eur J Neurosci*. 2000;12(12):4215-4221. doi:10.1046/j.1460-9568.2000.01309.x

60. Dev KK, Nakajima Y, Kitano J, Braithwaite SP, Henley JM, Nakanishi S. PICK1 interacts with and regulates PKC phosphorylation of mGLUR7. *J Neurosci*. 2000;20(19):7252-7257. doi:10.1523/jneurosci.20-19-07252.2000

61. Flor PJ, Van Der Putten H, Rüegg D, et al. A novel splice variant of a metabotropic glutamate receptor, human mGluR7b. *Neuropharmacology*. 1997;36(2):153-159. doi:10.1016/S0028-3908(96)00176-1

62. Corti C, Restituito S, Rimland JM, et al. Cloning and characterization of alternative mRNA forms for the rat metabotropic glutamate receptors mGluR7 and mGluR8. *Eur J Neurosci*. 1998;10(12):3629-3641. doi:10.1046/j.1460-9568.1998.00371.x

63. Kinoshita A, Shigemoto R, Ohishi H, van der Putten H, Mizuno N. Immunohistochemical localization of metabotropic glutamate receptors, mGluR7a and mGluR7b, in the central nervous system of the adult rat and mouse: A light and electron microscopic study. *J Comp Neurol*. 1998;393(3):332-352. doi:10.1002/(SICI)1096-9861(19980413)393:3<332::AID-CNE6>3.0.CO;2-2

64. Schulz HL, Stohr H, Weber BHF. Characterization of three novel isoforms of the metabotrobic glutamate receptor 7 (GRM7). *Neurosci Lett*. 2002;326(1):37-40. doi:10.1016/S0304-3940(02)00306-3

65. Shigemoto R, Kulik A, Roberts JDB, et al. Target-cell-specific concentration of a metabotropic glutamate receptor in the presynaptic active zone. *Nature*. 1996;381(6582):523-525. doi:10.1038/381523a0

66. Somogyi P, Dalezios Y, Luján R, Roberts JDB, Watanabe M, Shigemoto R. High level of mGluR7 in the presynaptic active zones of select populations of GABAergic terminals innervating interneurons in the rat hippocampus. *Eur J Neurosci*. 2003;17(12):2503-2520. doi:10.1046/j.1460-9568.2003.02697.x

67. Dalezios Y, Luján R, Shigemoto R, Roberts JDB, Somogyi P. Enrichment of mGluR7a in the presynaptic active zones of GABAergic and non-GABAergic terminals on interneurons in the rat somatosensory cortex. *Cereb Cortex*. 2002. doi:10.1093/cercor/12.9.961

68. Sansig G, Bushell TJ, Clarke VR, et al. Increased seizure susceptibility in mice lacking metabotropic glutamate receptor 7. *J Neurosci*. 2001;21(22):8734-8745.

69. Doumazane E, Scholler P, Zwier JM, Trinquet E, Rondard P, Pin J. A new approach to analyze cell surface protein complexes reveals specific heterodimeric metabotropic glutamate receptors. *FASEB J*. 2011;25(1):66-77. doi:10.1096/fj.10-163147

70. Lee J, Munguba H, Gutzeit VA, Kristt M, Dittman JS, Levitz J. Defining the Homo- and Heterodimerization Propensities of Metabotropic Glutamate Receptors. *Cell Rep*. 2020;31(5):107605. doi:10.1016/j.celrep.2020.107605

71. Habrian CH, Levitz J, Vyklicky V, et al. Conformational pathway provides unique sensitivity to a synaptic mGluR. *Nat Commun*. 2019;10(1). doi:10.1038/s41467-019-13407-8

72. O'Connor V, El Oussama F, Bofill-Cardona E, et al. Calmodulin dependence of presynaptic metabotropic glutamate receptor signaling. *Science (80-)*. 1999;286(5442):1180-1184. doi:10.1126/science.286.5442.1180

73. Jalan-Sakrikar N, Field JR, Klar R, et al. Identification of Positive Allosteric Modulators VU0155094 (ML397) and VU0422288 (ML396) Reveals New Insights into the Biology of Metabotropic Glutamate Receptor 7. *ACS Chem Neurosci*. 2014;5(12):1221-1237. doi:10.1021/cn500153z

74. Martín R, Torres M, Sánchez-Prieto J. mGluR7 inhibits glutamate release through a PKC-independent decrease in the activity of P/Q-type Ca2+ channels and by diminishing cAMP in hippocampal nerve terminals. *Eur J Neurosci*. 2007;26(2):312-322. doi:10.1111/j.1460-9568.2007.05660.x

75. Iacovelli L, Felicioni M, Nisticò R, Nicoletti F, De Blasi A. Selective regulation of recombinantly expressed mGlu7 metabotropic glutamate receptors by G protein-coupled receptor kinases and arrestins. *Neuropharmacology*. 2014;77:303-312. doi:10.1016/j.neuropharm.2013.10.013

76. Kammermeier PJ. Constitutive activity of metabotropic glutamate receptor 7. *BMC Neurosci*. 2015;16(1). doi:10.1186/s12868-015-0154-6

77. Tassin V, Girard B, Chotte A, et al. Phasic and Tonic mGlu7 Receptor Activity Modulates the Thalamocortical Network. *Front Neural Circuits*. 2016;10(APR):31. doi:10.3389/fncir.2016.00031

78. Stachniak TJ, Sylwestrak EL, Scheiffele P, Hall BJ, Ghosh A. Elfn1-induced constitutive activation of mglur7 determines frequency-dependent recruitment of somatostatin interneurons. *J Neurosci*. 2019;39(23):4461-4474. doi:10.1523/JNEUROSCI.2276-18.2019

79. Millán C, Luján R, Shigemoto R, Sánchez-Prieto J. The inhibition of glutamate release by metabotropic glutamate receptor 7 affects both [Ca2+]c and cAMP. Evidence for a strong reduction of Ca2+ entry in single nerve terminals. *J Biol Chem*. 2002;277(16):14092-14101. doi:10.1074/jbc.M109044200

80. Millán C, Castro E, Torres M, Shigemoto R, Sánchez-Prieto J. Co-expression of metabotropic glutamate receptor 7 and N-type Ca2+ channels in single cerebrocortical nerve terminals of adult rats. *J Biol Chem*. 2003;278(26):23955-23962. doi:10.1074/jbc.M211471200

81. Perroy J, El Far O, Bertaso F, et al. PICK1 is required for the control of synaptic transmission by the metabotropic glutamate receptor 7. *EMBO J*. 2002;21(12):2990-2999. doi:10.1093/emboj/cdf313

82. Perroy J, Prezeau L, De Waard M, Shigemoto R, Bockaert J, Fagni L. Selective blockade of P/Q-type calcium channels by the metabotropic glutamate receptor type 7 involves a phospholipase C pathway in neurons. *J Neurosci*. 2000;20(21):7896-7904. doi:10.1523/jneurosci.20-21-07896.2000

83. Bertaso F, Lill Y, Airas JM, et al. MacMARCKS interacts with the metabotropic glutamate receptor type 7 and modulates G protein-mediated constitutive inhibition of calcium channels. *J Neurochem*. 2006;99(1):288-298. doi:10.1111/j.1471-4159.2006.04121.x

84. Martín R, Durroux T, Ciruela F, Torres M, Pin JP, Sánchez-Prieto J. The metabotropic glutamate receptor mGlu7 activates phospholipase C, translocates munc-13-1 protein, and potentiates glutamate release at cerebrocortical nerve terminals. *J Biol Chem*. 2010;285(23):17907-17917. doi:10.1074/jbc.M109.080838

85. Ferrero JJ, Bartolomé-Martín D, Torres M, Sánchez-Prieto J. Potentiation of mGlu7 receptor-mediated glutamate release at nerve terminals containing N and P/Q type Ca2+ channels. *Neuropharmacology*. 2013;67:213-222. doi:10.1016/j.neuropharm.2012.10.032

86. Suh YH, Pelkey KA, Lavezzari G, et al. Corequirement of PICK1 Binding and PKC Phosphorylation for Stable Surface Expression of the Metabotropic Glutamate Receptor mGluR7. *Neuron*. 2008;58(5):736-748. doi:10.1016/j.neuron.2008.03.028

87. Suh YH, Park JY, Park S, Jou I, Roche PA, Roche KW. Regulation of metabotropic glutamate receptor 7 (mGluR7) internalization and surface expression by Ser/Thr protein phosphatase 1. *J Biol Chem*. 2013;288(24):17544-17551. doi:10.1074/jbc.M112.439513

88. Lavezzari G, Roche KW. Constitutive endocytosis of the metabotropic glutamate receptor mGluR7 is clathrin-independent. *Neuropharmacology*. 2007;52(1):100-107. doi:10.1016/j.neuropharm.2006.07.011

89. Pelkey KA, Yuan X, Lavezzari G, Roche KW, McBain CJ. mGluR7 undergoes rapid internalization in response to activation by the allosteric agonist AMN082. *Neuropharmacology*. 2007;52(1):108-117. doi:10.1016/j.neuropharm.2006.07.020

90. Lee S, Park S, Lee H, et al. Nedd4 E3 ligase and beta-arrestins regulate

ubiquitination, trafficking, and stability of the mGlu7 receptor. *Elife*. 2019;8. doi:10.7554/eLife.44502

91. Dunn HA, Patil DN, Cao Y, Orlandi C, Martemyanov KA. Synaptic adhesion protein ELFN1 is a selective allosteric modulator of group III metabotropic glutamate receptors in trans. *Proc Natl Acad Sci U S A*. 2018;115(19):5022-5027. doi:10.1073/pnas.1722498115

92. Dunn HA, Zucca S, Dao M, Orlandi C, Martemyanov KA. ELFN2 is a postsynaptic cell adhesion molecule with essential roles in controlling group III mGluRs in the brain and neuropsychiatric behavior. *Mol Psychiatry*. 2019;24(12):1902-1919. doi:10.1038/s41380-019-0512-3

93. Bliss TVP, Collingridge GL. A synaptic model of memory: Long-term potentiation in the hippocampus. *Nature*. 1993;361(6407):31-39. doi:10.1038/361031a0

94. Takeuchi T, Duszkiewicz AJ, Morris RGM. The synaptic plasticity and memory hypothesis: Encoding, storage and persistence. *Philos Trans R Soc B Biol Sci*. 2014;369(1633). doi:10.1098/rstb.2013.0288

95. Laezza F, Doherty JJ, Dingledine R. Long-term depression in hippocampal interneurons: Joint requirement for pre- and postsynaptic events. *Science (80-)*. 1999;285(5432):1411-1414. doi:10.1126/science.285.5432.1411

96. Pelkey KA, Lavezzari G, Racca C, Roche KW, McBain CJ. MGluR7 is a metaplastic switch controlling bidirectional plasticity of feedforward inhibition. *Neuron*. 2005;46(1):89-102. doi:10.1016/j.neuron.2005.02.011

97. Pelkey KA, Topolnik L, Lacaille JC, McBain CJ. Compartmentalized Ca2+ Channel Regulation at Divergent Mossy-Fiber Release Sites Underlies Target Cell-

Dependent Plasticity. *Neuron*. 2006;52(3):497-510. doi:10.1016/j.neuron.2006.08.032

98. Sylwestrak EL, Ghosh A. Elfn1 Regulates Target-Specific Release Probability at CA1-Interneuron Synapses. *Science (80-)*. 2012;338(6106):536-540. doi:10.1126/science.1222482

99. Summa M, Di Prisco S, Grilli M, Usai C, Marchi M, Pittaluga A. Presynaptic mGlu7 receptors control GABA release in mouse hippocampus. *Neuropharmacology*. 2013;66:215-224. doi:10.1016/j.neuropharm.2012.04.020

100. Klar R, Walker AG, Ghose D, et al. Activation of metabotropic glutamate receptor 7 is required for induction of long-term potentiation at SCCA1 synapses in the hippocampus. *J Neurosci*. 2015;35(19):7600-7615. doi:10.1523/JNEUROSCI.4543-14.2015

101. Jiang Y, Armstrong D, Albrecht U, et al. Mutation of the Angelman Ubiquitin Ligase in Mice Causes Increased Cytoplasmic p53 and Deficits of Contextual Learning and Long-Term Potentiation. *Neuron*. 1998;21(4):799-811. doi:10.1016/S0896-6273(00)80596-6

102. Von Der Brelie C, Waltereit R, Zhang L, Beck H, Kirschstein T. Impaired synaptic plasticity in a rat model of tuberous sclerosis. *Eur J Neurosci*. 2006;23(3):686-692. doi:10.1111/j.1460-9568.2006.04594.x

103. Moretti P, Levenson JM, Battaglia F, et al. Learning and memory and synaptic plasticity are impaired in a mouse model of Rett syndrome. *J Neurosci*. 2006;26(1):319-327. doi:10.1523/JNEUROSCI.2623-05.2006

104. Baskys A, Malenka RC. Agonists at metabotropic glutamate receptors

presynaptically inhibit EPSCs in neonatal rat hippocampus. *J Physiol*. 1991;444(1):687-701. doi:10.1113/jphysiol.1991.sp018901

105. Ayala JE, Niswender CM, Luo Q, Banko JL, Conn PJ. Group III mGluR regulation of synaptic transmission at the SC-CA1 synapse is developmentally regulated. *Neuropharmacology*. 2008;54(5):804-814. doi:10.1016/j.neuropharm.2007.12.009
106. Reed CW, McGowan KM, Spearing PK, et al. VU6010608, a Novel mGlu7 NAM from a Series of N-(2-(1H-1,2,4-Triazol-1-yl)-5-(trifluoromethoxy)phenyl)benzamides. *ACS Med Chem Lett*. 2017;8(12):1326-1330. doi:10.1021/acsmedchemlett.7b00429
107. Bushell TJ, Sansig G, Collett VJ, van der Putten H, Collingridge GL. Altered Short-Term Synaptic Plasticity in Mice Lacking the Metabotropic Glutamate Receptor mGlu7. *ScientificWorldJournal*. 2002;2:730-737. doi:10.1100/tsw.2002.146
108. Dammann F, Kirschstein T, Guli X, et al. Bidirectional shift of group III metabotropic glutamate receptor-mediated synaptic depression in the epileptic hippocampus. *Epilepsy Res*. 2018;139:157-163. doi:10.1016/j.eplepsyres.2017.12.002
109. Martín R, Ferrero JJ, Collado-Alsina A, et al. Bidirectional modulation of glutamatergic synaptic transmission by metabotropic glutamate type 7 receptors at Schaffer collateral–CA1 hippocampal synapses. *J Physiol*. 2018;596(5):921-940. doi:10.1113/JP275371
110. Sigurdsson T, Doyère V, Cain CK, LeDoux JE. Long-term potentiation in the amygdala: A cellular mechanism of fear learning and memory. *Neuropharmacology*. 2007;52(1):215-227. doi:10.1016/j.neuropharm.2006.06.022
111. Brasted PJ, Bussey TJ, Murray EA, Wise SP. Role of the hippocampal system in

associative learning beyond the spatial domain. *Brain*. 2003;126(5):1202-1223. doi:10.1093/brain/awg103

112. Fendt M, Schmid S, Thakker DR, et al. mGluR7 facilitates extinction of aversive memories and controls amygdala plasticity. *Mol Psychiatry*. 2008;13(10):970-979. doi:10.1038/sj.mp.4002073

113. Fendt M, Imobersteg S, Peterlik D, et al. Differential roles of mGlu7 and mGlu8 in amygdala-dependent behavior and physiology. *Neuropharmacology*. 2013;72:215-223. doi:10.1016/j.neuropharm.2013.04.052

114. Gee CE, Peterlik D, Neuhäuser C, et al. Blocking metabotropic glutamate receptor subtype 7 (mGlu7) via the Venus flytrap domain (VFTD) inhibits amygdala plasticity, stress, and anxiety-related behavior. *J Biol Chem*. 2014;289(16):10975-10987. doi:10.1074/jbc.M113.542654

115. Masugi M, Yokoi M, Shigemoto R, et al. Metabotropic glutamate receptor subtype 7 ablation causes deficit in fear response and conditioned taste aversion. *J Neurosci*. 1999;19(3):955-963.

116. Goddyn H, Callaerts-Vegh Z, Stroobants S, et al. Deficits in acquisition and extinction of conditioned responses in mGluR7 knockout mice. *Neurobiol Learn Mem*. 2008;90(1):103-111.

117. Goddyn H, Callaerts-Vegh Z, D'Hooge R. Functional Dissociation of Group III Metabotropic Glutamate Receptors Revealed by Direct Comparison between the Behavioral Profiles of Knockout Mouse Lines. *Int J Neuropsychopharmacol*. 2015;18(11):pyv053. doi:10.1093/ijnp/pyv053

118. Callaerts-Vegh Z, Beckers T, Ball SM, et al. Concomitant deficits in working

memory and fear extinction are functionally dissociated from reduced anxiety in metabotropic glutamate receptor 7-deficient mice. *J Neurosci*. 2006;26(24):6573-6582. doi:10.1523/JNEUROSCI.1497-06.2006

119. Hikichi H, Murai T, Okuda S, et al. Effects of a novel metabotropic glutamate receptor 7 negative allosteric modulator, 6-(4-methoxyphenyl)-5-methyl-3-pyridin-4-ylisoxazonolo[4,5-c]pyridin-4(5H)-one (MMPIP), on the central nervous system in rodents. *Eur J Pharmacol*. 2010;639(1-3):106-114. doi:10.1016/j.ejphar.2009.08.047
120. Klakotskaia D, Ramsey AK, Fowler SW, Serfozo P, Simonyi A, Schachtman TR. Effects of group II and III metabotropic glutamate receptor ligands on conditioned taste aversion learning. *Behav Brain Res*. 2013;253:9-16. doi:10.1016/j.bbr.2013.06.032
121. Palazzo E, Romano R, Luongo L, et al. MMPIP, an mGluR7-selective negative allosteric modulator, alleviates pain and normalizes affective and cognitive behavior in neuropathic mice. *Pain*. 2015;156(6):1060-1073. doi:10.1097/j.pain.0000000000000150
122. Niswender CM, Johnson KA, Miller NR, et al. Context-dependent pharmacology exhibited by negative allosteric modulators of metabotropic glutamate receptor 7. *Mol Pharmacol*. 2010;77(3):459-468. doi:10.1124/mol.109.058768
123. Dobi A, Sartori SB, Busti D, et al. Neural substrates for the distinct effects of presynaptic group III metabotropic glutamate receptors on extinction of contextual fear conditioning in mice. *Neuropharmacology*. 2013;66:274-289. doi:10.1016/j.neuropharm.2012.05.025

124. Siegl S, Flor PJ, Fendt M. Amygdaloid metabotropic glutamate receptor subtype 7 is involved in the acquisition of conditioned fear. *Neuroreport*. 2008;19(11):1147-1150. doi:10.1097/WNR.0b013e328307f295

125. Toth I, Dietz M, Peterlik D, et al. Pharmacological interference with metabotropic glutamate receptor subtype 7 but not subtype 5 differentially affects within- and between-session extinction of Pavlovian conditioned fear. *Neuropharmacology*. 2012;62(4):1619-1626. doi:10.1016/j.neuropharm.2011.10.021

126. Slattery DA, Neumann ID, Flor PJ, Zoicas I. Pharmacological modulation of metabotropic glutamate receptor subtype 5 and 7 impairs extinction of social fear in a time-point-dependent manner. *Behav Brain Res*. 2017;328:57-61. doi:10.1016/j.bbr.2017.04.010

127. Ahnaou A, Raeyemaekers L, Huysmans H, Drinkenburg WHIM. Off-target potential of AMN082 on sleep EEG and related physiological variables: Evidence from mGluR7 (-/-) mice. *Behav Brain Res*. 2016;311:287-297. doi:10.1016/j.bbr.2016.05.035

128. Abe M, Seto M, Gogliotti RG, et al. Discovery of VU6005649, a CNS Penetrant mGlu7/8 Receptor PAM Derived from a Series of Pyrazolo[1,5-a]pyrimidines. *ACS Med Chem Lett*. 2017;8(10):1110-1115. doi:10.1021/acsmedchemlett.7b00317

129. Bertaso F, Zhang C, Scheschonka A, et al. PICK1 uncoupling from mGluR7a causes absence-like seizures. *Nat Neurosci*. 2008;11(8):940-948. doi:10.1038/nn.2142

130. Zhang CS, Bertaso F, Eulenburg V, et al. Knock-in mice lacking the PDZ-ligand motif of mGluR7a show impaired PKC-dependent autoinhibition of glutamate

release, spatial working memory deficits, and increased susceptibility to pentylenetetrazol. *J Neurosci*. 2008;28(34):8604-8614. doi:10.1523/JNEUROSCI.0628-08.2008

131. Dolan J, Mitchell KJ. Mutation of Elfn1 in Mice Causes Seizures and Hyperactivity. Ruhrberg C, ed. *PLoS One*. 2013;8(11):e80491. doi:10.1371/journal.pone.0080491
132. Matson JL, Cervantes PE. Commonly studied comorbid psychopathologies among persons with autism spectrum disorder. *Res Dev Disabil*. 2014;35(5):952-962. doi:10.1016/j.ridd.2014.02.012
133. Shin LM, Liberzon I. The neurocircuitry of fear, stress, and anxiety disorders. *Neuropsychopharmacology*. 2010;35(1):169-191. doi:10.1038/npp.2009.83
134. Cryan JF, Kelly PH, Neijt HC, Sansig G, Flor PJ, Van Der Putten H. Antidepressant and anxiolytic-like effects in mice lacking the group III metabotropic glutamate receptor mGluR7. *Eur J Neurosci*. 2003;17(11):2409-2417. doi:10.1046/j.1460-9568.2003.02667.x
135. Kalinichev M, Rouillier M, Girard F, et al. ADX71743, a potent and selective negative allosteric modulator of metabotropic glutamate receptor 7: In vitro and in vivo characterization. *J Pharmacol Exp Ther*. 2013;344(3):624-636. doi:10.1124/jpet.112.200915
136. Pałucha-Poniewiera A, Pilc A. A selective mGlu7 receptor antagonist MMPIP reversed antidepressant-like effects of AMN082 in rats. *Behav Brain Res*. 2013;238(1):109-112. doi:10.1016/j.bbr.2012.10.004
137. O'Connor RM, Cryan JF. The effects of $mGlu_7$ receptor modulation in behavioural models sensitive to antidepressant action in two mouse strains. *Behav Pharmacol*.

2013;24(2):105-113. doi:10.1097/FBP.0b013e32835efc78

138. Gogliotti RG, Senter RK, Fisher NM, et al. mGlu 7 potentiation rescues cognitive, social, and respiratory phenotypes in a mouse model of Rett syndrome. *Sci Transl Med*. 2017;9(403):eaai7459. doi:10.1126/scitranslmed.aai7459
139. Neul JL, Kaufmann WE, Glaze DG, et al. Rett syndrome: Revised diagnostic criteria and nomenclature. *Ann Neurol*. 2010;68(6):944-950. doi:10.1002/ana.22124
140. Amir RE, Van Den Veyver IB, Wan M, Tran CQ, Francke U, Zoghbi HY. Rett syndrome is caused by mutations in X-linked MECP2, encoding methyl- CpG-binding protein 2. *Nat Genet*. 1999;23(2):185-188. doi:10.1038/13810
141. Carney RM, Wolpert CM, Ravan SA, et al. Identification of MeCP2 mutations in a series of females with autistic disorder. *Pediatr Neurol*. 2003;28(3):205-211. doi:10.1016/S0887-8994(02)00624-0
142. Couvert P, Bienvenu T, Aquaviva C, et al. MECP2 is highly mutated in X-linked mental retardation. *Hum Mol Genet*. 2001;10(9):941-946. doi:10.1093/hmg/10.9.941
143. Guy J, Cheval H, Selfridge J, Bird A. The role of MeCP2 in the brain. *Annu Rev Cell Dev Biol*. 2011;27:631-652. doi:10.1146/annurev-cellbio-092910-154121
144. Tate P, Skarnes W, Bird A. The methyl-CpG binding protein MeCP2 is essential for embryonic development in the mouse. *Nat Genet*. 1996;12(2):205-208. doi:10.1038/ng0296-205
145. Shahbazian MD, Antalffy B, Armstrong DL, Zoghbi HY. Insight into Rett syndrome: MeCP2 levels display tissue- and cell-specific differences and correlate with neuronal maturation. *Hum Mol Genet*. 2002;11(2):115-124.

doi:10.1093/hmg/11.2.115

146. Bedogni F, Gigli CC, Pozzi D, et al. Defects during Mecp2 Null Embryonic Cortex Development Precede the Onset of Overt Neurological Symptoms. *Cereb Cortex*. 2016;26(6):2517-2529. doi:10.1093/cercor/bhv078

147. Guy J, Gan J, Selfridge J, Cobb S, Bird A. Reversal of neurological defects in a mouse model of Rett syndrome. *Science (80-)*. 2007;315(5815):1143-1147. doi:10.1126/science.1138389

148. McGraw CM, Samaco RC, Zoghbi HY. Adult neural function requires MeCP2. *Science (80-)*. 2011;333(6039):186. doi:10.1126/science.1206593

149. Chao HT, Chen H, Samaco RC, et al. Dysfunction in GABA signalling mediates autism-like stereotypies and Rett syndrome phenotypes. *Nature*. 2010;468(7321):263-269. doi:10.1038/nature09582

150. Holscher C, Schmid S, Pilz PKD, Sansig G, van der Putten H, Plappert CF. Lack of the metabotropic glutamate receptor subtype 7 selectively modulates Theta rhythm and working memory. *Learn Mem*. 2005;12(5):450-455. doi:10.1101/lm.98305

151. Lai MC, Lombardo M V., Baron-Cohen S. Autism. In: *The Lancet*. Vol 383. Lancet Publishing Group; 2014:896-910. doi:10.1016/S0140-6736(13)61539-1

152. Sandin S, Lichtenstein P, Kuja-Halkola R, Hultman C, Larsson H, Reichenberg A. The heritability of autism spectrum disorder. *JAMA - J Am Med Assoc*. 2017;318(12):1182-1184. doi:10.1001/jama.2017.12141

153. Gai X, Xie HM, Perin JC, et al. Rare structural variation of synapse and neurotransmission genes in autism. *Mol Psychiatry*. 2012;17(4).

154. Liu Y, Zhang Y, Zhao D, et al. Rare de novo deletion of metabotropic glutamate

receptor 7 (GRM7) gene in a patient with autism spectrum disorder. *Am J Med Genet Part B Neuropsychiatr Genet*. 2015;168(4):258-264. doi:10.1002/ajmg.b.32306

155. Sanders SJ, Murtha MT, Gupta AR, et al. De novo mutations revealed by whole-exome sequencing are strongly associated with autism. *Nature*. 2012;485(7397):237-241. doi:10.1038/nature10945
156. Yang Y, Pan C. Role of metabotropic glutamate receptor 7 in autism spectrum disorders: A pilot study. *Life Sci*. 2013;92(2):149-153. doi:10.1016/j.lfs.2012.11.010
157. Noroozi R, Taheri M, Movafagh A, et al. Glutamate receptor, metabotropic 7 (GRM7) gene variations and susceptibility to autism: A case-control study. *Autism Res*. 2016;9(11):1161-1168. doi:10.1002/aur.1640
158. Chen M, Tominaga K, Pereira-Smith OM. Emerging role of the MORF/MRG gene family in various biological processes, including aging. In: *Annals of the New York Academy of Sciences*. Vol 1197. Blackwell Publishing Inc.; 2010:134-141. doi:10.1111/j.1749-6632.2010.05197.x
159. Park S, Jung S-WW, Kim B-NN, et al. Association between the GRM7 rs3792452 polymorphism and attention deficit hyperacitiveity disorder in a Korean sample. *Behav Brain Funct*. 2013;9(1):1. doi:10.1186/1744-9081-9-1
160. Akutagava-Martins G, Salatino-Oliveira A, Bruxel E, et al. Lack of association between the GRM7 gene and attention deficit hyperactivity disorder. *Psychiatr Genet*. 2014;24(6):281-282. doi:10.1097/YPG.0000000000000059
161. Park S, Kim B-N, Cho S-C, et al. The Metabotropic Glutamate Receptor Subtype 7 rs3792452 Polymorphism Is Associated with the Response to Methylphenidate in

Children with Attention-Deficit/Hyperactivity Disorder. *J Child Adolesc Psychopharmacol*. 2014;24(4):223-227. doi:10.1089/cap.2013.0079

162. Firth H V., Richards SM, Bevan AP, et al. DECIPHER: Database of Chromosomal Imbalance and Phenotype in Humans Using Ensembl Resources. *Am J Hum Genet*. 2009;84(4):524-533. doi:10.1016/j.ajhg.2009.03.010
163. Fisher NMNM, Gogliotti RGRG, Vermudez SADSADSAD, Stansley BJBJBJ, Conn PJJ, Niswender CMCM. Genetic Reduction or Negative Modulation of mGlu 7 Does Not Impact Anxiety and Fear Learning Phenotypes in a Mouse Model of MECP2 Duplication Syndrome. *ACS Chem Neurosci*. 2018;9(9):2210-2217. doi:10.1021/acschemneuro.7b00414
164. Neul JL, Fang P, Barrish J, et al. Specific mutations in methyl-CpG-binding protein 2 confer different severity in Rett syndrome. *Neurology*. 2008;70(16):1313-1321. doi:10.1212/01.wnl.0000291011.54508.aa
165. del Gaudio D, Fang P, Scaglia F, et al. Increased MECP2 gene copy number as the result of genomic duplication in neurodevelopmentally delayed males. *Genet Med*. 2006;8(12):784-792. doi:10.1097/01.gim.0000250502.28516.3c
166. Van Esch H, Bauters M, Ignatius J, et al. Duplication of the MECP2 region is a frequent cause of severe mental retardation and progressive neurological symptoms in males. *Am J Hum Genet*. 2005;77(3):442-453. doi:10.1086/444549
167. Sztainberg Y, Chen HM, Swann JW, et al. Reversal of phenotypes in MECP2 duplication mice using genetic rescue or antisense oligonucleotides. *Nature*. 2015;528(7580):123-126. doi:10.1038/nature16159
168. Bradley SR, Rees HD, Yi H, Levey AI, Conn PJ. Distribution and developmental

regulation of metabotropic glutamate receptor 7a in rat brain. *J Neurochem*. 1998;71(2):636-645.

169. Collins AL, Levenson JM, Vilaythong AP, et al. Mild overexpression of MeCP2 causes a progressive neurological disorder in mice. *Hum Mol Genet*. 2004;13(21):2679-2689. doi:10.1093/hmg/ddh282
170. Na ES, Nelson ED, Adachi M, et al. A mouse model for MeCP2 duplication syndrome: MeCP2 overexpression impairs learning and memory and synaptic transmission. *J Neurosci*. 2012;32(9):3109-3117. doi:10.1523/JNEUROSCI.6000-11.2012
171. Stansley BJ, Fisher NM, Gogliotti RG, Lindsley CW, Conn PJ, Niswender CM. Contextual fear extinction induces hippocampal metaplasticity mediated by metabotropic glutamate receptor 5. *Cereb Cortex*. 2018;28(12). doi:10.1093/cercor/bhx282
172. Samaco RC, Mandel-Brehm C, McGraw CM, Shaw CA, McGill BE, Zoghbi HY. Crh and Oprm1 mediate anxiety-related behavior and social approach in a mouse model of MECP2 duplication syndrome. *Nat Genet*. 2012;44(2):206-221. doi:10.1038/ng.1066
173. Lu H, Ash RT, He L, et al. Loss and Gain of MeCP2 Cause Similar Hippocampal Circuit Dysfunction that Is Rescued by Deep Brain Stimulation in a Rett Syndrome Mouse Model. *Neuron*. 2016;91(4):739-747. doi:10.1016/j.neuron.2016.07.018
174. Gogliotti RG, Senter RK, Rook JM, et al. mGlu5 positive allosteric modulation normalizes synaptic plasticity defects and motor phenotypes in a mouse model of Rett syndrome. *Hum Mol Genet*. 2016;25(10):1990-2004.

doi:10.1093/hmg/ddw074

175. Fisher NM, Gould RW, Gogliotti RG, et al. Phenotypic profiling of mGlu 7 knockout mice reveals new implications for neurodevelopmental disorders . *Genes, Brain Behav*. April 2020. doi:10.1111/gbb.12654

176. Ohtsuki T, Koga M, Ishiguro H, et al. A polymorphism of the metabotropic glutamate receptor mGluR7 (GRM7) gene is associated with schizophrenia. *Schizophr Res*. 2008;101(1-3):9-16. doi:10.1016/j.schres.2008.01.027

177. Noroozi R, Taheri M, Omrani MD, Ghafouri-Fard S. Glutamate receptor metabotropic 7 (GRM7) gene polymorphisms in mood disorders and attention deficit hyperactive disorder. *Neurochem Int*. 2019;129:104483. doi:10.1016/J.NEUINT.2019.104483

178. Bozzi Y, Casarosa S, Caleo M. Epilepsy as a Neurodevelopmental Disorder. *Front Psychiatry*. 2012;3:19. doi:10.3389/fpsyt.2012.00019

179. Robinson-Shelton A, Malow BA. Sleep Disturbances in Neurodevelopmental Disorders. *Curr Psychiatry Rep*. 2016;18(1):6. doi:10.1007/s11920-015-0638-1

180. Mick E, Neale B, Middleton FA, McGough JJ, Faraone S V. Genome-wide association study of response to methylphenidate in 187 children with attention-deficit/hyperactivity disorder. *Am J Med Genet Part B Neuropsychiatr Genet*. 2008;147B(8):1412-1418. doi:10.1002/ajmg.b.30865

181. Masugi-Tokita M, Flor PJ, Kawata M. Metabotropic Glutamate Receptor Subtype 7 in the Bed Nucleus of the Stria Terminalis is Essential for Intermale Aggression. *Neuropsychopharmacology*. 2016;41(3):726-735. doi:10.1038/npp.2015.198

182. Masugi-Tokita M, Yoshida T, Kageyama S, Kawata M, Kawauchi A. Metabotropic

glutamate receptor subtype 7 has critical roles in regulation of the endocrine system and social behaviours. *J Neuroendocrinol*. 2018;30(3):e12575. doi:10.1111/jne.12575

183. Gryksa K, Mittmann L, Bauer A, et al. Metabotropic glutamate receptor subtype 7 controls maternal care, maternal motivation and maternal aggression in mice. *Genes, Brain Behav*. December 2019. doi:10.1111/gbb.12627
184. Friedman RA, Van Laer L, Huentelman MJ, et al. GRM7 variants confer susceptibility to age-related hearing impairment. *Hum Mol Genet*. 2009;18(4):785-796. doi:10.1093/hmg/ddn402
185. Kosinski CM, Risso Bradley S, Conn PJ, et al. Localization of metabotropic glutamate receptor 7 mRNA and mGluR7a protein in the rat basal ganglia. *J Comp Neurol*. 1999;415(2):266-284.
186. Girard B, Tuduri P, Moreno MP, et al. The mGlu7 receptor provides protective effects against epileptogenesis and epileptic seizures. *Neurobiol Dis*. 2019;129:13-28. doi:10.1016/j.nbd.2019.04.016
187. Luppi P-H, Gervasoni D, Verret L, et al. Paradoxical (REM) sleep genesis: The switch from an aminergic–cholinergic to a GABAergic–glutamatergic hypothesis. *J Physiol*. 2006;100(5-6):271-283. doi:10.1016/j.jphysparis.2007.05.006
188. Rasch B, Born J. About sleep's role in memory. *Physiol Rev*. 2013;93(2):681-766. doi:10.1152/physrev.00032.2012
189. Lee ML, Katsuyama ÂM, Duge LS, et al. Fragmentation of Rapid Eye Movement and Nonrapid Eye Movement Sleep without Total Sleep Loss Impairs Hippocampus-Dependent Fear Memory Consolidation. *Sleep*. 2016;39(11):2021-

2031. doi:10.5665/sleep.6236

190. Fort P, Bassetti CL, Luppi P-H. Alternating vigilance states: new insights regarding neuronal networks and mechanisms. *Eur J Neurosci*. 2009;29(9):1741-1753. doi:10.1111/j.1460-9568.2009.06722.x

191. Gonzalez-Burgos G, Hashimoto T, Lewis DA. Alterations of Cortical GABA Neurons and Network Oscillations in Schizophrenia. *Curr Psychiatry Rep*. 2010;12(4):335-344. doi:10.1007/s11920-010-0124-8

192. Le Van Quyen M, Khalilov I, Ben-Ari Y. The dark side of high-frequency oscillations in the developing brain. *Trends Neurosci*. 2006;29(7):419-427. doi:10.1016/j.tins.2006.06.001

193. Benchenane K, Tiesinga PH, Battaglia FP. Oscillations in the prefrontal cortex: a gateway to memory and attention. *Curr Opin Neurobiol*. 2011;21(3):475-485. doi:10.1016/j.conb.2011.01.004

194. Franzen JD, Wilson TW. Amphetamines modulate prefrontal γ oscillations during attention processing. *Neuroreport*. 2012;23(12):731-735. doi:10.1097/WNR.0b013e328356bb59

195. Klein MO, Battagello DS, Cardoso AR, Hauser DN, Bittencourt JC, Correa RG. Dopamine: Functions, Signaling, and Association with Neurological Diseases. *Cell Mol Neurobiol*. 2019;39(1):31-59. doi:10.1007/s10571-018-0632-3

196. Katz DM, Berger-Sweeney JE, Eubanks JH, et al. Preclinical research in Rett syndrome: setting the foundation for translational success. *Dis Model Mech*. 2012;5(6):733-745. doi:10.1242/dmm.011007

197. Gould RW, Nedelcovych MT, Gong X, et al. State-dependent alterations in

sleep/wake architecture elicited by the M<inf>4</inf> PAM VU0467154 - Relation to antipsychotic-like drug effects. *Neuropharmacology*. 2016;102. doi:10.1016/j.neuropharm.2015.11.016

198. Rook JM, Xiang Z, Lv X, et al. Biased mGlu5-Positive Allosteric Modulators Provide InVivo Efficacy without Potentiating mGlu5 Modulation of NMDAR Currents. *Neuron*. 2015;86(4):1029-1040. doi:10.1016/j.neuron.2015.03.063
199. Nedelcovych MT, Gould RW, Zhan X, et al. A rodent model of traumatic stress induces lasting sleep and quantitative electroencephalographic disturbances. *ACS Chem Neurosci*. 2015;6(3). doi:10.1021/cn500342u
200. Marafi D, Mitani T, Isikay S, et al. Biallelic *GRM7* variants cause epilepsy, microcephaly, and cerebral atrophy. *Ann Clin Transl Neurol*. April 2020. doi:10.1002/acn3.51003
201. Han G, Hampson DR. Ligand binding to the amino-terminal domain of the mGluR4 subtype of metabotropic glutamate receptor. *J Biol Chem*. 1999;274(15):10008-10013. doi:10.1074/JBC.274.15.10008
202. Robbins MJ, Ciruela F, Rhodes A, Mcilhinney RAJ. *Characterization of the Dimerization of Metabotropic Glutamate Receptors Using an N-Terminal Truncation of MGluR1*. Vol 72.; 1999.
203. Beqollari D, Kammermeier PJ. Venus Fly Trap Domain of mGluR1 Functions as a Dominant Negative Against Group I mGluR Signaling. *J Neurophysiol*. 2010;104(1):439-448. doi:10.1152/jn.00799.2009
204. Chang K, Roche KW. Structural and molecular determinants regulating mGluR5 surface expression. *Neuropharmacology*. 2017;115:10-19.

doi:10.1016/j.neuropharm.2016.04.037

205. Park D, Park S, Song J, et al. N-linked glycosylation of the mGlu7 receptor regulates the forward trafficking and transsynaptic interaction with Elfn1. *FASEB J*. September 2020. doi:10.1096/fj.202001544R

206. Ruggiano A, Foresti O, Carvalho P. ER-associated degradation: Protein quality control and beyond. *J Cell Biol*. 2014;204(6):869-879. doi:10.1083/jcb.201312042

207. Niswender CM, Johnson KA, Luo Q, et al. A novel assay of Gi/o-linked G protein-coupled receptor coupling to potassium channels provides new insights into the pharmacology of the group III metabotropic glutamate receptors. *Mol Pharmacol*. 2008;73(4):1213-1224. doi:10.1124/mol.107.041053

208. Meng X, Wang W, Lu H, et al. Manipulations of MeCP2 in glutamatergic neurons highlight their contributions to rett and other neurological disorders. *Elife*. 2016;5(JUN2016). doi:10.7554/eLife.14199

209. Balakrishnan S, Mironov SL. CA1 Neurons Acquire Rett Syndrome Phenotype After Brief Activation of Glutamatergic Receptors: Specific Role of mGluR1/5. *Front Cell Neurosci*. 2018;12:363. doi:10.3389/fncel.2018.00363

210. Zeitz C, Forster U, Neidhardt J, et al. Night blindness-associated mutations in the ligand-binding, cysteine-rich, and intracellular domains of the metabotropic glutamate receptor 6 abolish protein trafficking. *Hum Mutat*. 2007;28(8):771-780. doi:10.1002/humu.20499

211. Kolodziejczyk K, Saab AS, Nave KA, Attwell D. Why do oligodendrocyte lineage cells express glutamate receptors? *F1000 Biol Rep*. 2010;2(1). doi:10.3410/B2-57

212. Káradóttir R, Attwell D. Neurotransmitter receptors in the life and death of

oligodendrocytes. *Neuroscience*. 2007;145(4):1426-1438. doi:10.1016/j.neuroscience.2006.08.070

213. Luyt K, Varadi A, Molnar E. Functional metabotropic glutamate receptors are expressed in oligodendrocyte progenitor cells. *J Neurochem*. 2003;84(6):1452-1464. doi:10.1046/j.1471-4159.2003.01661.x
214. Spampinato SF, Merlo S, Chisari M, Nicoletti F, Sortino MA. Glial metabotropic glutamate receptor-4 increases maturation and survival of oligodendrocytes. *Front Cell Neurosci*. 2015;8(JAN):462. doi:10.3389/fncel.2014.00462
215. Tasic B, Yao Z, Graybuck LT, et al. Shared and distinct transcriptomic cell types across neocortical areas. *Nature*. 2018;563(7729):72-78. doi:10.1038/s41586-018-0654-5
216. Stowell JN, Craig AM. Axon/dendrite targeting of metabotropic glutamate receptors by their cytoplasmic carboxy-terminal domains. *Neuron*. 1999;22(3):525-536. doi:10.1016/S0896-6273(00)80707-2
217. Fuccillo M V. Striatal circuits as a common node for autism pathophysiology. *Front Neurosci*. 2016;10(FEB):27. doi:10.3389/fnins.2016.00027
218. Peça J, Feliciano C, Ting JT, et al. Shank3 mutant mice display autistic-like behaviours and striatal dysfunction. *Nature*. 2011;472(7344):437-442. doi:10.1038/nature09965
219. Mahgoub M, Adachi M, Suzuki K, et al. MeCP2 and histone deacetylases 1 and 2 in dorsal striatum collectively suppress repetitive behaviors. *Nat Neurosci*. 2016;19(11):1506-1512. doi:10.1038/nn.4395
220. Sellings LHL, Clarke PBS. Segregation of amphetamine reward and locomotor

stimulation between nucleus accumbens medial shell and core. *J Neurosci*. 2003;23(15):6295-6303. doi:10.1523/jneurosci.23-15-06295.2003

221. Li X, Xi ZX, Markou A. Metabotropic glutamate 7 (mGlu7) receptor: A target for medication development for the treatment of cocaine dependence. *Neuropharmacology*. 2013;66:12-23. doi:10.1016/j.neuropharm.2012.04.010
222. Sukoff Rizzo SJ, Leonard SK, Gilbert A, et al. The metabotropic glutamate receptor 7 allosteric modulator AMN082: A monoaminergic agent in disguise? *J Pharmacol Exp Ther*. 2011;338(1):345-352. doi:10.1124/jpet.110.177378
223. Ehninger D, Li W, Fox K, Stryker MP, Silva AJ. Reversing Neurodevelopmental Disorders in Adults. *Neuron*. 2008;60(6):950-960. doi:10.1016/j.neuron.2008.12.007
224. Vashi N, Justice MJ. Treating Rett syndrome: from mouse models to human therapies. *Mamm Genome*. 2019;30(5-6):90-110. doi:10.1007/s00335-019-09793-5
225. Xia W, Liu Y, Jiao J. GRM7 regulates embryonic neurogenesis via CREB and YAP. *Stem Cell Reports*. 2015;4(5):795-810. doi:10.1016/j.stemcr.2015.03.004